2013

Exploring Electric Field-Induced Changes in Astrocyte Behavior

Doel Dhar
Virginia Commonwealth University

EXPLORING ELECTRIC FIELD-INDUCED CHANGES IN ASTROCYTE BEHAVIOR

A Thesis submitted in partial fulfillment of the requirements for the degree of Master of Science in Anatomy & Neurobiology at Virginia Commonwealth University

by

DOEL DHAR
Bachelor of Science, Neuroscience, College of William & Mary, 2010

Director: RAYMOND J. COLELLO, D. PHIL.
ASSOCIATE PROFESSOR, DEPARTMENT OF ANATOMY AND NEUROBIOLOGY

Virginia Commonwealth University
Richmond, Virginia
July 2013

Acknowledgement

I would first like to recognize and thank my advisor, Dr. Raymond Colello, for his support and advice over the last year. His encouraging words and constructive criticisms, both towards my project and future career goals, have shaped this year into more than just a research experience.

I would also like to give thanks to Dr. John Bigbee, Dr. Jeffery Dupree, Dr. Dong Sun, and Dr. David Simpson for their time and advice regarding my project. I would additionally like to thank Dr. Scott Henderson for his help and time with the microscope and associated computer software.

I am thankful for the help provided by my lab members, in particular Matt Baer for his guidance and pearls of wisdom & Damien Brown for his assistance with microscopy and indulgence of endless questions. I would also like to recognize other people associated with the lab – Adam Goodreau, Raghu Madiraju, Ryan Mischel, and Michelle Tran – who have contributed in some form to my project.

Lastly, I would like to thank my family and friends, both new & old, for their love and continued support. I wouldn't be where I am today without the chats over frozen yogurt, inevitable arguments, and spontaneous 'adventures' that remind me to enjoy the little things in life.

Table of Contents

List of Tables

Page

List of Figures

Abstract

EXPLORING ELECTRIC FIELD-INDUCED CHANGES IN ASTROCYTE BEHAVIOR

By Doel Dhar, M.S.

A Thesis submitted in partial fulfillment of the requirements for the degree of Master of Science in Anatomy & Neurobiology at Virginia Commonwealth University

Virginia Commonwealth University, 2013

Major Director: Raymond J. Colello, D. Phil.
Associate Professor, Department of Anatomy and Neurobiology

Electric fields, which are generated by the movement of charged ions across membranes, are found in all biological systems and can influence cellular components ranging from amino acids to biological macromolecules. Physiological field strengths range from 1 – 200 $^{mV}/_{mm}$, and these electric fields are especially elevated at sites of cellular growth during development and regeneration. It has previously been demonstrated that elevated electric fields induce alignment of astrocyte processes *in vitro*, enhancing the rate of neurite outgrowth. It is believed that electric fields of varying physiological strength affect other astrocytic responses associated with regeneration. To characterize the duration over which these changes emerge, cultured rat astrocytes were exposed to different direct-current electric field strengths. The resulting cellular behaviors were recorded every three minutes with an inverted microscope equipped with DIC optics and a stage incubator. Electric fields were found to induce astrocyte responses similar to those observed during periods of

neurodevelopment and regeneration. Changes in astrocyte movement, proliferation, & morphology emerged within the first hour and persisted through the course of the electric field application, leading mammalian astrocytes to revert to an earlier maturation state resembling those seen in amphibian astrocytes associated with central nervous system regeneration. Collectively, these results suggest that applied electric fields lead to astrocyte dedifferentiation, with certain electric field strengths eliciting and enhancing specific cell responses.

CHAPTER 1 Introduction

The study of mammalian regeneration has historically been a topic of much research and discussion due to the enormous impact any breakthrough would have on modern medicine (Okada, 1996). The term regeneration can be used to describe two related mechanisms, referring to either everyday renewal of worn-down tissue or the regrowth of entire limbs and organs (also known as epimorphic regeneration) (Stewart et al., 2007). While epimorphic regeneration is observed in non-mammalian vertebrates, mainly amphibians, this regeneration does not occur naturally in mammals following a traumatic injury. Unlike the peripheral nervous system, minimal neural regeneration is seen in mammalian central nervous systems. This lack of regrowth is due in part to supporting glial cells sealing off the injury site and releasing inhibitory secreting inhibitory extracellular matrix proteins that block regeneration of lost neural and spinal pathways.

Damaged tissue exhibit electrical fields generated from the post-injury disruption of endogenous ionic currents. These electric fields, which are linked to repair and regrowth of injury sites, are also observed during embryonic development – a similar permissive environment is required for proper growth and formation during both development and regeneration. Electric fields promote regrowth following an injury by changing and eliciting a range of cellular behaviors, including cell migration, proliferation, and differentiation. Of the many cell types affected by electric fields, glial astrocytes in particular are closely associated with central nervous system regeneration. Mature astrocytes are largely responsible for the post-injury inhibitory environment, adapting a reactive morphology with an altered cytoskeletal makeup, proliferating and migrating towards the site of injury, and finally releasing factors to sequester the damaged tissue (Kornyei et al., 2000).

Manipulating post-injury astrocytic responses that lead to this inhibitory environment may play a critical role in promoting mammalian central nervous system regeneration. A method that can be used to direct cellular behavior is the application of electric fields generated using a power supply and metal-ion electrodes. These external electric fields can mimic and enhance the endogenous electric fields which are essential for normal embryonic development and tissue regeneration in amphibians. Mammalian astrocytes, in conjunction with external electric fields that modify astrocytic behaviors, could be utilized to promote central nervous system regeneration (Alexander et al., 2006). However, the extent to which astrocytes adjust their behavior in response to specific electric field strengths has yet to be defined.

This study examines the application of electric fields to mammalian astrocyte cultures in order to document the range of elicited changes in astrocyte activities. Externally applied electric fields are hypothesized to elicit behavioral & intracellular changes resembling those seen in organisms capable of central nervous system regeneration. Since astrocytes play a key role in inhibiting mammalian central nervous system regeneration, electric fields can then be tailored to modify or induce specific cellular behaviors that promote post-injury regrowth. Once fully understood, applied electric fields could be utilized to create a viable post-injury therapy for mammalian regeneration, specifically to reestablish neural and spinal pathways damaged and regain functionality following a traumatic injury.

Overview of Astrocytes

Since their discovery in the 1800s, glial cells have been a major focus of study in neurobiology research (Somjen, 1988). During development, neural stem cells generate either neuronal precursor cells or glial precursor cells that differentiate into neurons or glial cells, respectively, as the cells begin to migrate (Morest & Silver, 2003). Some of the most prevalent glial precursor cells, as well

as their possible differentiated daughter cells, are presented in Figure 1.1. The glial cells found in the central nervous system are divided into two classes – macroglia (comprising of astrocytes, oligodendrocytes, and ependymal cells) & microglia. Among the macroglial cells, astrocytes are the most abundant cell type with the widest range of functions in the central nervous system. Astrocytes have a characteristic star-shape with a number of processes that overlap and integrate with synapses between neurons – the branching processes from one astrocyte are able to contact thousands of synapses, modulating numerous neurons at once (Sofroniew, 2009). Astrocytes also form intercellular gap junctions, creating a syncytium that uses calcium to communicate with neighboring cells and to initiate signaling pathways (Giaume & Venance, 1998). Astrocytes and their interactions with other components of the central nervous system are further discussed in Figure 1.2. Astrocytes also express numerous sodium and potassium channels that establish ionic currents; however, unlike neurons, these cells do not generate or propagate action potentials.

Up to 50% of the total volume of the brain is comprised of astrocytes, which are found throughout the entire central nervous system in a non-overlapping array (Montgomery, 1994). Each regional population expresses differing compositions of cytoskeletal and extracellular proteins, making them markedly different from each other (Batter et al., 1992). Cortical astrocytes play key roles in structural development and normal neuronal functioning of the central nervous system, while Bergmann glial cells play a similar role with Purkinje cells in the cerebellum (Xu et al., 2013). Pituicytes in the hypothalamus modulate neuroendocrine signaling and bodily homeostasis (Stern & Filosa, 2013). Subventricular zone astrocytes can behave as neural stem cells, promoting neurogenesis by generating a network of migrating neuroblasts through division (Doetsch et al., 1999). These different astrocyte regions are generated locally through symmetric divisions; the differentiated progeny cells then integrate into the neighboring astrocyte network (Ge et al., 2012).

Figure 1.1: Glial Precursor Cells
As neural stem cells differentiate and participate in neurodevelopment, these cells form intermediate neural or glial precursor cells. Due to the large volume and diversity of astrocytes in the central nervous system, a variety of progenitor cells can mature and generate astrocytes. Adapted from Liu & Rao, 2004.

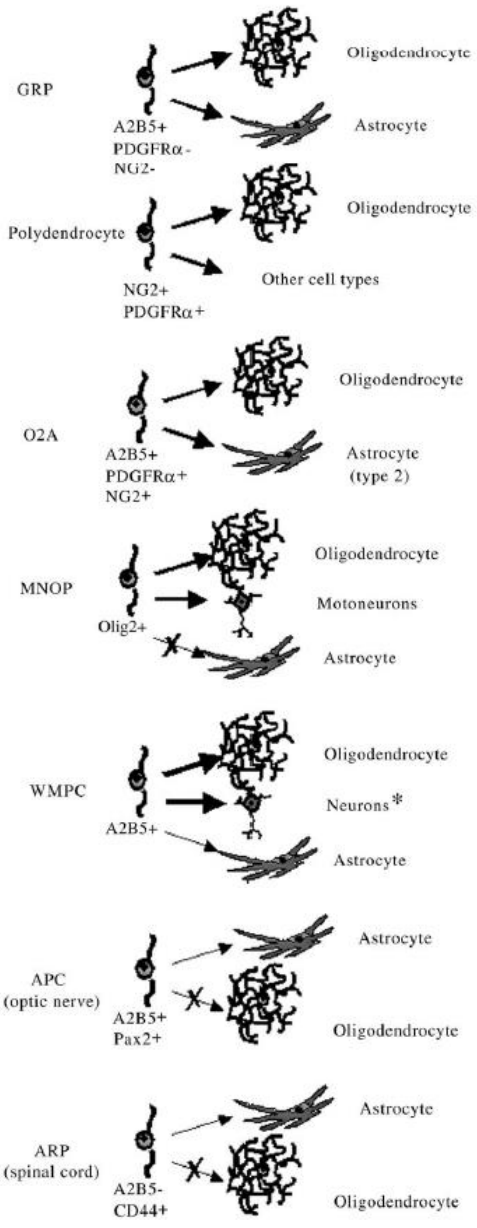
GRP
A2B5+
PDGFRα-
NG2-
Oligodendrocyte
Astrocyte
Polydendrocyte
NG2+
PDGFRα+
Oligodendrocyte
Other cell types
O2A
A2B5+
PDGFRα+
NG2+
Oligodendrocyte
Astrocyte
(type 2)
MNOP
Olig2+
Oligodendrocyte
Motoneurons
Astrocyte
WMPC
A2B5+
Oligodendrocyte
Neurons*
Astrocyte
APC
(optic nerve)
A2B5+
Pax2+
Astrocyte
Oligodendrocyte
ARP
(spinal cord)
A2B5-
CD44+
Astrocyte
Oligodendrocyte

Figure 1.2: Astrocyte Interactions within the Mammalian Central Nervous System
Astrocytes (shown in black) are up to ten times more numerous than neurons (seen in gray) in the mammalian central nervous system. Astrocyte processes form a network between the pia mater and ependyma, allowing a single astrocyte to contact and modulate multiple neurons. Astrocyte processes **(a)** surround synapses between a presynaptic terminal and postsynaptic terminal, creating a tripartite synapse that allows bidirectional contact between astrocytes and neurons. Astrocyte processes also **(b)** surround the intermodal regions of myelinated axons (M). Foot processes of astrocytes can **(c)** encompass blood vessels (BV), forming a tight barrier as well as structural support around the central nervous system. Adapted from Montgomery, 1994.

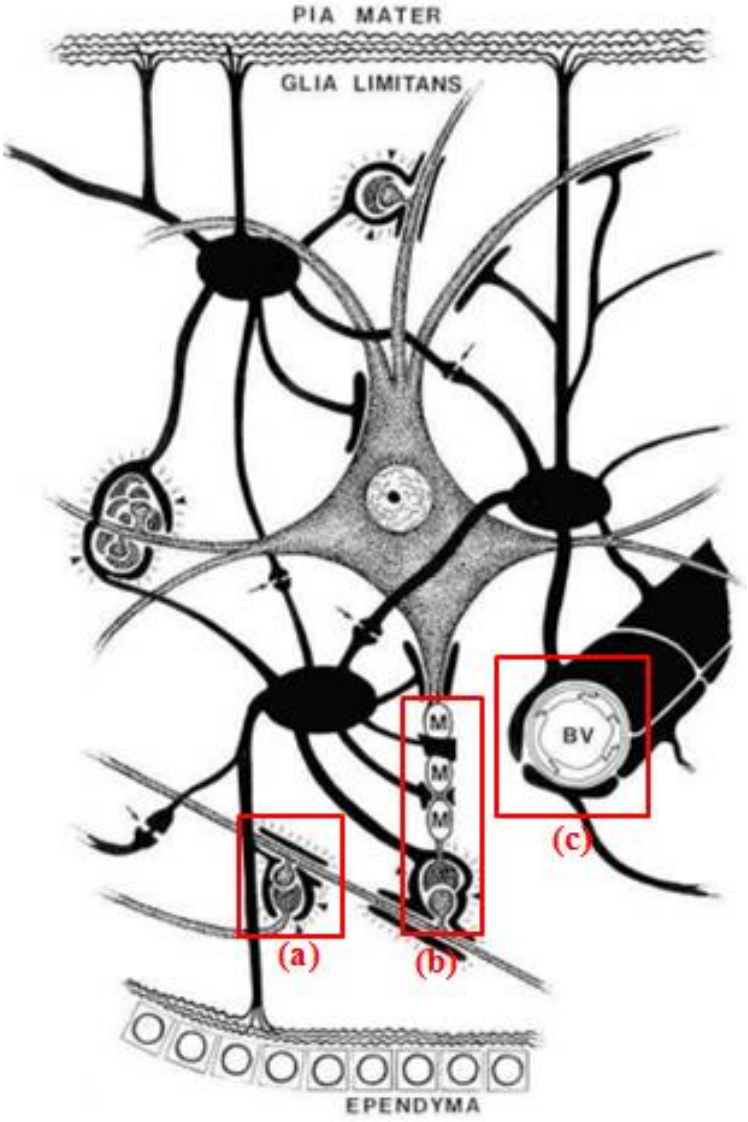
PIA MATER
GLIA LIMITANS
M
M
M
BV
(a)
(b)
(c)
EPENDYMA

Cortical astrocytes have generally been classified based on morphology – fibrous astrocytes with long, fiber-like processes are found in white matter, while larger protoplasmic astrocytes with short, branching processes are found in the gray matter. The human cerebral cortex also possesses interlaminar astrocytes, which extend processes through various cortical layers, and the uncommon polarized astrocytes (Nag, 2011). A more recent classification divides astrocytes into type I and type II that are analogous to protoplasmic astrocytes and fibrous astrocytes, respectively – these subdivisions are based on immunohistochemistry and progenitor cell lineage. Type I astrocytes stain positively for the antibody marking intermediate filament glial fibrillary acidic protein (GFAP) and negatively for the monoclonal antibody A2B5; type II astrocytes stain positively for both GFAP and A2B5 (Raff et al., 1983). Since both types of astrocytes are GFAP-positive, GFAP is considered the prevalent marker for mature astrocyte identification.

Unlike neurons, astrocytes retain the ability to resume proliferation and up-regulate cellular features seen in development (Buffo et al., 2008) – this shift to an earlier maturation state is referred to as dedifferentiation. Immature astrocytes express low levels of GFAP and instead express different proteins, such as the intermediate filaments vimentin and RC2 (a modified form of the intermediate filament nestin). The production of Olig2, a transcription factor seen in mature astrocytes that inhibits astrocyte differentiation, is down-regulated upon returning to an immature stage. In addition to the changes in cytoskeletal proteins and other intracellular markers, immature astrocytes also display a more elongated, bipolar morphology than the polygonal, star-shape associated with mature astrocytes (Sharif et al., 2007). This ability of astrocytes to dedifferentiate into an earlier maturation stage implies a certain level of plasticity in the central nervous system (Mao et al., 2009).

Astrocytes Functioning in Normal Environments

Astrocytes play a major role in the central nervous system, beginning with development and establishing proper neuronal structures and functions. During embryonic development, a subpopulation of astrocytes expressing both vimentin and glial fibrillary acidic protein (GFAP), referred to as radial glia, provide a scaffold for migrating neuroblasts. Once the neurons reach their final cortical location, these radial glia can either differentiate into mature astrocytes or become adult neural stem cells (Merkle et al., 2004). Astrocytes then express the appropriate extracellular matrix proteins, adhesion molecules, and receptors to stabilize neuronal structures and can release neurotrophic factors to promote neuronal survival. In addition, astrocytes are also capable of releasing gliotransmitters, allowing astrocytes in tripartite synapses to have an active role throughout synaptogenesis, synapse maturation, and synaptic pruning (Sofroniew & Vinters, 2010). Another crucial element of the central nervous system, the blood-brain barrier, requires tight junctions between astrocyte process endfeet to surround cerebral endothelial cells and control the substances entering the brain – astrocyte contacts between blood vessels and endothelial cells also regulate neuronal blood flow and promote angiogenesis (Abbott et al., 2006).

Astrocyte processes encompassing synapses can also regulate the synaptic fluid in the extracellular space between cells. Astrocytes contain the appropriate enzymes to allow neurotransmitter reuptake and recycling, ultimately regulating neural signaling. Another enzyme found in astrocytes is carbonic anhydrase, allowing pH regulation in conjunction with O_2 consumption and lactate production. Astrocytes also contain various ion channels – for example, spatial buffering of potassium ions through potassium channels regulates neuronal functioning. Additionally, astrocytes are capable of detoxification as well as phagocytosis, acting as antigen-presenting cells. The multiple roles astrocytes play in proper neurotransmission illustrate the importance of these particular glial cells in both the immature and mature central nervous system (Montgomery, 1994).

Astrocytes Functioning in Abnormal Environments

Beyond gliomas, astrocytes are believed to be involved in a number of other diseases, including neurodegenerative diseases (such as Alzheimer's disease, Parkinson's disease, & Huntington's disease), traumatic brain injuries, neurovascular disease, and epilepsy (Nag, 2011). In response to a brain or spinal cord injury, astrocytes demonstrate reactive astrogliosis – however, the extent of this response depends on the nature and severity of the injury. These reactive astrocytes are generally defined by their astrocytic swelling and astrocytic hypertrophy-hyperplasia, with characteristic increases in glial fibrillary acidic protein (GFAP) production. Astrocyte hypertrophy and hyperplasia lead to enlarged cell bodies, with increased levels of additional intermediate filaments vimentin and nestin, as well as increased proliferation and ultimately migration that is not limited to the area of injury (Montgomery, 1994).

While astrogliosis generally has a negative connotation associated with it, it can exert both deleterious & beneficial effects on the surrounding injured tissues. Initially post-injury, reactive astrocytes promote a pro-inflammatory response through a variety of mechanisms. Astrocytes produce and release cytokines & neurotoxic levels of various substances that compromise the blood-brain barrier, allowing foreign cells and substances to enter the nervous system. Astrocytes can also interact with microglia to elicit rapid local inflammation (Ridet et al., 1997). Over time, however, astrocytes begin to restrict the spread of infection and inflammation, especially at the border between damaged and healthy tissue. These reactive astrocytes are now promoting anti-inflammatory responses by uptaking and degrading neurotoxic substances, protecting from oxidative stress, and expediting blood-brain barrier repair.

In mild to moderate injuries, the astrocytes are capable of returning to a normal, healthy state. More severe, penetrating injuries, however, with vast tissue damage lead to the formation of long-lasting

glial scars. These glial scars provide a barrier, separating the injury site and subsequent inflammation from the remaining healthy tissue. During glial scar formation, a proportion of quiescent mature astrocytes re-enter the cell cycle and resume proliferation upon injury, generating reactive astrocytes. These newly proliferated cells then migrate towards the sites of injury and contribute to the glial scar, where the processes of these astrocytes overlap and are held together by tight junctions (Sofroniew, 2009). This tightly packed pattern of astrocyte processes, as well as the restructuring of astrocytic cellular components (mainly cytoskeletal proteins) creates a protective structural barrier that prevents post-injury neurite regeneration. Substances released from astrocytes, such as extracellular matrix protein chondroitin sulfate proteoglycans (CSPGs), make up the second part of this glial scar and create an additional biochemical barrier. The presence of these additional inhibitory substances around the injury site act to further inhibit neuronal regeneration and neurite regrowth (Fawcett et al., 1994). The varying levels of injury severity, along with the resulting reactive astrogliosis and potential for recovery, are presented in Figure 1.3.

Invasive injuries that are sufficiently damaging to generate permanent glial scars also disrupt the epithelial layer at the site of injury. The resultant shift in ion flow creates an outward electric current, and the moving charges generate an electric field (Altizer et al., 2001). These fields, known as injury potentials, are similar to the electric fields observed during embryonic development. The crucial presence of physiological electric fields in the central nervous system during both normal development and post-injury regeneration implies a major functional significance of electric fields in biological systems.

Electric Fields *In vivo*

Cells, the basic unit of living organisms, are filled with numerous positively and negatively charged ions separated from their extracellular environment by cell membranes. Electric potential (ψ)

Figure 1.3: Different Levels of Post-Injury Reactive Astrogliosis
Depending on the severity of the injury, the resulting reactive astrogliosis can have either a favorable or adverse effect on the damaged tissue. (a) Mild or moderate injuries cause astrocytes to hypertrophy while migrating to the site of injury, displaying an altered state with changed cellular components and altered cell behavior. As the damage from injuries lessens and eventually disappears, these astrocytes return to their natural state while an anti-inflammatory state is established. (b) More severe injuries, however, lead to the formation of a persisting glial scar around the damaged tissue. Astrocytes in these glial scars are no longer restricted to domains; overlap occurs between their processes as they release specific substances into the environment, creating a structural and biochemical barrier around the injury site. This glial scar inhibits neurite outgrowth and the potential for central nervous system regeneration. Seen in Sofroniew, 2009.

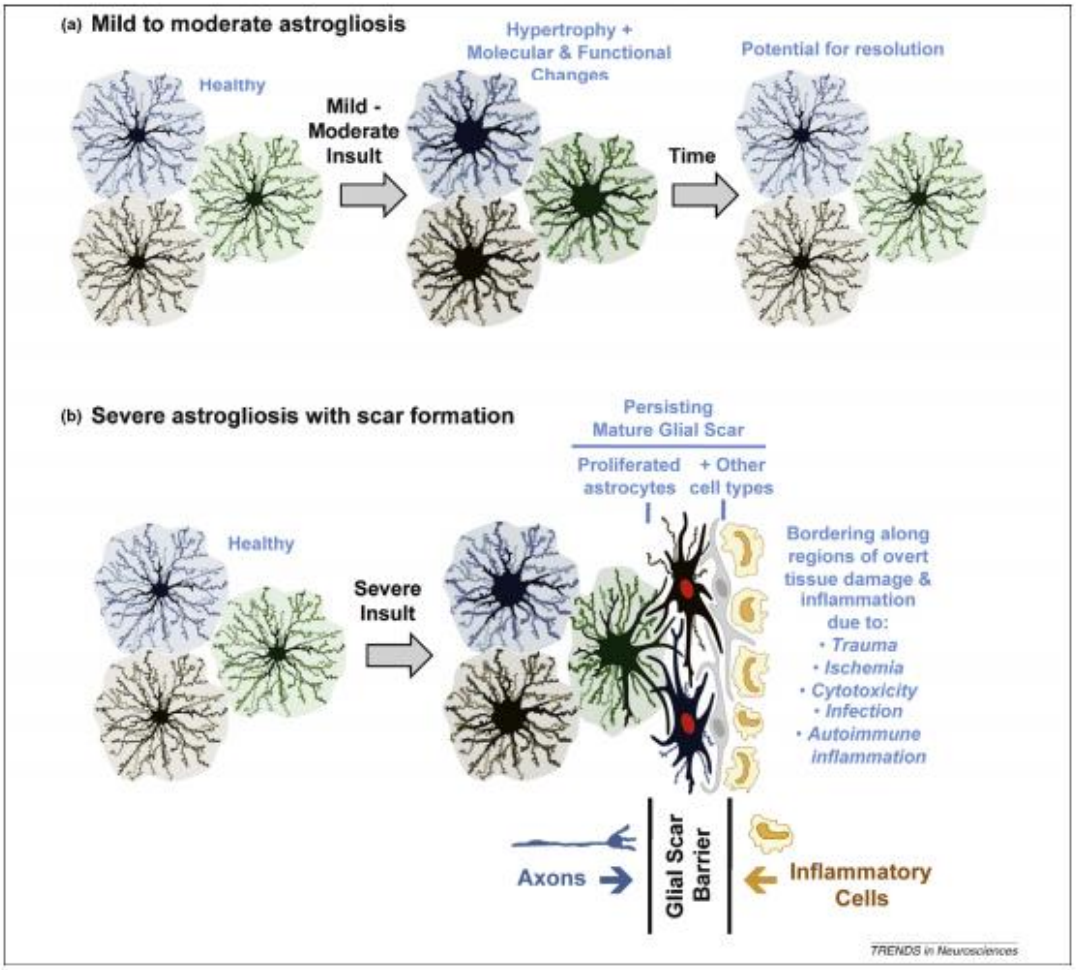
(a) Mild to moderate astrogliosis
Healthy
Mild - Moderate Insult
Hypertrophy + Molecular & Functional Changes
Time
Potential for resolution
(b) Severe astrogliosis with scar formation
Persisting Mature Glial Scar
Proliferated astrocytes
+ Other cell types
Healthy
Severe Insult
Bordering along regions of overt tissue damage & inflammation due to:
• Trauma
• Ischemia
• Cytotoxicity
• Infection
• Autoimmune inflammation
Axons
Glial Scar Barrier
Inflammatory Cells
TRENDS in Neurosciences

defines the electric potential energy that a single charge contains in either a static or dynamic state. Due to various attractive & repulsive forces present in the environment, the differences in electric potential across the system force charged particles to move through resistive areas. This net movement of electrons creates an electric current, which is conventionally defined as the flow of positive charges. The electric current is dependent on the resistance of the material through which the current is flowing and the electric potential difference across a distance, referred to as voltage. This relationship between voltage (V), current (I) and resistance (R) is summarized by Ohm's law, or V = I x R (Floyd, 2007).

The movement of charged particles through a system, in the form of electric current, creates an electric field. An electric field (E) is a vector field that exists around a charged particle and can be described by the formula $E = \frac{F}{q}$, where F is the force experienced by a charged particle within an electric field and q is the charge of the particle. The static electric field of a charged particle thus describes the magnitude and direction of the force per unit charge that is applied by other charged particles in its proximity (Colello & Alexander, 2003). The electric fields of moving charged particles can be described by electric field lines that depict the vector movement of each particle in the presence of attractive or repulsive forces – for example, electric field lines for a positively charged particles would point away from areas of positive charge and point towards areas of negative charge. This concept of electric fields and their representation by electric field lines is illustrated in Figure 1.4.

Electric fields have been found to exist naturally in biological systems. All cells are capable of transporting ions across their membranes through a variety of ion channels, creating an electric current from the movement of charged particles. The flow of ionic current in biological systems can create electric fields ranging in strength from 1 to 1000 $^{mV}/_{mm}$ (Nuccitelli, 1992). Normal developing

Figure 1.4: Electric Fields Generated in Electrical Circuits
(a) In a closed electrical circuit, negatively-charged electrons (e–) spontaneously flow from the negative terminal to the positive terminal of a battery. This leads to a loss of electrons (or oxidation) at the negative terminal and a gain of electrons (or reduction) at the positive terminal, creating a difference in electric potential. Since electric current is conventionally defined as the movement of positive charges, the current (I) is moving in the opposite direction of the electron flow, or from the positive terminal to the negative terminal of the battery. This movement of charges creates an electric field that describes the magnitude and direction a particular charge moves in response to neighboring attractive and repulsive forces. The electric field lines visualizing the electric field experienced by a positive charge in a circuit, therefore, point away from the positive terminal (due to repulsion) and towards the negative terminal (due to attraction). **(b)** The resistor in a circuit has a constant cross-sectional area, so each point in the resistor has the same electric resistance. As charged particles move through the resistor as an electric current, an electric field is generated – since the current experiences equal resistance throughout the resistor, each charged particle experiences the same electric field. The electric field lines passing through the resistor therefore are all constant in magnitude & direction and parallel to one another. In a cell culture chamber, the culture media can take the place of the resistor in the electric circuits. As the current passes through a constant cross-sectional area of culture media (with a constant resistivity), this generates similar equal, parallel electric fields lines. This demonstractes a constant generated electric field through the cell culture chamber that mimics those seen in an electric circuit.

(a)

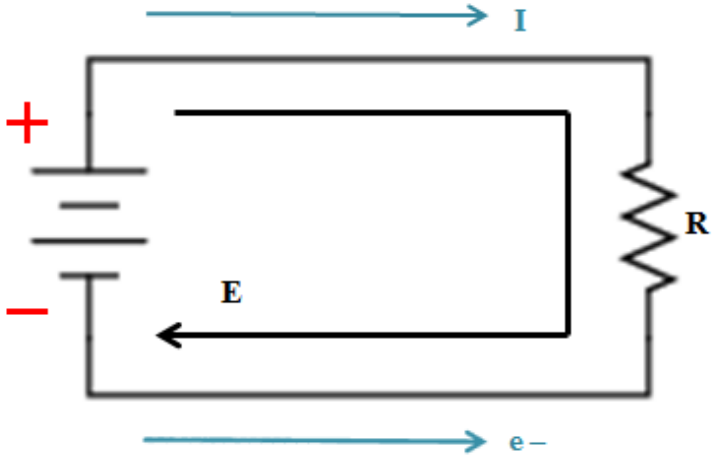

(b)

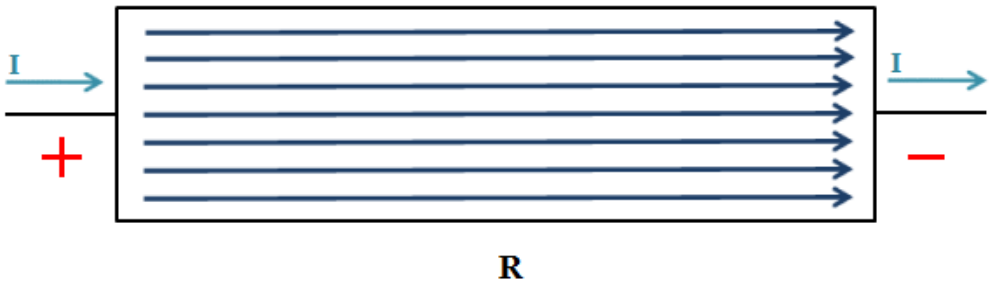

mammalian tissue exhibit electric fields ranging between 20 & 50 $^{mV}/_{mm}$ (Hotary & Robinson, 1994), while adult mammalian tissue exhibit electric fields between 1 & 5 $^{mV}/_{mm}$ (Cao et al., 2013). These physiological electric fields are three to four orders of magnitude smaller than the ones generated by action potentials seen in neurons (McCaig, 2005) and about 500 times smaller than the field strength required to contract skeletal muscle (Messerli & Graham, 2011).

In mammals, electric fields result from the movement of sodium ions beneath the epithelium. Cells in the epithelial layer have an outer apical surface and an inner basolateral surface and are connected by tight junctions. The apical surface of epithelial cells pumps in sodium ions from the space between the outer keratinized layer of mammalian skin and epithelial cells. The basolateral Na^+/K^+ ATPase simultaneously pumps sodium ions out of the epithelial cells. This leads to a net movement of sodium ions into the extracellular space beneath the epithelial cells. These cells are held together by tight junctions, which create a high resistance seal that prevents movement of soluble substances between cells. The tight junctions prevent sodium ion movement back through to the apical surface of the cells; this buildup of positive charge creates a potential difference across the epidermis (Lodish et al., 2008).

Upon injury, the epithelial layer is damaged, and the potential difference is no longer present. The positively charged sodium ions leak out at the injury site towards the apical surface of the epithelium, creating an outward electric current. This outward movement of ions draws in additional sodium ions from surrounding regions to the injury site. The movement of charged ions underneath the epidermis creates an electric field known as an injury potential (McCaig, 2005). The generation of these injury potentials following disruption of ionic currents is illustrated in Figure 1.5. The post-injury outward current in injured mammalian tissue is measured to be between 1 & 10 $^{\mu A}/_{cm^2}$, generating injury potentials between 40 and 200 $^{mV}/_{mm}$ (Barker et al., 1982). However, injured non-mammalian tissue from vertebrates capable of regeneration show a much more elevated outward

Figure 1.5: Generation of Injury Potentials in Mammals
(a) Apical Na^+ pumps and basolateral Na^+/K^+ ATPase pumps lead to a net movement of sodium ions beneath epithelial cells, and tight junctions prevents backflow of sodium ions. This causes a buildup of positively-charged sodium ions underneath mammalian epidermis. **(b)** Following an injury, the ruptured epidermis causes sodium ions to leak out at the site of injury and create an outward current. This creates a local decrease in sodium ions, pulling in more sodium ions from the environment surrounding the injury site. The arrows illustrate the post-injury movement of sodium ions and resultant electric field, known as the injury potential. This electric field, generated under the epidermis, follows the movement of charged ions and, as illustrated by the electric field lines, faces inward towards the site of injury. Adapted from Stewart et al., 2007 & Lodish et al., 2008.

(a)

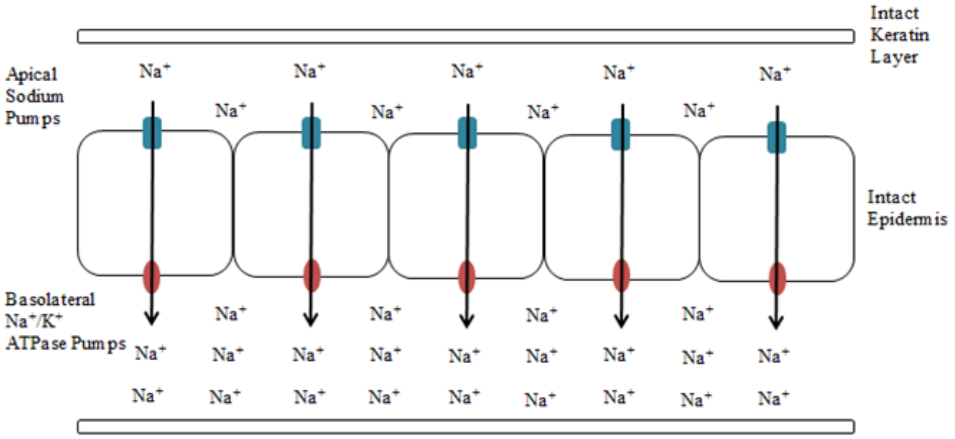
Intact
Keratin
Layer
Apical
Sodium
Pumps
Intact
Epidermis
Basolateral
Na+/K+
ATPase Pumps
Na+

(b)

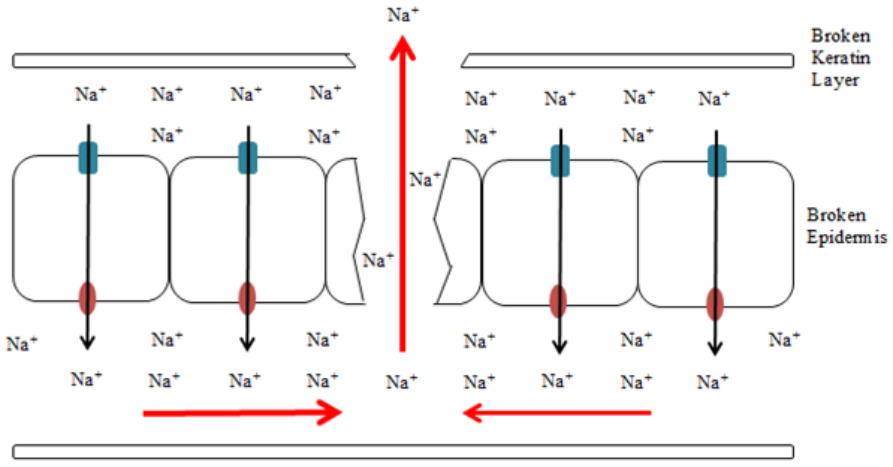
Broken
Keratin
Layer
Broken
Epidermis
Na+

current, between 10 & 100 $^{\mu A}/_{cm^2}$ depending on the location and type of damaged tissue (Borgens et al., 1977). This produces electric fields of much higher field strengths (200+ $^{mV}/_{mm}$) that are related to enhanced wound healing and subsequent regeneration observed in these animals.

Modifying the strength of these post-injury potentials changes the rate of wound healing, and removing the electric field altogether blocks any current restorative process. Pharmacological treatments of the drug furosemide, which blocks the sodium-potassium transport system, in a mammalian wounded cornea model reduced the strength of the current and resultant electric field. This leads to a decreased wound healing rate and increased post-injury recovery time when compared to control wounded corneas. On the other hand, the drug aminophylline, which stimulates ion transport, increases the electric field strength and led to an increased wound healing rate (Reid et al., 2005). These studies indicate that the magnitude of the endogenous injury potential is related to the rate of wound healing.

Regenerating limbs in newts and salamanders display a similar post-amputation outward current and electric field. Reducing this current using pharmacological methods, however, results in minimal or deficient limb regeneration when compared to control injured newts (Borgens et al., 1977). Other methods to reduce the endogenous electric field, such as grafting skin over the amputation site, lead to a similar deficit in limb regeneration (Altizer et al., 2002). Blocking these injury potentials completely arrests limb regeneration in amphibians (Jenkins et al., 1996). Additionally, enhancing the outward current at the site of amputation in frogs, which normally do not regenerate in their adult state, also enhanced regeneration (Borgens et al., 1977). Similar to studies done with mammalian corneal wound healing, these studies indicate that the magnitude of the post-amputation injury potential in amphibians is related to the regeneration rate, and removing the injury potential entirely following an amputation blocks any current regenerative process.

Interestingly, endogenous electric fields similar to injury potentials are also observed in various phases throughout normal development. An outward current appears before limb buds forms during vertebrate limb development and localizes as the limb bud grows (Altizer et al., 2001). The size, location, and timing of these electric fields can also influence cell behavior during central nervous system development. Physiological electric fields have been detected at the neural plate and neural folds, aligning the body axes for further cell division, migration, and differentiation (Yao et al., 2011); disrupting these endogenous electric fields can lead to neural and skeletal abnormalities (Hotary & Robinson, 1992). While different channels expressed only during development are involved in generating the electric fields seen in the developing brain (Davies et al., 1996), the resulting effects from altering embryonic electric fields confirm their crucial role in proper development.

Changing the magnitude of physiological electric fields clearly impacts activities critical for post-injury repair & regeneration as well as development. Since many of the same cell behaviors are observed during both development and regeneration, this suggests that electric fields may be a triggering cue for these behaviors.

Electric Fields *In vitro*

Electric fields similar to those seen in nature, particularly in development, wound healing, and regeneration, can also be generated externally and applied to a biological system. A constant direct current can be generated across a cell culture chamber using a power supply. Since charged particles move as a current through electric circuits, there must also be an electric field present. The created electric field can be described by the equation $E = \frac{\rho \times I}{A}$, where the strength of the electric field (E) is dependent on the resistivity of the culture media (ρ), the constant current (I), and the cross-sectional area of the cell culture (A) (Alexander et al., 2006).

The cell culture chamber resembles an electrolytic cell, where a nonspontaneous electrochemical reaction is forced by introducing a power supply through metal-ion electrodes. Electric current, or the flow of positive charge, moves from the positive end to the negative end of the battery. The flow of negatively-charged electrons is therefore in the opposite direction of the electric current. The anode is defined as the site of oxidation, or the loss of electrons, while the cathode is defined as the site of reduction, or the gain of electrons. Therefore, the electrons are being forced to move from the anode, giving it a positive charge, to the cathode, which gains a negative charge (Berman & Awayda, 2013). Figure 1.6 diagrams the flow of electrons from the positively charged anode to the negatively charged cathode.

In a cell culture chamber, the culture media acts as a resistor seen in traditional electric circuits. The current passes through the media in a constant cross-sectional area, ensuring a constant resistance; therefore, the electric field is constant in magnitude and direction at all points in the culture media. This electric field passing through the cell culture chamber can be illustrated by electric field lines; when passing through the culture media, or 'resistor', the electric field lines are all parallel to each other, again demonstrating a constant generated electric field through the cell culture chamber. Electric field lines passing through a resistor can be revisited in Figure 1.4.

Exposure to these external electric fields can elicit different cell behaviors, including galvanotaxis (directional cell movement towards charged ends in response to an electric current), altered cell migration rate, altered cell alignment, altered cell division rate & orientation, and altered cell morphology (Wang & Zhao, 2010). These behaviors occur with respect to the orientation of the generated electric field – cells often realign themselves perpendicular to the electric field lines.

Figure 1.6: Electrolytic Cell
Generating an electric current through an electrotactic chamber using electrodes and a power supply creates an electrolytic cell. The power supply creates an electric current; negatively-charged electrons move in the opposite direction, from the negative terminal of the battery to the positive terminal. This flow of electrons through an electrochemical reaction creates a positive and negative electrode. The anode is oxidized, or loses electrons; this means the less negative (or positive) electrode is the anode. The electrons from the anode move towards the cathode, leading to a gain of electrons, or reduction. Therefore, the more negative (or negative) electrode is the cathode.

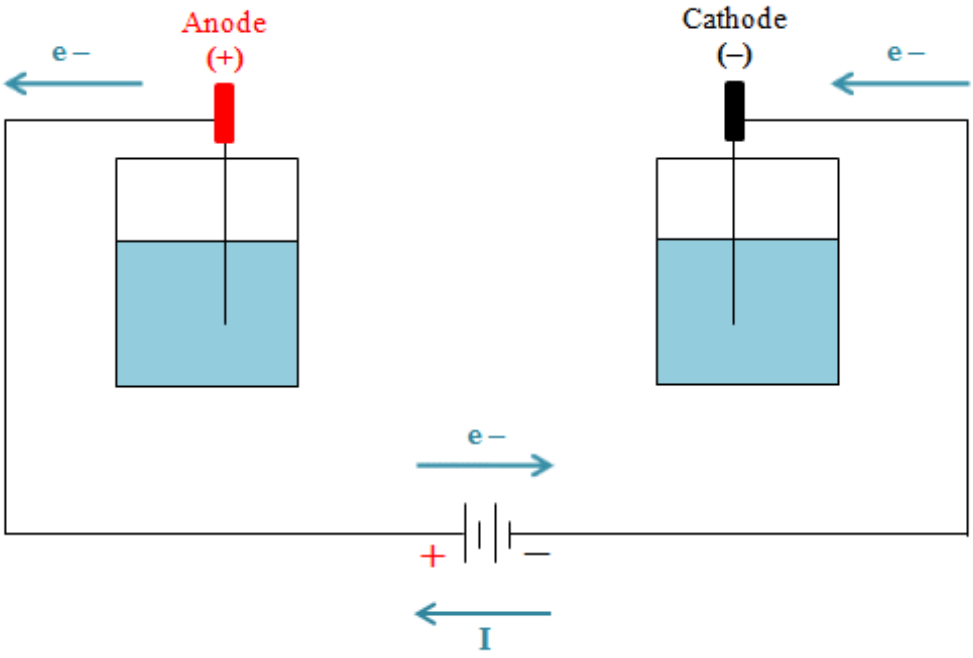
Anode
(+)
Cathode
(–)
e –
e –
e –
+
–
I

However, specific electric field-induced cellular behaviors depend on the magnitude of the electric field and the cell type. The effects of these applied electrical fields are also reversible once the field is disrupted, either by pharmacological methods or an applied electric field of opposite polarity (Messerli & Graham, 2011). Keratinocytes migrate when exposed to an applied electric field (Sheridan et al., 1996) while epithelial cells either migrate or reorient themselves in response to different electric field strengths (Zhao et al., 1997) – both of these responses are essential steps in initial wound healing. Taking advantage of the effects external electric fields have on keratinocytes and epithelial cells, applied electric fields have been used to enhance the healing of human skin wounds (Gentzknow, 1993). A more detailed list of electric field-induced cellular behaviors in a variety of cell types, adapted from Alexander et al., 2006, can be seen in Table 1.1.

Cell Type	Electric Field Strength ($^{mV}/_{mm}$)	Cell Behaviors	Reference
Epithelial Cells	150 25 – 250	Orientation of cell division Migration towards cathode	Zhao et al., 1999 Zhao et al., 1996
Keratinocytes	100 – 400	Migration towards cathode	Sheridan et al., 1996
Chondrocytes	80 – 1000	Migration towards cathode	Chao et al., 2000
Fibroblasts	1 – 400	Perpendicular elongation Migration towards cathode	Erickson & Nuccitelli, 1984
Muscle Cells			
Myoblasts	36 – 170	Perpendicular elongation	Hinkle et al., 1981
Cardiomyocytes	250 – 500	Cell differentiation	Sauer et al., 1999
Osteoblasts	100 – 1000	Migration towards cathode	Ferrier et al., 1986
Osteoclasts	100 – 1000	Migration towards anode	Ferrier et al., 1986
Endothelial Cells	150 – 400	Migration towards anode Perpendicular alignment	Bai et al., 2004
Leukocytes	150 – 200	Migration towards cathode	Lin et al., 2008
Neural Stem Cells	250	Migration towards cathode	Li et al., 2008
Neurons			
Neural Crest	7 – 390	Migration towards cathode	Gruler & Nuccitelli, 1991
Dorsal Root Ganglion	7 – 140	Growth towards cathode	Jaffe & Poo, 1979
Hippocampal	28 – 219	Orientation of growth	Rajnicek et al., 1992
PC12 Cells	1 – 5	Growth towards anode	Cork et al., 1994
Astrocytes	0.03 50 – 500	Enhanced glycolysis rate Perpendicular alignment	Huang et al., 1997 Borgens et al., 1994
Schwann Cells	3 – 100	Migration towards anode	McKasson et al., 2008

Table 1.1: Electric Field-Induced Cell Behaviors

Astrocytes are among the cell types affected by electric fields, displaying different cell behaviors in response to different field strengths. Due to their role in creating an inhibitory, non-permissive environment, astrocytes are a major focus in central nervous system regeneration in mammals. An applied low voltage electric field of 0.03 $^{mV}/_{mm}$ enhances the rate of glycolysis in astrocytes (Huang et al., 1997). However, higher electric fields, in the range of 50 to 500 $^{mV}/_{mm}$, cause astrocytes to reorient their processes and align themselves perpendicularly to the direction of the electric field vector (Borgens et al., 1994). Since astrocytes play a prominent role in normal development and regeneration, these *in vitro* electric fields can be used to modify astrocyte behavior in order to eliminate inhibitory effects in the central nervous system while promoting post-injury repair and regrowth.

Astrocytes in Epimorphic Regeneration

Following an injury, several non-mammalian vertebrates can completely regenerate damaged tissue, including entire limbs (Brockes, 1997) and major organs such as the heart (Poss et al., 2002). Mammalian epimorphic regeneration, however, is confined to a few organs such as the liver, skin, and skeletal muscle (Singh et al., 2010). This capacity for regeneration is inversely related to an organism's complexity – following limb amputation, amphibians can fully regenerate the missing limb, while higher vertebrates, such as mice, are incapable of regenerating the limb (Masaki & Ide, 2007). The close phylogenetic relationship between lower vertebrates and mammals, presented in Figure 1.7, however, suggests that mammals may possess a similar regenerative potential that could be elicited under the right conditions. African spiny mice can regenerate skin, hair, and cartilage following the loss of ear tissue (Seifert et al., 2012), and humans are capable of growing back amputated fingertips (Illingworth & Barker, 1980). These findings suggest that mammals may have

Figure 1.7: Phylogenetic Tree of Vertebrate Lineages
Humans & other mammals have a close evolutionary history with amphibians, vertebrates that have demonstrated post-injury or post-amputation epimorphic regeneration. This implies that mammals may retain the capacity for regeneration of limbs, organs, and entire body systems and that it may be possible to induce regeneration in animals that do not normally regenerate. Adapted from Meyer & Zardoya, 2003.

Phylum **Chordata**
Subphylum **Vertebrata**

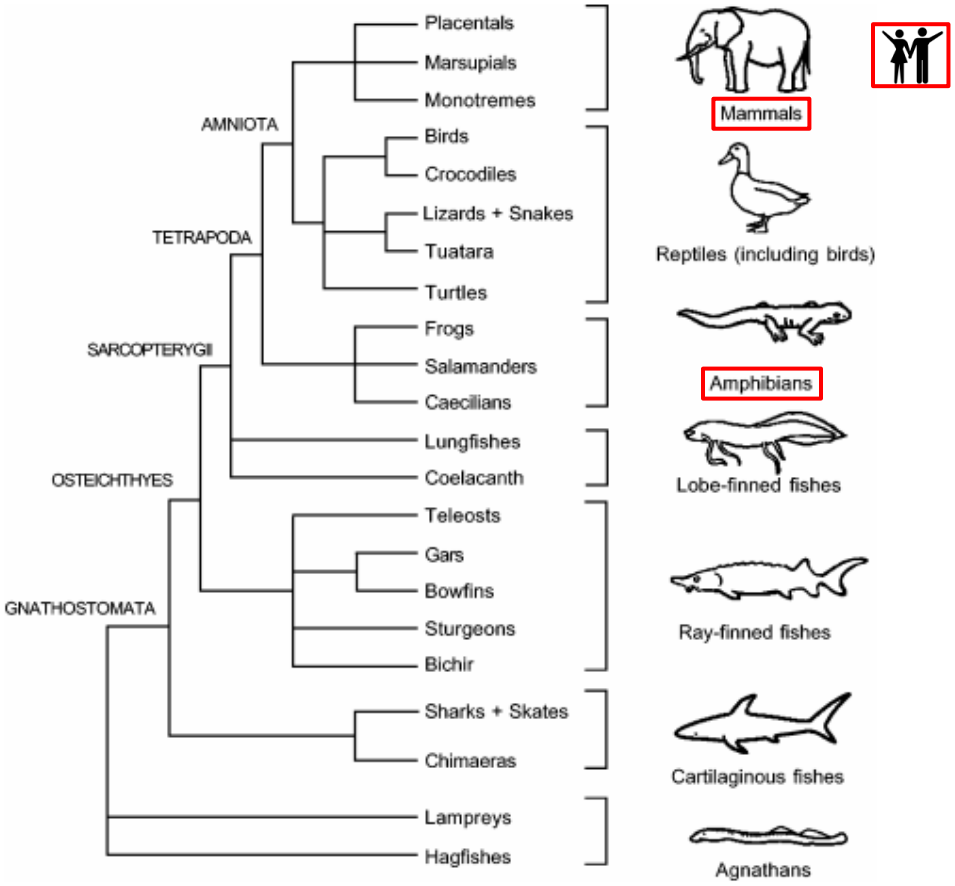

a higher capacity for tissue regeneration than previously seen, and the optimal stimulus could further expand this regenerative capacity.

When looking at unforced central nervous system regeneration *in vivo*, animals display a range in their regenerative capacity. Tailed amphibians (including newts & salamanders) are capable of regenerating the spinal cord following amputation of the tail, as well as regeneration of parts of the telencephalon (Iten & Bryant, 1976). Tailless amphibians (such as frogs), however, only have the ability to regenerate neural structures, spinal structures, and tails post-amputation early on as tadpoles; this regenerative ability is lost as they mature into adults (Reid et al., 2009). Among mammals, marsupial opossums can regenerate the spinal cord for a few days postnatal. This regenerative capacity decreases and is eventually lost as opossums continue to develop and grow (Terman et al., 2000).

Upon injury or amputation, the wounded epithelium releases a variety of growth factors and cytokines in addition to creating an injury potential. The injury potentials play a crucial role in controlling wound healing (Song et al., 2004) and epimorphic regeneration – blocking these electric fields arrests amphibian limb regeneration completely (Jenkins et al., 1996). Successful tissue regeneration following wound healing requires cellular migration, proliferation, dedifferentiation and/or redifferentiation, and finally functional integration at the injury site (Bonfanti & Peretto, 2011). In vertebrates capable of central nervous system regeneration, one of the early events seen is the movement of glial cells into the damaged tissue. These areas then show high levels of cell division, which correspond to reparation and elongation of the regenerating region (Walder et al., 2003). This greatly contrasts with non-regenerating mammalian glial cells, where proliferating astrocytes release cytokines and chemokines to recruit other cell types, ultimately creating a tightly packed pattern of processes that form the glial scar, as well as secreting extracellular substances to seal off the wound.

Once in the damaged region, markers of early development can be seen in these cells, indicating cellular dedifferentiation in response to the injury. Some of these markers include the intermediate filament vimentin and nestin, a neural precursor cell marker. The presence of these markers suggests that these dedifferentiated cells have neural precursor potential. In addition to vimentin and nestin, an increase in the astrocyte-specific intermediate filament GFAP is also seen. However this increase is temporary – the GFAP levels are down-regulated following asymmetric division of the neural precursor cells (Dawley et al., 2012). Therefore, the highest levels of GFAP are seen in the non-damaged areas of the central nervous system that are not responding to injury as well as the newly formed, undifferentiated region being regenerated. These GFAP-expressing cells are a distinct subpopulation of astrocytes that have no clear differentiated state and ultimately behave as neural precursor cells (Doetsch, 2003).

Interestingly, these dedifferentiated cells resemble radial glia, bipolar-shaped cells seen during proper neurodevelopment, which maintain contact with the pial membrane. This connection is lost in vertebrates lacking the ability to regenerate the central nervous system, leading to a loss of these radial glia-like cells (Walder et al., 2003). Astrocytes in particular shift from a flat, polygonal morphology with distinct extensions of cytoplasm, or lamellipodia (Rodnight & Gottfried, 2013), to a bipolar morphology similar to radial glial cells. This intracellular rearrangement includes elongation of the nucleus, retraction of the cytoplasm, and extension of two processes in opposite directions (Sharif et al., 2007).

Once fully understood, applied electric fields could also be used to direct axonal regeneration for mammalian nervous system repair and regrowth. During neuronal development, neurons extend neurites (future axons & dendrites) to reach their appropriate target; as development continues, the environment becomes less permissive to neurite outgrowth. This active inhibition, which keeps the

central nervous system from repairing itself, is believed to be caused in part by astrocytes, as well as other glial cells (Fawcett et al, 1994). Following a traumatic injury that leads to the formation of a glial scar, astrocytes release extracellular substances that further enhance this inhibitory environment. Reducing this inhibition promotes neural regeneration – for example, using chondroitinase ABC to break down the inhibitory molecule CSPG, in conjunction with astrocytes, permits regeneration at the site of injury (Filous et al., 2010).

The crucial step in central nervous system regeneration is reestablishing the neural and spinal connections lost post-injury, where the key requirements are having an adequate number of neuronal & glial precursor cells and the ability for growing axons to successfully innervate the target destination (Ferretti et al., 2003). Directed axon outgrowth is required to ensure that the growing neurons reach their intended target, allowing these pathways to reform properly. Growing neurites can be directed by diffusible released factors (chemotropism) or by applied electric fields (galvanotropism) (Purves & Lichtman, 1985). The direction and rate of neurite outgrowth can be controlled using these external electric fields (Patel & Poo, 1982) – this growth occurs due the dynamic movements of actin & microtubules at growth cones in the tip of neurites. Astrocytes can further guide neurite outgrowth by providing a structural foundation for neurites to grow along upon electric field application, ensuring they reach the proper destination (Prochiantz, 1985). This is achieved by generating specific cell-adhesive guidance cues for correct neurite outgrowth along astrocyte processes, allowing regenerating axons to circumvent the inhibitory regions preventing outgrowth (Neugebauer et al., 1988). Introducing an electric field of physiological strength (500 $^{mV}/_{mm}$) further enhances this directed neurite outgrowth towards its appropriate final target (Alexander et al., 2006). Astrocytes are capable of playing an active role in central nervous system regeneration, and external electric fields of varying strengths may promote other astrocytic behaviors favorable to central nervous system regeneration once fully investigated.

Astrocytes and applied electric fields have been shown to positively influence central nervous system regeneration in mammals, both individually and in conjunction with each other. Collecting further information regarding astrocyte behaviors seen at specific electric field strengths would help tailor treatments & therapeutic options to regulate the rate and extent of regeneration seen post-injury. Applied electric fields could then be used, possibly in the form of an implant, as a method to promote reestablishment of lost neural & spinal pathways in patients with traumatic brain or spinal cord injuries.

CHAPTER 2 Materials & Methods

Astrocyte Cell Cultures

ScienCell cerebellar rat astrocytes (RA-c), harvested and cryopreserved from a 8-day old rat cerebellum, were cultured using ScienCell Astrocyte Medium-animal (AM-a). The astrocyte media consists of basal medium with 2% fetal bovine serum (FBS), 1% astrocyte growth supplement-animal (AGS-a), 1% penicillin/streptomycin (P/S), and phenolsulfonphthalein (phenol red) as a visual pH indicator. Frozen astrocytes (1×10^6 cells) were then thawed in a 37^OC water bath; when completely thawed, the 1 mL vial was sterilized with 70% ethanol and transferred into a sterile environment. The cells were then re-suspended with 15 mL of astrocyte medium in a poly-L-lysine-coated T-75 flask (that was previously treated with 15 µL ScienCell poly-L-lysine (10 mg/mL) & 10 mL sterile deionized water for an hour at 37^OC, then washed twice with deionized water). The culture was placed in a 37^OC, 5.0% CO_2 incubator and subsequently monitored daily. The growth medium was changed the next day to eliminate residual freezing medium and unattached cells; the astrocyte medium was then changed every two to three days afterwards depending on the confluency of the cells attached to the bottom of the flask and the color of the media (indicating the pH of the cell culture).

When cells had reached approximately 90+% confluency within the T-75 flask, the cells were prepared for subcultures using Hank's Balanced Salt Solution (HBSS) & 0.25% Trypsin/EDTA (T/E) solution. Upon removal of the astrocyte media from the flask, warmed (37^OC) 8 mL HBSS and 2 mL T/E were added and the flask was transferred to the 37^OC incubator for two minutes. At

the end of this time, the flask was gently tapped so that the astrocytes detached from the bottom of the flask and appeared as sheets under a microscope. The HBSS/trypsin containing the newly detached cells was removed and added to a 50mL centrifuge tube containing 5mL fetal bovine serum (FBS) to deactivate the enzyme trypsin. The T-75 flask was placed back into the incubator for an additional two minutes, then rinsed twice, 5mL each, with warmed trypsin neutralization solution (TNS) (10% FBS in HBSS) to harvest additional cells still plated onto the flask. A pipette was used to break up any cell clumps; the astrocytes were then spun down in a centrifuge at 1000 RPM for five minutes. The resulting supernatant was then discarded and the remaining cell pellet was re-suspended with 1 mL warmed astrocyte medium.

A hemacytometer was then used to count the number of astrocytes present. 10 µL of the re-suspended cells was transferred into the chamber with a coverslip in place to create a specified volume; capillary action pulls the media to completely fill the chamber and cover the gridded surface. Each of the 25 squares in the 5×5 grid has an area of 0.04 mm^2; while the coverslip creates a depth of 0.1 mm for the media; therefore, the entire 5×5 grid represents a volume of 0.1 mm^3. Using the conversion 1 cm^3 = 1 mL, the astrocyte concentration per mL can be approximated as [the average number of cells counted in the 5×5 grid × 10^4]. This cell concentration can then be used to approximate the total number of cells present – the cells were then split accordingly into either poly-L-lysine coated T-75 flasks for future culturing or fibronectin-treated Petri dishes for electrotactic chambers.

Electrotactic Chamber Setup

Electric fields are present *in vivo* during development as well as regeneration, where fields are generated in response to damaged tissue. Electrotactic chambers can be used to create electric fields of equivalent field strengths *in vitro* that can influence cell behaviors such as directional cell

movement (galvanotaxis), proliferation, and changes in cellular morphology & composition. The electrotactic chambers are built to control a direct current passing through a cell culture with a constant cross-sectional area, providing an equal electric field at all points in the culture. These electrotactic chambers were created on WillCo 50 mm polystyrene Petri dishes, with a 40 mm diameter, #1.5 thickness glass bottom.

Invitrogen bovine plasma fibronectin (1 µL/mL) was pre-coated onto a confined area of the Petri dish to enhance astrocyte attachment to the bottom of the fish. After 30 minutes, the fibronectin was removed and the area was washed twice with sterile deionized water. Astrocytes, which at this point have been trypsinized and are ready to be subcultured, were plated onto the dish along with plating media consisting of warmed astrocyte media & 0.5% Invitrogen G5 supplement (used to induce astrocyte stellation). The hemacytometer was used to plate a seeding density of approximately 1×10^4 astrocytes onto the fibronectin-coated area of each Petri dish to achieve approximately 50% confluency per dish. These newly subcultured Petri dishes were then placed in the 37^{O}C, 5.0% CO_2 incubator overnight (minimum 12 hours) to allow cells to attach to the Petri dish surface. Once inoculated, the cell-plated Petri dishes can be incubated for up to a week with daily monitoring.

Once astrocytes were plated onto the Petri dish and ready for application of electric fields to cell subcultures, the electrotactic chamber was constructed. One Fisherbrand 22×22 mm #1.5 thickness coverslip was cut in half using a diamond-tip pen and then sterilized. The two coverslip strips were then adhered to the glass bottom Petri dish using Dow Corning DC4 high vacuum grease, which is non-toxic to cell cultures. The two strips were placed parallel to each other, leaving a constant distance between the two pieces where the astrocyte culture was present and plated onto the Petri dish. This distance between the 'base' coverslip strips is one of the components to determining the strength of the electric field being generated. The plating media was then replaced with 5mL warmed astrocyte media (without the G5 supplement). A second sterile 22×22 mm coverslip was

glued onto the halved cover glasses with DC4 vacuum grease; this 'roof' covered the subcultured cells and created a chamber with a constant cross-sectional area, seen in Figure 2.1.

Scotch double-sided mounting tape, cut lengthwise into strips, was placed along the two edges of the top coverslip, running from one wall of the Petri dish to the other. These tape strips were perpendicular to the gap created by the base cover slips, where the astrocyte culture is plated onto the dish. The tape formed a barrier on each side of the top cover slip, establishing two wells on opposite sides of the Petri dish that could be filled with astrocyte medium. These wells connected the astrocyte-coated area between the surface of the Petri dish and the top cover slip, creating the electrotactic chamber and providing a continuous system for electric current flow. The four corners where the double-sided tape reached the Petri dish wall were sealed with DC4 vacuum grease to ensure water-tight barriers and avoid leakage of cell media. The two wells were then each filled with 1mL warmed astrocyte media; therefore, the Petri dish contained a total of 2.5 mL astrocyte media. The complete electrotactic chamber is shown in Figure 2.1.

Electric Field Application

The electric field was introduced to the electrotactic chamber via a connected system created from salt bridges, Steinberg's solution, and silver electrodes in a sterile environment. The resultant cell behaviors were then monitored using time-lapse microscopy. Salt bridge molds were made using a Bunsen burner to melt plastic pipettes into an U-shape and then sawed down, ensuring a constant cross-sectional area. The salt bridge molds were further configured to fit around the microscope apparatus, as seen in Figure 2.2.

Per electrotactic chamber, two salt bridges were filled with agarose. 2% Bioline multi-purpose agar powder was dissolved in astrocyte media and heated up to 60^{O}C – once the agar-media began to

Figure 2.1: Electrotactic Chamber Setup with Astrocyte Subculture
(a) This diagram shows the basic setup of the astrocyte subculture on Petri dish. The cells are coated down at the desired seeding density onto the fibronectin pre-coated bottom of the dish. 22X22 coverslips are used to fashion a 'base' and a 'roof' around the cell subculture. **(b) – (c)** The 'base' and 'roof' coverslips are seen from the side, illustrating the cross-sectional area created for the cell culture and accompanying culture medium. This constant cross-sectional area (A) is created by ensuring an equidistance between the 'base' coverslip pieces (d) and using coverslips with a constant thickness (h). **(d)** Tape and DC4 vacuum grease are used to create distinct media-filled wells on opposite sides of the Petri dish. This provides a continuous source of media to the cell subculture underneath the 'roof' coverslip.

(a)

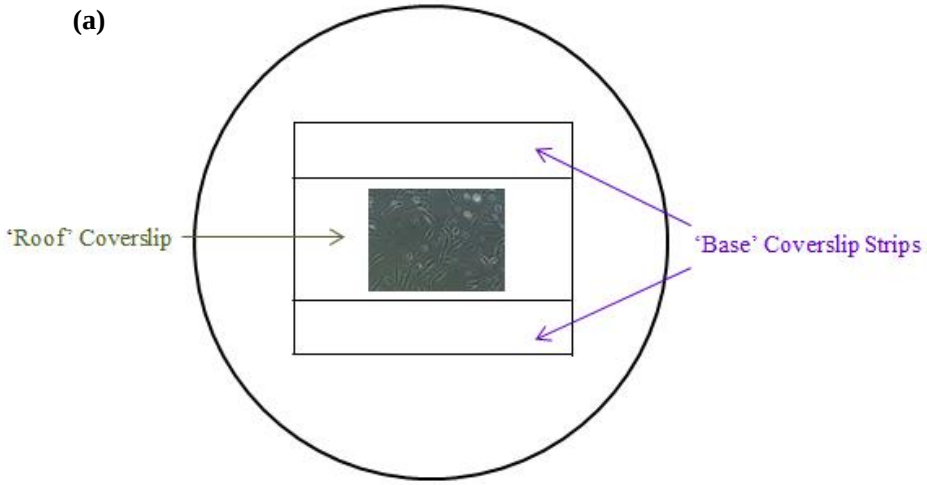
'Roof' Coverslip
'Base' Coverslip Strips

(b)

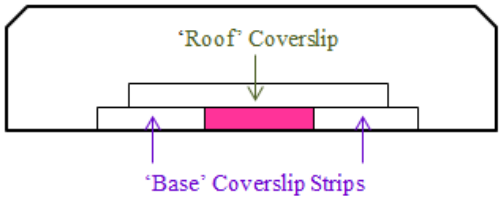
'Roof' Coverslip
'Base' Coverslip Strips

(c)

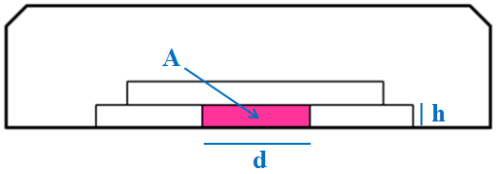
A
h
d

(d)

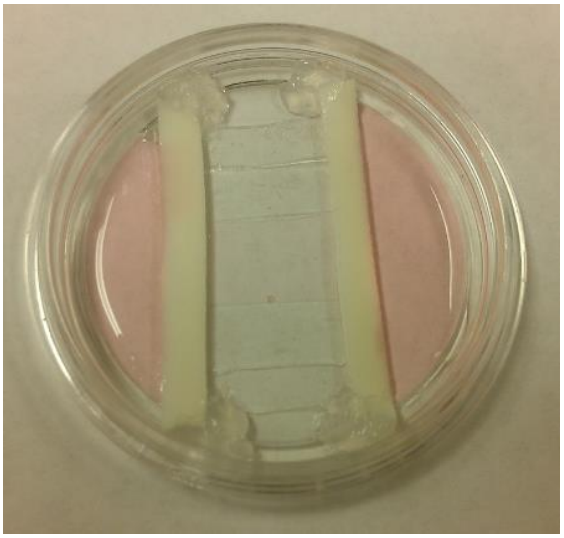

Figure 2.2: Application of an Electric Field to an Electrotactic Chamber
(a) The power supply generates a current running from the positive electrode to the negative electrode. These electrodes sit in electrolytic Steinberg's solution, which are connected to the cell culture through 2% agarose salt bridges. The astrocyte subculture is plated onto an area of known dimensions, which is created using side 'base' coverslips and a top 'roof' coverslip, and is filled with culture media to create a constant cross-sectional area. The two wells on opposite sides of the electrotactic chamber are also filled with culture media to create a continuous path for electric current flow. **(b)** The electrotactic chamber setup is placed in an incubated stage inside a Zeiss Spinning Disk Confocal microscope. The agarose salt bridge molds are shaped around the microscope apparatus to maximize the path of the current, preventing electrode byproducts from entering the cell culture. The Steinberg's solution was placed in small, covered vials with holes drilled in to allow the salt bridges and electrodes to sit snugly. These vials were then placed in small trays, selected to fit the space around the microscope, to prevent any accidental solution leakage.

(a)

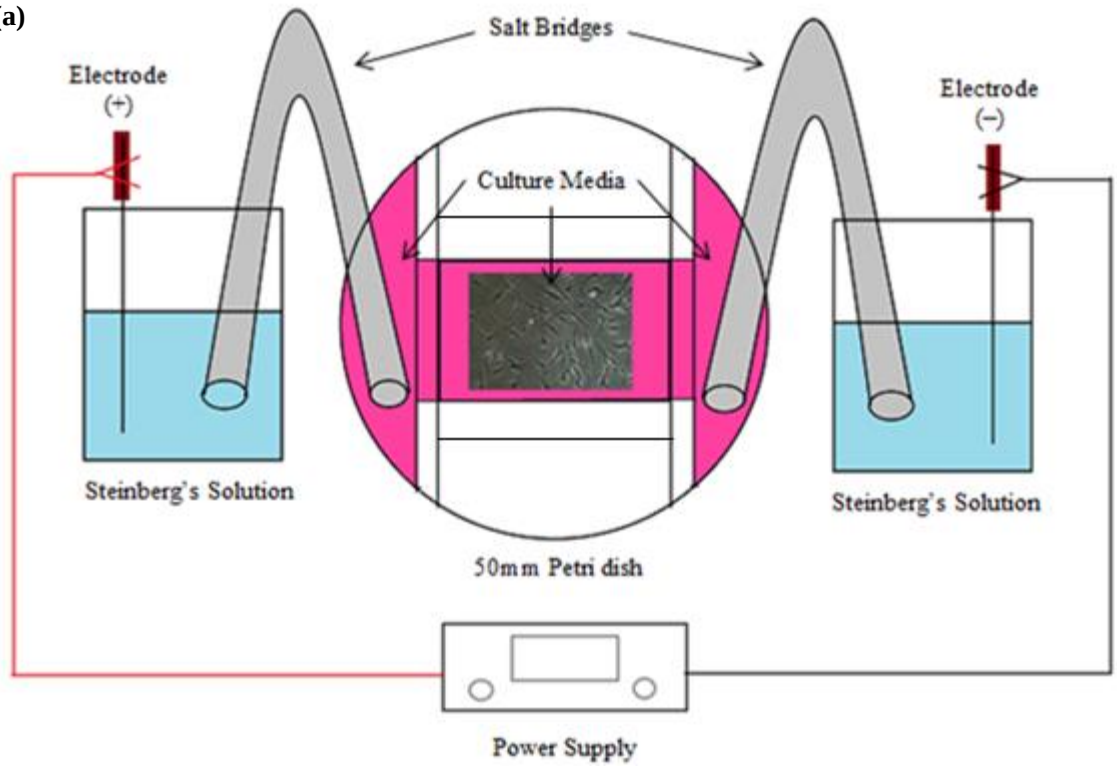
Salt Bridges
Electrode
(+)
Electrode
(–)
Culture Media
Steinberg's Solution
Steinberg's Solution
50mm Petri dish
Power Supply

(b)


NA 0.55
WD 26 mm

boil, the agar was carefully injected into the salt bridge using a 3cc syringe to avoid introducing air bubbles. After cooling, the salt bridges were sterilized for use with the electrotactic chamber. One end of the U-shaped filled salt bridge was placed in the astrocyte media in one of the wells of the electrotactic chambers; two separate salt bridges were used for each media-filled well in the Petri dish. However, in order for the salt bridges to reach the media, the Petri dish lid needed to be modified. A soldering iron was used to melt two small holes corresponding with the astrocyte medium wells at the ends of the dish into the polystyrene Petri dish lid. The holes for the salt bridges fit snugly around the salt bridges so that they could make contact with the wells containing astrocyte media in order to apply an electric field. A rectangle was cut out from the middle of the Petri dish lid and replaced by a #1.5 thickness coverslip attached with DC4 vacuum grease on the sides – this coverslip enhanced the time-lapse imaging. This Petri dish lid was sterilized and reused in later experiments. The modified Petri dish lid can be seen in Figure 2.2.

With one end of the agar-filled salt bridge in the electrotactic chamber astrocyte media well, held firmly in place by the Petri dish lid, the other end of the salt bridge was placed in a beaker filled with an electrolyte solution to enhance electric current flow. Since there were two salt bridges exiting the electrotactic chamber, one on each side of the Petri dish, there were two beakers filled with solution for each salt bridge. The particular electrolyte solution used was Steinberg's solution (60 mM NaCl, 0.7 mM KCl, 0.8 mM MgSO4•7H2O, 0.3 mM CaNO3•4H2O, and 1.4 mM Tris). Each of these beakers also contained an A-M Systems .015" diameter Ag/AgCl electrode – these electrodes were placed in an external salt solution rather than directly into the astrocyte media to avoid toxic buildup from the electrodes entering the cell culture in the electrotactic chamber. The Ag/AgCl electrodes were linked to a Bio-Rad PowerPac direct current power supply via wires and alligator clips. The PowerPac power supply provided a steady electric current that passed through the cathode, moving in through one salt bridge, entering the cell subculture and exiting out of the other salt bridge, finishing the current loop by passing through the anode and back to the PowerPac.

The overall setup of the complete electrotactic chamber, diagrammed in Figure 2.2, was adapted from Song et al., 2007.

Since the cell subculture in the electrotactic chamber had a constant cross-sectional area, the generated electric field was constant throughout the astrocytes. The electric field strength produced and applied to a cell culture can be calculated using the following equation (Alexander et al., 2006):

$$E = \frac{I \times \rho}{A} = \frac{I \times \rho}{d \times h}$$

(I) represents the electric current produced by the PowerPac power supply that is introduced to the cell culture via a connected system of electrodes and salt bridges. The current generated by the power supply can be manipulated by using an adjustable resistor in parallel with the electrotactic chamber setup. This ensures that the desired current, and resultant electric field (E), was applied on the cell subculture.

The resistivity of the astrocyte media (ρ) has been measured using an ammeter to be 700 Ω·mm – this value is constant since the same media was used per experiment. (A) represents the cross-sectional area of the astrocyte culture, created in the electrotactic chamber by coverslips and DC4 vacuum grease (Figure 2.1). This area can also be written as the distance between the two coverslip strips where the cells are subcultured onto the Petri dish (distance, or d) times the height of the coverslip representing the depth of subcultured area (height, or h). The thickness of multiple #1.5 thickness coverslips were measured using a micrometer to produce an average thickness of 0.175 mm – since the same #1.5 thickness coverslips were used in the electrotactic chamber, the average coverslip thickness remained constant. The creation of varying electric field strengths using different electric currents (I) and distance between coverslips, as mentioned earlier, can be seen in Table 2.1; these specific electric field strengths were chosen to mimic the range of electric field strengths seen in injured mammals and injured, regenerating non-mammals.

E ($^{mV}/_{mm}$)	I (mA)	ρ (Ω·mm)	d (mm)	h (mm)
400	1	700	10	0.175
100	0.2	700	8	0.175
40	0.1	700	10	0.175
10	0.02	700	8	0.175
4	0.01	700	10	0.175
0	0	700	10	0.175

Table 2.1: Generating Different Electric Field Strengths

Time-Lapse Recording

The electrotactic chamber (with the astrocyte culture, proper coverslips, tape-barriers, and astrocyte media), salt bridges, electrodes, and power supply were arranged around a Zeiss Spinning Disk Confocal microscope with an incubated (37^{O}C, 5.0% CO_2) stage and time-lapse recording capability seen in Figure 2.2. This inverted microscope with DIC live imaging capability was used to take images of randomly selected regions of interest (ROI) within the astrocyte culture every three minutes for 12 hours. This allowed for controlled observation of astrocytic responses to an applied electric field. Therefore, over a period of 720 minutes, 241 images were taken for each region of interest. The application of the electric field via a connected current path and microscope imaging were monitored every two hours during the 12 hour recording period. The electric field could be monitored visually due to the phenol red present in the astrocyte media. As the current passed through the cell culture in the electrotactic chamber, the negatively charged (at pH 7.4) phenol red compound is also drawn towards the cathode, or the site of electrochemical gain of electrons. Due to the humidified environment inside the microscope apparatus, 1 to 2 mL of astrocyte media was added to the electrotactic chamber wells approximately half-way through the duration of the recording to prevent the cells from drying out.

Directly after the 12 hour application of the electric field, the microscope imaging was shut off. The tape-barriers and cover slips were gently removed, opening up the area of the Petri dish plated with

the cell subculture. The remaining astrocyte media was aspirated off and the cells were washed thrice with 1X phosphate-buffered saline (PBS). After the final wash, 4% paraformaldehyde was applied for fifteen minutes at room temperature. At the end of the fifteen minute time period, the formaldehyde was removed and replaced with 1X PBS, and stored at $4^{O}C$ until staining (within a 48 hour time period).

Immunocytochemistry

Immunostaining was used to visualize internal cellular changes in protein expression and DNA distribution. Following electric field application and cell fixing, astrocytes were stained with fluorescent dyes for the intermediate filaments vimentin & glial fibrillary acidic protein (GFAP), markers for immature astrocytes and mature astrocytes respectively. Staining astrocyte cytoskeletal elements in the fixed culture was accomplished by using fluorescent secondary antibodies that specifically targeted primary antibodies against vimentin and GFAP. 4',6-diamidino-2-phenylindole (DAPI), an intercalating agent that binds to A-T-rich regions of double stranded DNA, was used create nuclear stains of the cell culture.

The astrocyte subcultures, having been fixed in paraformaldehyde, were washed three times with PBS, each wash lasting five minutes. The cells were then blocked for 30 minutes using a solution of 4% Vector Labs normal goat serum (NGS), 1% Triton X-100, and 0.5% Akron bovine serum albumin (BSA) in 1X PBS to permeabilize the cell membranes. The cultures were then incubated overnight at $4^{O}C$ in a humid setting with DAKO α-GFAP rabbit primary antibody (1:500) & Invitrogen α-Vimentin mouse primary antibody (1:500); both primary antibodies were diluted in the PBS/NGS/Triton/BSA block solution. The following day, the cells were washed three times with PBS, five minutes per wash. The cells were then incubated with Molecular Probes Alexa Fluor 488 goat α-rabbit IgG secondary antibody (1:200) & Molecular Probes Alexa Fluor 594 goat α-mouse

IgG secondary antibody (1:200), both diluted in 1X PBS. Following another series of three five-minute PBS washes, Invitrogen DAPI NucBlue Cell Stain (2 drops per mL 1X PBS) was added onto the cultures for five minutes at room temperature. The cells were then washed three times with PBS and three times with deionized water, then cover slipped with Vector Labs Vecta-Shield aqueous mounting medium; this acts as an anti-quenching agent to preserve the fluorescence intensity. These coverslips were sealed with clear nail polish to preserve the newly stained astrocyte culture.

Images were taken within 48 hours of random areas within the stained culture using a Zeiss 710 Laser Scanning Microscope at 40X. The different absorption and emission properties of the various fluorochromes used (the 568 & 488 secondary antibodies and the dye DAPI) allow them to appear as different fluorescent signals, as shown in Table 2.2 (adapted from Haugland, 1992).

Fluorochrome	Absorption Maximum (nm)	Emission Maximum (nm)	Color
568	578	603	Red
488	495	591	Green
DAPI	372	456	Blue

Table 2.2 – Maximum Absorption and Emission Wavelength of Fluorochromes

The 568 goat α-mouse antibody targeted the mouse α-vimentin primary antibody, causing the vimentin secondary antibody to emit a red fluorescent signal; similarly, the 488 goat α-rabbit antibody targeted the rabbit α-GFAP primary antibody, causing the GFAP secondary antibody to appear as a green fluorescent signal. The DAPI dye produced a blue fluorescent signal when bound to double stranded DNA. This combination of fluorescent secondary antibodies was chosen to minimize overlapping emission spectra from different components of the stained cell culture.

BrdU in Astrocyte Cultures

Experiments involving the application and staining of the synthetic nucleoside BrdU in astrocyte cultures followed a very similar protocol with minor adjustments. When initially building the electrotactic chambers (Figure 2.2) Invitrogen BrdU Labeling Reagent was diluted in astrocyte media to a concentration of 100 μM. The media was warmed to 37^{O}C and then used in place of the normal warm astrocyte media when filling the cell subculture and wells. The same BrdU-astrocyte media was used when replenishing the electrotactic chamber about halfway through recording.

Following electric field application and cell fixing using 4% paraformaldehyde, the cultures exposed to BrdU underwent a different staining procedure. Binding the α-BrdU antibody required denaturation of the DNA before staining. This was achieved by adding 1N HCl for ten minutes at 0^{O}C (in ice), followed by 2N HCl for an additional ten minutes at 25^{O}C (room temperature) then 2N HCl for 20 minutes at 37^{O}C. The acid was then neutralized with 0.1M borate buffer for ten minutes at room temperature. The borate buffer was rinsed off three times with 1X PBS, five minutes per wash. The remaining staining protocol for fluorescent antibodies and nuclear stains is similar to experiments lacking the BrdU; when blocking the culture with primary antibodies for intermediate filaments, a DAKO α-BrdU mouse primary antibody was added as well.

Cell Behavior Analysis

ImageJ was used to analyze changes in cellular behavior during the course of the time-lapse recordings, where images were takes every three minutes over a 12 hour period. The plug-in MTrackJ was used to manually track the movement of individual cells, calculating the cell velocity and direction of movement at every hour over 12 hours. Over four experiments conducted at 400 $^{mV}/_{mm}$, the velocity and direction of 553 cells were tracked over 20 regions of interest. The migration paths of 431 cells from 30 regions of interest were tracked from four experiments conducted at 0

$^{mV}/_{mm}$ – due to the minimal movement of cells not exposed to an electric field, more regions of interest were analyzed for experiments lacking an electric field. The differing number of tracked cells can also be attributed to slight variations in seeding/plating astrocytes. The obtained cell velocities were averaged at each hour point, giving a mean velocity at each time point for each tested electric field strength. In addition, the velocities and angle of movement at each hour were vector-summed for each cell to obtain the final position of the cell. These were averaged together to calculate an ultimate displacement and direction of movement.

ImageJ was also used to visualize and count the number of cell divisions and changes in cell proliferation during the 12 hour time-lapse recording. Again, 20 regions of interest were examined from 400 $^{mV}/_{mm}$ (n=4) and 30 regions of interest were examined from 0 $^{mV}/_{mm}$ (n=4). The hour period during which the observed division occurred was noted, and the divisions that occurred during the 12 one-hour blocks were summated. Additionally, a line was drawn along the cleavage plane of each dividing cell to obtain the orientation of division. The obtained values were doubled to account for the data being diametric; when carrying out statistical tests for significance, however, the original angle values were used (Marr, 2011). This average angle represents the mean axis of cell division in response to an electric field. Cell division and astrocyte proliferation were also studied using 5-bromo-2'-deoxyuridine (BrdU) studies – the nucleotide BrdU, which was added to astrocyte subcultures before application of an electric field, can be incorporated into newly synthesized DNA during S phase (Miller & Nowakowski, 1988). As cells divide over the course of the 12 hour recording, BrdU is incorporated into the cellular DNA – therefore, immunostaining with BrdU highlighted the cells that had undergone division after the BrdU had been introduced to the subculture and visualized the proliferation rate.

Lastly, ImageJ was used to quantify the changes in external morphology after the application of an electric field. The CellCounter plug-in was used to tag cells using different colored markers to

represent different categories. Cells displaying a bipolar morphology and cells with a more polygonal morphology were marked using two different colors at time points 0, 1, 6, and 12. By counting the two cell types and comparing the percentages of each value at different times, a shift in cell morphology from one cell type to another can be easily established. Immunocytochemistry using antibodies against astrocyte-specific intermediate filaments (in addition to corroborating that the cells in the subculture were indeed astrocytes) were also used to visualize internal changes in cell morphology. Staining for vimentin & GFAP highlighted changes in cytoskeletal structure and protein composition in response to an electric field, while the DAPI nuclear stain was used to examine nuclear changes.

Statistical Analysis

Microsoft Excel and the statistics software JMP were used to analyze the experimental data and create graphs; a variety of statistical hypothesis tests were then used to determine the significance of the data. Linear regression analysis was used to test the correlation between the electric field strength used and the resulting astrocyte behaviors. The regression correlation coefficient (r) was calculated from a trend line fit to the data – a r-value of 1 indicates complete linearity, implying that the observed astrocyte behavior (directional migration or cell proliferation rate) is directly proportional to the applied field strength (Orlov, 1996).

A paired student's t-test was used to test for differences between two sets of data with equal sample sizes (n); a one-way ANOVA test and Holm-Sidak test for post-hoc analysis were used for three or more sets of data with equal sample sizes. These statistical tests were carried out to test the null hypothesis that there was no significant difference between the sets of data being tested. The predetermined level of significance for statistical tests (α) was determined to be 0.05. Therefore, an obtained p-value, or probability of the null hypothesis being true, from statistical testing falling

above $\alpha = 0.05$ means that the null hypothesis has failed to be rejected. Conversely, a p-value falling below $\alpha = 0.05$ suggests that null hypothesis can be rejected and that the data can be considered statistically significant.

When analyzing angle measurements, a different set of statistical tests had to be used for circular data. When using linear tests, angles of value 0^O and 355^O seem to indicate a high level of variability, whereas in reality there is minimal difference between the two angles. An average vector was calculated to describe the distribution of angle values, using the sine and cosine values of each angle. The resultant angle direction of the vector represented the circular mean of the data, and the length of the vector represented the r-value, or the level of dispersion of the data – a r-value of 0 indicates complete random distribution, while a r-value of 1 indicates clustering of data towards a particular direction.

To test the significance of the observed directionality, a Rayleigh's test of directionality was used to test whether or not the circular distribution of the angle measurements was random. The null hypothesis, that the angle values were randomly distributed, was either accepted or rejected by comparing a calculated statistic to a table of predetermined critical values for a certain level of significance ($\alpha = 0.05$). If the calculated statistic is less than the critical statistic, the null hypothesis has failed to be rejected. If the calculated statistic is greater than the critical statistic, the null hypothesis can be rejected and the data can be considered statistically significant (Li & Hoffman-Kim, 2008).

A v-test for directionality can be used to further test if the measured angles are oriented towards a particular direction. While the same null hypothesis is used (that the angle values were randomly distributed), an additional alternative hypothesis is added that the angle values are not randomly distributed and are oriented with a certain predicted direction. Similar to the Rayleigh's test, a

critical value was calculated and compared to a table of critical values for $\alpha = 0.05$. If the calculated statistic is less than the critical statistic, the null hypothesis has failed to be rejected. If the calculated statistic is greater than the critical statistic, however, the null hypothesis has been rejected and the alternative hypothesis must be accepted as true – this would indicate the measured angles are distributed towards a particular angle or orientation (Zar, 1999).

CHAPTER 3 Results

Previous experiments involving the application of electric fields to astroglia cultures have shown that astrocytes realign themselves perpendicularly to the direction of the electric field (Borgens et. al., 1994). This induced alignment can direct and further enhance neurite outgrowth towards its appropriate final target (Alexander et. al., 2006), demonstrating that astrocytes are capable of playing a role in mammalian central nervous system regeneration. However, the range of elicited astrocyte behaviors in response to electric fields of varying field strengths has not been closely studied or documented and is the focus of this study.

Presence of Astrocytes Confirmed

Before beginning experiments with astrocyte cultures, the astrocytes were first tested to confirm the identity of the cells. When using neonatal brain tissue, there is a high chance of contamination with other cell types. Some of the most common contaminating cell types seen within an astrocyte culture include oligodendrocytes & microglia, which are recognizable by their distinctive surface and intracellular morphologies (Banker & Goslin, 1992). The purity of the culture can be established through immunological staining. An astrocyte subculture was fixed 12 hours after being plated onto an electrotactic chamber and incubated (representing a control electric field strength of 0 $^{mV}/_{mm}$). The fixed culture was then stained with astrocyte-specific markers.

Antibodies against the intermediate filaments vimentin and glial fibrillary acidic protein (GFAP) were used to visualize immature and mature astrocytes, respectively; 4',6-diamidino-2-phenylindole (DAPI), which binds to DNA to create a fluorescent stain of the nucleus, was also used in addition to the antibodies. Immunostaining and subsequent fluorescent microscopy imaging showed that

every DAPI-stain, which highlights the nucleus of a cell, was seen in conjunction with either vimentin, GFAP, or both. The presence of vimentin-positive and/or GFAP-positive cells indicated a predominantly astrocyte population within the culture with no other contaminating cell type present. The GFAP, vimentin, & DAPI staining can be seen in Figure 3.1.

Electric Field-Induced Astrocyte Directional Migration

Cellular migration is a crucial post-injury event seen *in vivo* during tissue repair and regeneration (Stewart et. al., 2007) – astrocytes in particular move in response to endogenous injury potentials. One of the aspects of astrocyte cultures studied was the induced cell migration seen *in vitro* in response to the application of an electric field, done by using ImageJ to track cell movement in time-lapse recordings. The initial positions of individual cells, along with their migration paths, are highlighted in Figure 3.2. Following a 12 hour exposure to an electric field strength of 400 $^{mV}/_{mm}$ (n=4), astrocytes began to almost immediately exhibit mass directional cell movement. However, control cells receiving no electric field, or 0 $^{mV}/_{mm}$ (n=4), failed to show similar movement patterns over a 12 hour period. The overall mean cell speed of all cells exposed to 400 $^{mV}/_{mm}$ was 26.63 $^{\mu m}/_{hr}$; the overall mean cell speed of the control cells was 12.40 $^{\mu m}/_{hr}$. Therefore, astrocytes that had an electric field with an applied field strength of 400 $^{mV}/_{mm}$ moved at over double the speed that control astrocytes lacking an electric field did.

The average speeds of astrocyte movement at each time point over the 12 hour recording period for all eight experiments are presented in Figure 3.3. The cell speeds from all experiments conducted at a specific field strength were then averaged and compared to each other, also seen in Figure 3.3. Cells exposed to an electric field of 400 $^{mV}/_{mm}$ displayed average cell migration speeds between 20 $^{\mu m}/_{hr}$ & 30 $^{\mu m}/_{hr}$ over a 12 hour period, while control cells not exposed to an electric field (0 $^{mV}/_{mm}$) displayed cell migration speeds between 5 $^{\mu m}/_{hr}$ & 15 $^{\mu m}/_{hr}$ over the same time period. A paired

Figure 3.1: Astrocyte Culture Immunostaining
Immunological staining and fluorescence microscopy was used to test the purity of astrocyte cultures. Specific primary antibodies & fluorescent secondary antibodies were used to visualize astrocyte-specific intermediate filaments – **(a)** the secondary antibody used to tag vimentin emits a red fluorescent signal and **(b)** the secondary antibody used to tag glial fibrillary acidic protein (GFAP) emits a green fluorescent signal. The DAPI dye produces a blue fluorescent signal when bound to double-stranded DNA. **(c)** Every DAPI-stained nucleus is seen in conjunction with at least one cytoskeletal element –in some instances both vimentin and GFAP can be seen, producing an intermediate orange-yellow color (highlighted). The presence of astrocyte-specific markers proves that the stained culture is predominantly comprised of astrocytes.

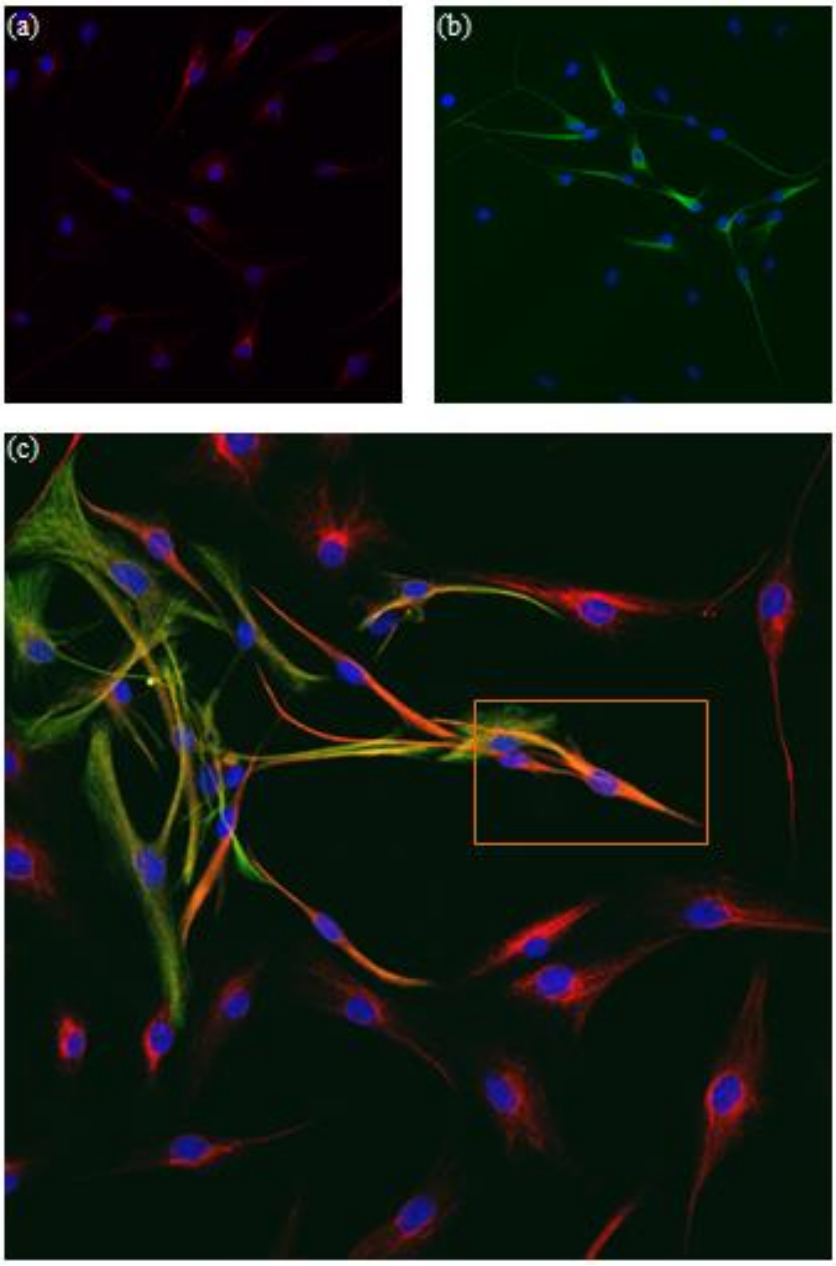
(a)
(b)
(c)

Figure 3.2: Tracking Directional Cell Movement
Following application of an electric field (E = 400 $^{mV}/_{mm}$), astrocytes began to show directional cell movement, while cells receiving no electric field failed to show similar movement patterns. The ImageJ plug-in MTrackJ was used to track specific cells, recording distances travelled in between time points to calculate cell velocities & angles of movement. **(a)** Multiple regions of interest from the same experiment are shown at the last time point at 12 hours. Each colored line represents the migration path travelled by an individual cell, with its location marked at each hour. Control cells receiving no electric field showed minimal movement – although there are occasional cells that seem to move around a bit, most of the movement appears to be random and contained to a limited distance, with cells circling themselves. Exposure to an electric field, however, caused immediate mass downwards movement. The full migration path for every tracked cell is visible for as long as the cell remained in the region of interest. **(b)** The initial positions of specific cells were noted and tracked over time. These particular cells, tracked every two hours, are shown at 10 hours rather than 12 hours in order to include the last marked position before leaving the region of interest.

.

(a)

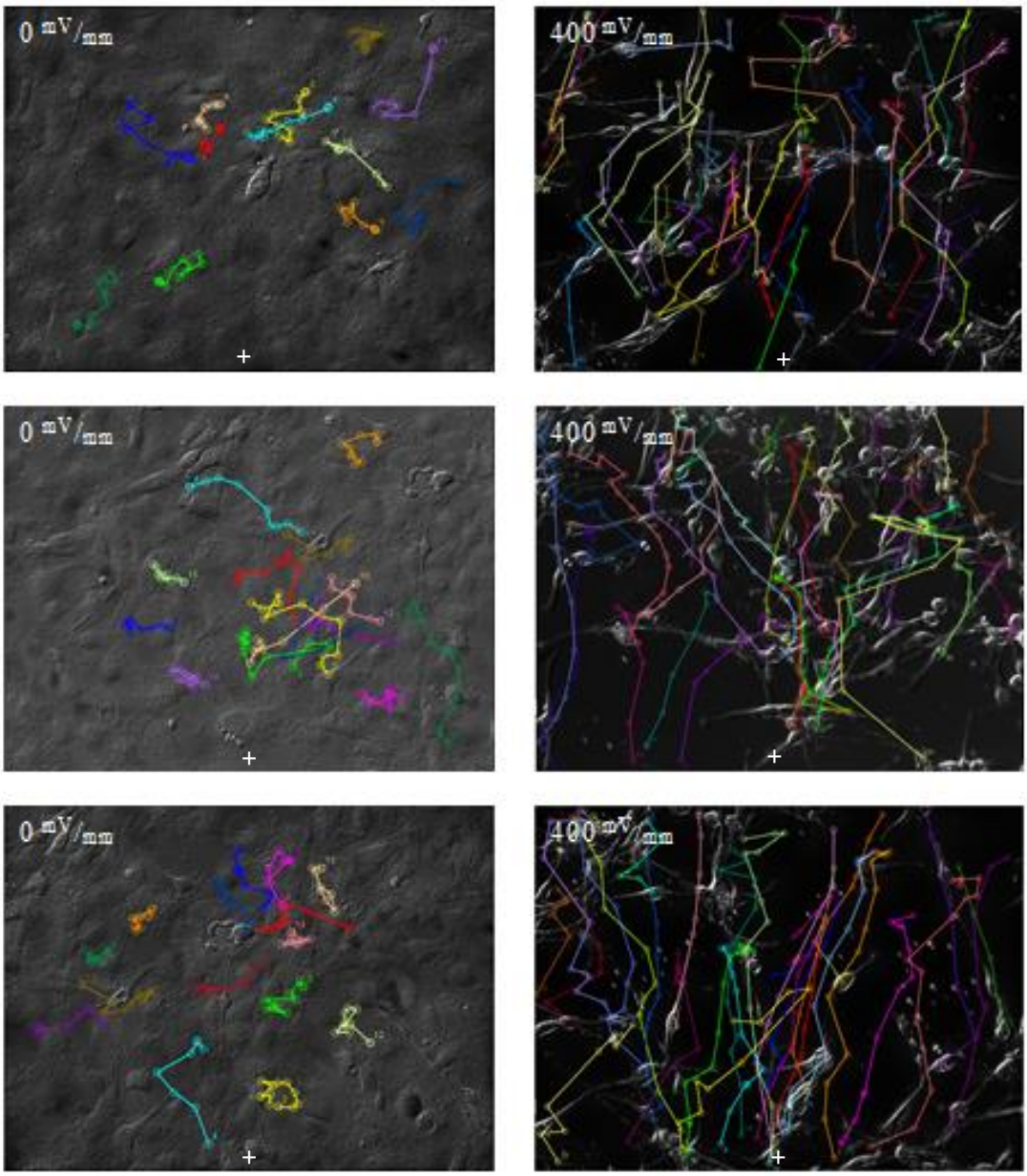

(b)

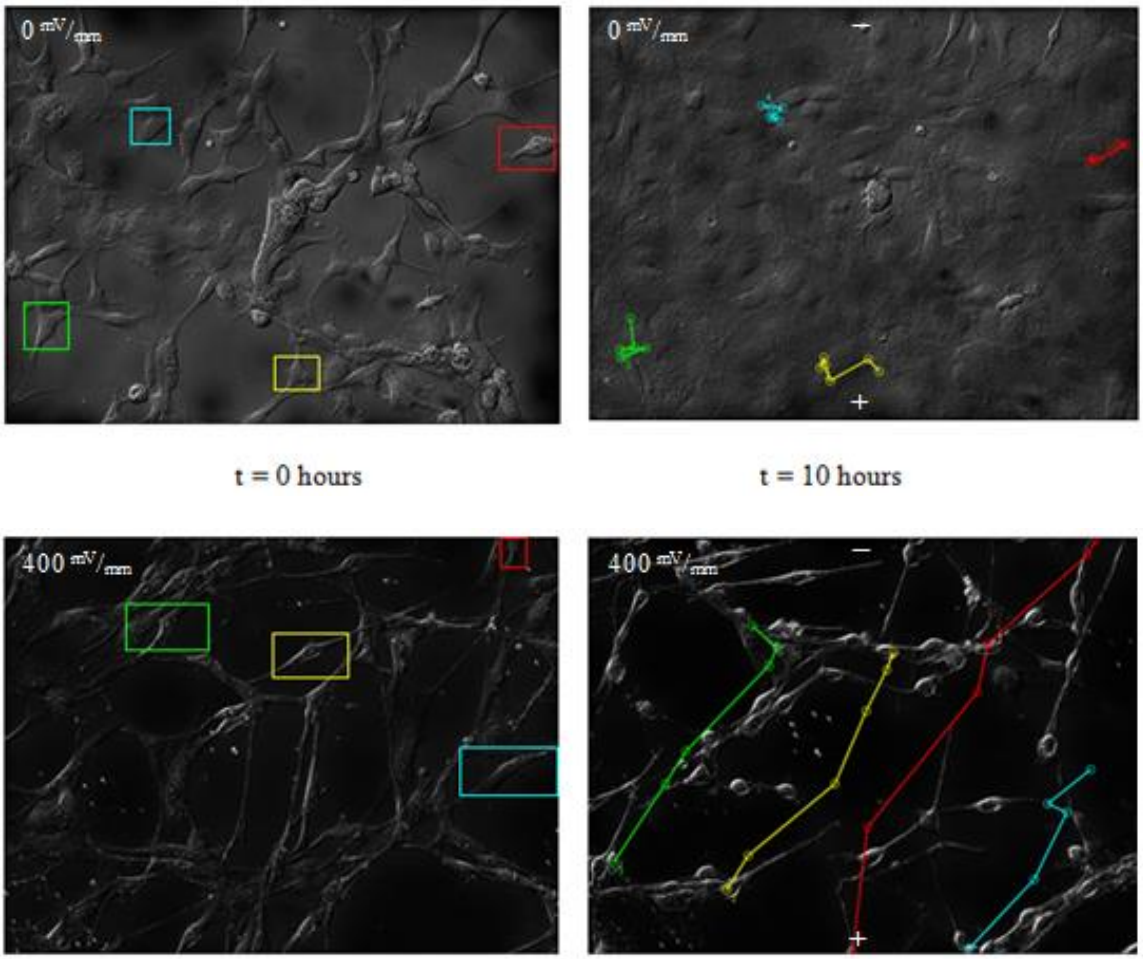

Figure 3.3: Average Cell Speeds Upon Electric Field Exposure
(a) The mean speeds of astrocytes undergoing induced cell migration are shown from each individual experiment at electric field strengths of 400 $^{mV}/_{mm}$ and $0^{mV}/_{mm}$. This highlights the variety of observed speeds by individual cells at different time points as well as the clear difference between the cell speeds seen at differing electric field strengths. **(b)** The mean cell speeds of all tracked cells at specific field strengths, along with their corresponding standard error bars, show that cells exposed to an electric field of 400 $^{mV}/_{mm}$ for 12 hours show a higher migration rate than control cells, or 0 $^{mV}/_{mm}$. Additionally, the average speed of cell migration appears to be proportional to the electric field strength applied to an astrocyte subculture.

(a)

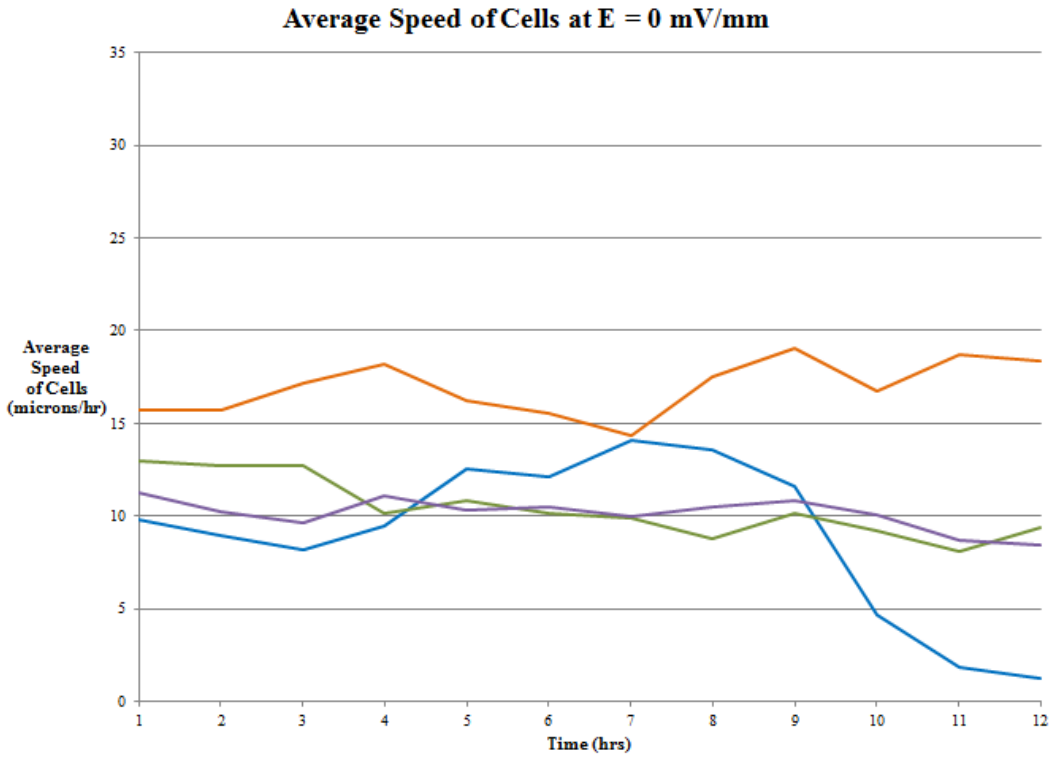
Average Speed of Cells at E = 0 mV/mm
Average Speed of Cells (microns/hr)
35
30
25
20
15
10
5
0
1
2
3
4
5
6
7
8
9
10
11
12
Time (hrs)

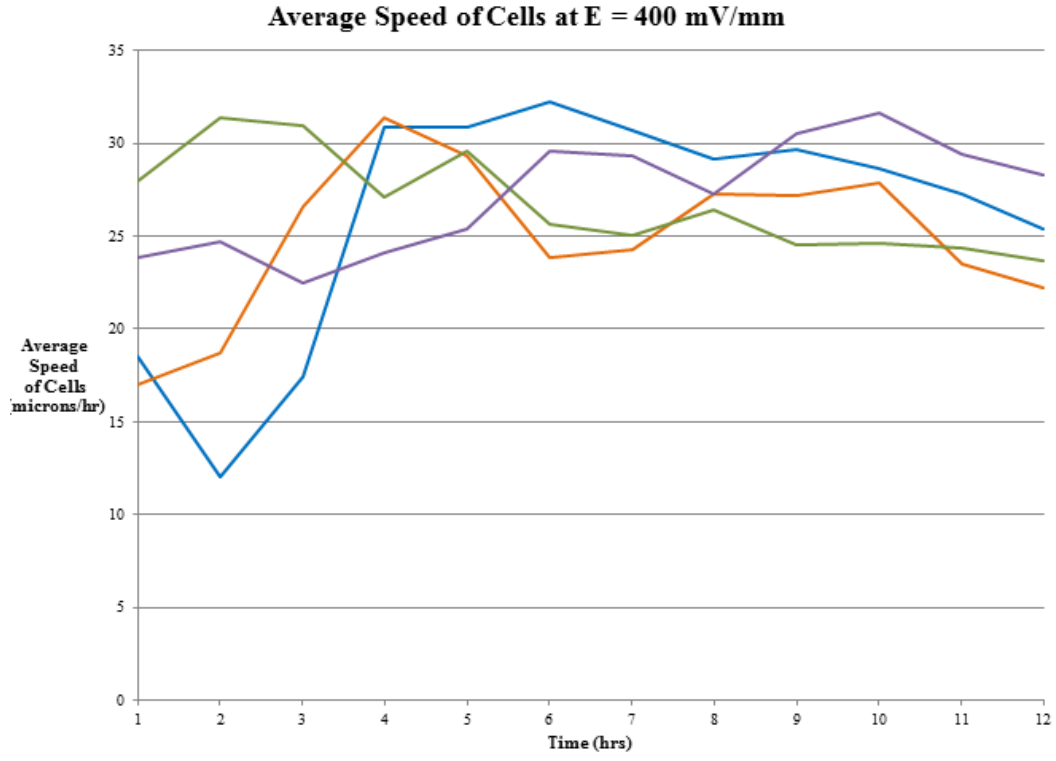
Average Speed of Cells at E = 400 mV/mm
Average Speed of Cells (microns/hr)
35
30
25
20
15
10
5
0
1
2
3
4
5
6
7
8
9
10
11
12
Time (hrs)

(b)

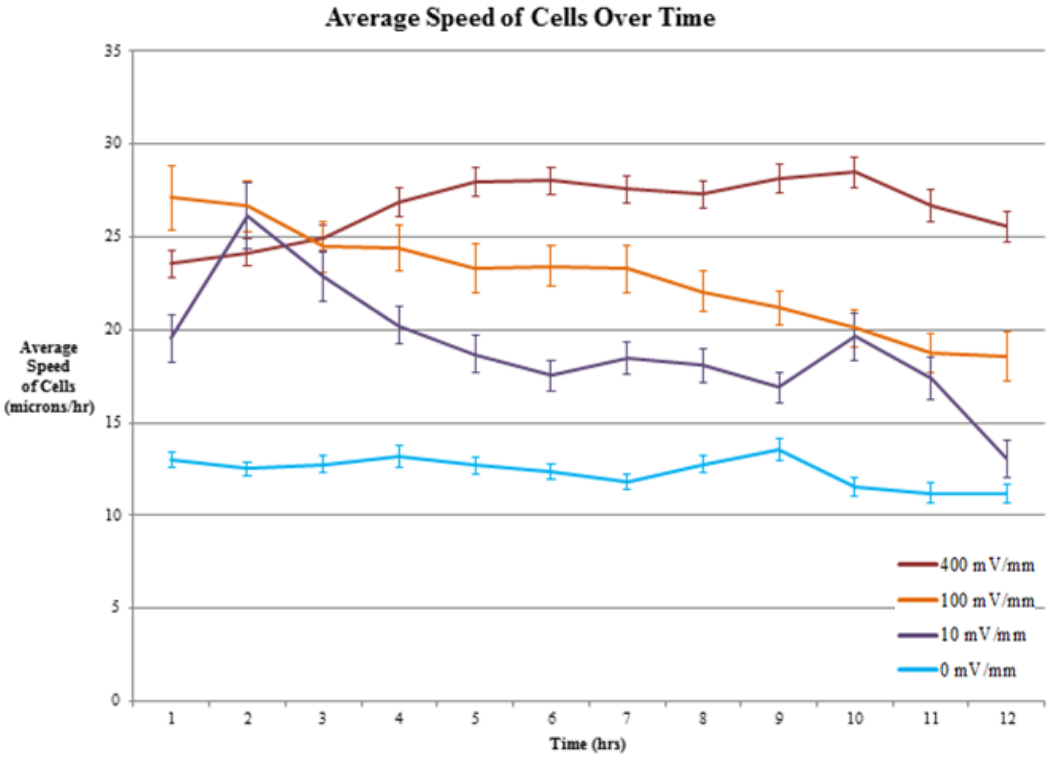
Average Speed of Cells Over Time
Average Speed of Cells (microns/hr)
35
30
25
20
15
10
5
0
1
2
3
4
5
6
7
8
9
10
11
12
Time (hrs)
400 mV/mm
100 mV/mm
10 mV/mm
0 mV/mm

student's t-test was carried out to compare the average speeds from each distinct electric field strength at each time point. The obtained p-value from the data was 3.13×10^{-11}; this value was substantially lower than the level of significance $\alpha = 0.05$ and showed that there is a statistically significant difference between the cell speeds at 400 $^{mV}/_{mm}$ and 0 $^{mV}/_{mm}$.

The application of electric fields on induced cell migration in an astrocyte culture appears to have a graded effect. Results from additional experiments run at electric field strengths of 100 $^{mV}/_{mm}$ (n=1) and 10 $^{mV}/_{mm}$ (n=1) are also displayed in Figure 3.3; this data is compared with data from experiments at 400 $^{mV}/_{mm}$ (n=4) and 0 $^{mV}/_{mm}$ (n=4) for a preliminary visual comparison. Although experiments at 100 $^{mV}/_{mm}$ & 10 $^{mV}/_{mm}$ didn't have comparable numbers of repeated experiments, there were a sufficient number of cells (121 and 157, respectively) to assume a normal distribution. The mean cell speed of the cells from the 100 $^{mV}/_{mm}$ experiment was 22.75 $^{\mu m}/_{hr}$, while the mean speed of cells from the 10 $^{mV}/_{mm}$ experiment was 19.04 $^{\mu m}/_{hr}$. These values fall between the values seen at 400 $^{mV}/_{mm}$ (26.63 $^{\mu m}/_{hr}$) and 0 $^{mV}/_{mm}$ (12.40 $^{\mu m}/_{hr}$), showing that the magnitude of the applied electric field had a proportional effect on induced cell migration speed. The calculated regression correlation coefficient (r) from a fitted trend line was 0.99. Since a r-value of 1 demonstrates complete linearity, this indicated that the induced cell speed is directly proportional to the applied electric field strength. A one-way ANOVA test was used to further compare the cell speeds from the four differing electric field strengths. The p-value for the four groups of data was 4.04×10^{-18}, which is less than the level of significance $\alpha = 0.05$. An additional post-hoc analysis was carried out using the Holm-Sidak method; this test showed that migration speeds at all electric field strengths were statistically different from each other with p-values < 0.001.

When measuring the velocities from induced-astrocyte migration, the obtained vector quantities have two components – the magnitude of the change in rate of position (measured as a speed) and the direction of motion (measured as an angle). Upon exposure to an electric field of 400 $^{mV}/_{mm}$,

mass directional cell migration was seen towards the positively-charged electrode (which can be revisited in Figure 3.2); since the electrotactic chamber mimics an electrolytic cell, this electrode was the anode. The angle values ranged from -180^{O} to 180^{O}, where 0^{O} was parallel to the positive x-axis, 90^{O} was parallel to the positive y-axis, -90^{O} was parallel to the negative y-axis, and 180^{O}/ -180^{O} was parallel to the negative x-axis. First, the vectors representing the circular dispersion of the data (represented by r) were calculated. For the measured angles from cells exposed to a field strength of 400 $^{mV}/_{mm}$, the calculated r-value was 0.95, suggesting that the direction of migrating cells was oriented towards a certain direction. The r-value for measured angles from cells exposed to a control field strength (0 $^{mV}/_{mm}$) was 0.07, meaning the data was uniformly scattered and that there was no particular direction cell move preferentially towards. The average directions of movement at electric field strengths of 400 $^{mV}/_{mm}$ and 0 $^{mV}/_{mm}$ are visually summarized in Figure 3.4.

In order to test whether these cells showed directionality in their movement, a Rayleigh's test for uniformity was used to test the distribution and potential clustering of the angle measurements. Using the critical values and desired level of significance ($\alpha = 0.05$), the null hypothesis that measured angles from a field strength of 400 $^{mV}/_{mm}$ were uniformly scattered was rejected. This indicated that the overall cell migration paths were distributed non-randomly and displayed some level of directionality. However, the null hypothesis that measured angles from a field strength of 0 $^{mV}/_{mm}$ were uniformly scattered did not meet the criteria to be rejected, confirming that the cell migration patterns were randomly distributed.

To further establish the overall direction of movement in response to an electric field, a v-test for directionality was conducted on the angle measurements from a field strength of 400 $^{mV}/_{mm}$. Using live cell imaging and ImageJ, the cell migration patterns appeared to mainly be moving downwards towards the positively-charged anode. For the v-test, the null hypothesis was that the measured

Figure 3.4: Average Angle of Directional Cell Migration
The range of angles, from -180^{O} to 180^{O}, represents a full circle. Assuming that all tracked cells start at the origin (0,0), each point on the scatterplot represents the final position of an individual moving cell. Cells not exposed to an electric field, shown in blue, displayed completely random movement in a wide range of directions, which was confirmed with statistical testing. Cells experiencing an electric field of 400 $^{mV}/_{mm}$, in addition to moving faster, also showed downwards movement towards the positively-charged electrode, or anode. The corresponding summary vector shows that these cells have an average direction of movement of -93.07^{O} with an ultimate displacement of 186.81 μm. This confirms that electric fields induce directional, anodal astrocyte migration.

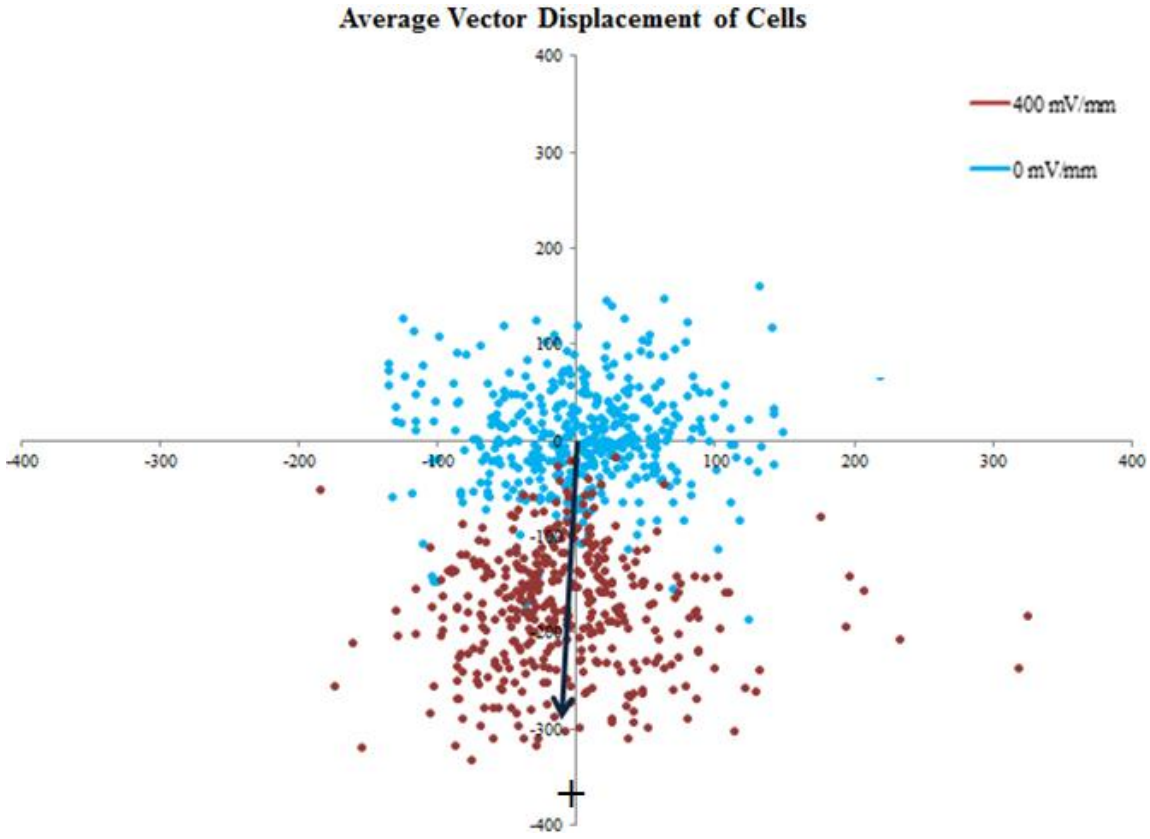
Average Vector Displacement of Cells
400 mV/mm
0 mV/mm
400
300
200
100
0
-100
-200
-300
-400
-400
-300
-200
-100
100
200
300
400

angles were randomly scattered, with an alternative hypothesis that the cells were clustered towards -90^{O}, or the direction of the anode. The circular mean, calculated to be -93.29^{O}, was compared to -90^{O}; using the critical values and desired level of significance ($\alpha = 0.05$), the null hypothesis was rejected. Therefore, the alternative hypothesis that the cells are migrating downwards towards the anode was accepted as true. This corroborates the visual observation that cells were moving towards the positive anode. This also indicates that without exposure to an electric field, cells had no directional movement in addition to limited cell migration.

Electric Field-Induced Astrocyte Proliferation

In vivo, astrocytes undergo symmetric division to both maintain the large glial population in the mammalian central nervous system as well as to generate new cells post-injury. The physical characteristics and time course of a single astrocyte cell dividing can be seen in Figure 3.5. Changes in astrocyte division and proliferation rate following exposure to an electric field were studied using time-lapse recording and 5-bromo-2'-deoxyuridine (BrdU) incorporation into DNA.

Upon application of an electric field with a field strength of 400 $^{mV}/_{mm}$, the number of divisions in astrocytes showed a marked increase, as seen in Figure 3.6. When examining time-lapse recordings, a total of 171 divisions were seen across the experiments conducted at 400 $^{mV}/_{mm}$, while only 38 divisions were seen in the control experiments at 0 $^{mV}/_{mm}$. The rate of cell division in response to an electric field of 400 $^{mV}/_{mm}$ appears to be consistent throughout the 12 hour time period, with no major fluctuations between time points. A paired student's t-test was carried out to compare the changes in cumulative astrocyte proliferation at different electric field strengths over a 12 hour time frame. The p-value from the obtained data was 3.22×10^{-7} and lower than $\alpha = 0.05$, showing that there was a statistically significant difference between the cell divisions at 400 $^{mV}/_{mm}$ and 0 $^{mV}/_{mm}$.

Figure 3.5: Astrocyte Division
A typical astrocyte division, shown with the characteristic rounding of the cell, produces two daughter cells in approximately 0.3 hours, or between 15 and 20 minutes.

t = 0 hrs

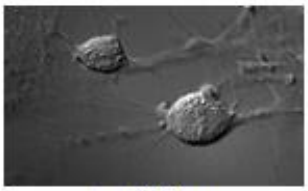

t = 0.1 hrs

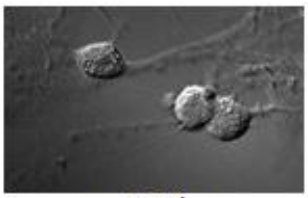

t = 0.2 hrs

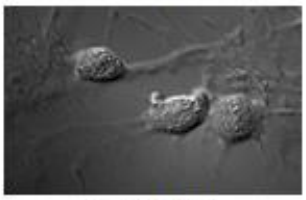

t = 0.3 hrs

Figure 3.6: Astrocyte Proliferation over Time
ImageJ was used to count the number of divisions viewed in each 12 hour recording in one region of interest. The divisions from 20 regions of interest from experiments carried out at field strengths of 400 $^{mV}/_{mm}$ & 0 $^{mV}/_{mm}$ were tallied based on the hour period during which the division occurred. The rate of astrocyte proliferation increases upon application of an electric field, with a larger number of cell divisions occurring in the same 12 hour time frame as control subcultures. Cell division continues to occur throughout the 12 hour period – there doesn't appear to be any time point that has unusually high or low cell divisions.

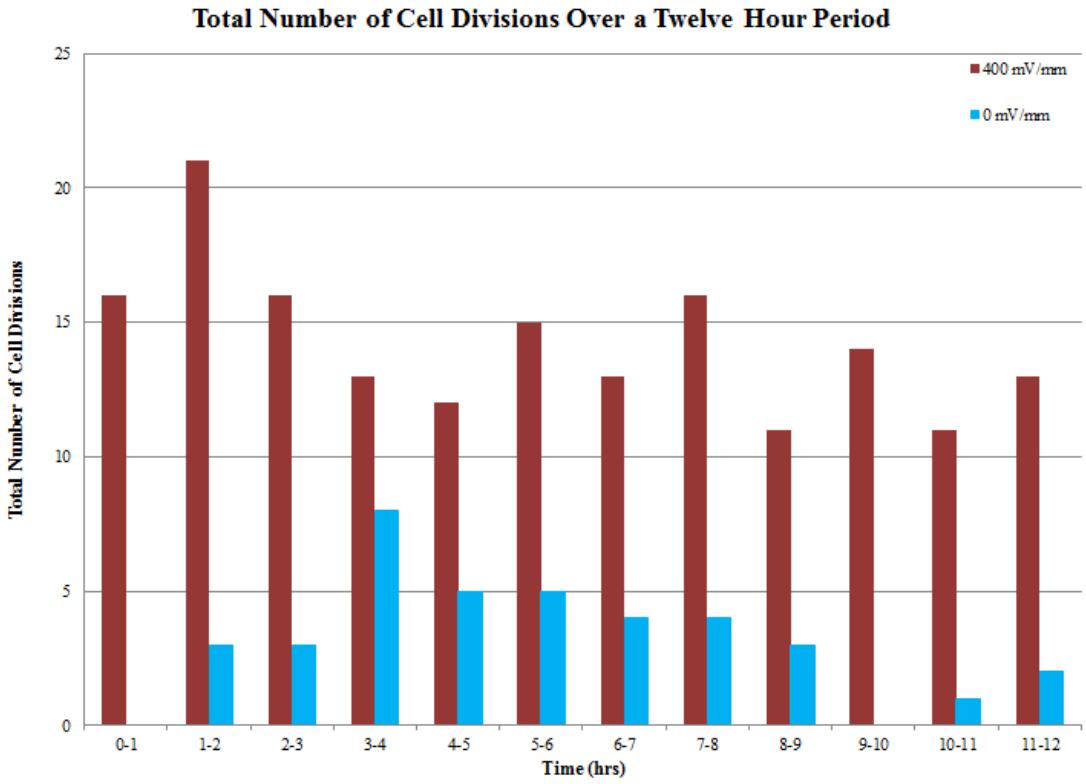
Total Number of Cell Divisions Over a Twelve Hour Period
Total Number of Cell Divisions
25
20
15
10
5
0
400 mV/mm
0 mV/mm
0-1
1-2
2-3
3-4
4-5
5-6
6-7
7-8
8-9
9-10
10-11
11-12
Time (hrs)

Using electric fields with field strengths between 400 $^{mV}/_{mm}$ and 0 $^{mV}/_{mm}$ may also have a graded effect on cell proliferation similar to the effects on cell migration, though not as pronounced. Electric field strengths of 100 $^{mV}/_{mm}$ and 10 $^{mV}/_{mm}$ were applied for a 12 hour time period; however, for both 100 $^{mV}/_{mm}$ and 10 $^{mV}/_{mm}$, five regions of interest were analyzed rather than twenty due to the limited number of experiments for these field strengths (n=1). Over the course of 12 hours, 35 divisions were seen following an exposure to a field strength of 100 $^{mV}/_{mm}$, while 10 divisions were seen over the same time period during an exposure to a field strength of 10 $^{mV}/_{mm}$. Due to the uneven number of experiments for the various electric field strengths, the proliferation rate was instead measured as divisions per region of interest.

When looking at the four field strengths tested, the cumulative number of divisions per region of interest was calculated to be 400 $^{mV}/_{mm}$ (8.6), 100 $^{mV}/_{mm}$ (7), 10 $^{mV}/_{mm}$ (2), and 0 $^{mV}/_{mm}$ (1.9). The induced changes in cell division appear to be proportional to the magnitude of the electric field strength, with a clear difference between the number of divisions seen at field strengths of 400 $^{mV}/_{mm}$ & 100 $^{mV}/_{mm}$ and the number of divisions seen at 10 $^{mV}/_{mm}$ & 0 $^{mV}/_{mm}$. The r-value from the fitted trend line for average cumulative divisions per region of interest was 0.86, meaning that there was a fairly strong correlation between electric field strength and proliferation rate. A one-way ANOVA test between the four electric field strengths gave a p-value of 6.86×10^{-6}; since this value was less than $\alpha = 0.05$, this showed that there is significance between proliferation rates from each electric field strength.

The velocity & nature of astrocyte migration make it problematic to study proliferation in the same set of cells using time-lapse recordings. Therefore, these results were further confirmed using BrdU incorporation studies, which are presented in Figure 3.7. Data collected from the ImageJ-tracked cells showed that astrocytes that underwent a 12 hour exposure to an electric field of strength 400 $^{mV}/_{mm}$ had a marked increase in cell division when compared to control cells. Therefore, it would be

Figure 3.7: BrdU Staining
The high velocity of induced astrocyte migration makes it difficult to study the same set of cells continuously for 12 hours, as cells move in and out of the region of interest. **(a)** Immunostaining and fluorescence microscopy was conducted on astrocyte subcultures treated with BrdU immediately before the recording period. Since BrdU incorporates into the DNA during replication, cell staining positive for BrdU have undergone division during the 12 hour exposure to an electric field. Per region of interest, there were far more BrdU-positive astrocytes in subcultures exposed to 400 $^{mV}/_{mm}$ that control subcultures, or 0 $^{mV}/_{mm}$. This further confirms the finding that the application of an electric field enhances the rate of astrocyte division. **(b)** The fluorescent BdrU image is superimposed onto the DIC image of the same region of interest, highlighting the BrdU-stained cell nucleus. There are clearly more BrdU-stained cells following an electric field of 400 $^{mV}/_{mm}$ than at 0 $^{mV}/_{mm}$.

(a)

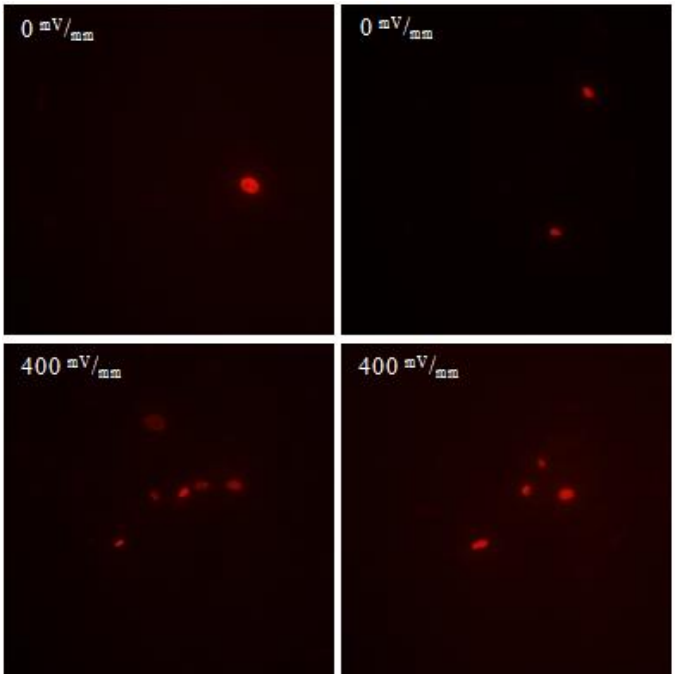

(b)

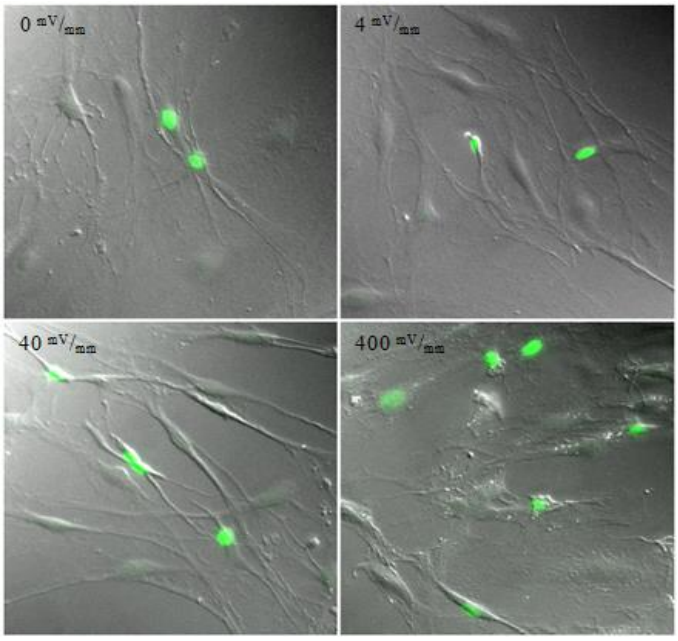

expected that cells from an experiment at 400 $^{mV}/_{mm}$ would show a higher number of BrdU-positive astrocytes – a higher proliferation rate would mean that more dividing cells incorporate BrdU into their DNA over a period of time. As expected, immunostaining and fluorescence microscopy showed a greater number of cells that stained positively for BrdU. This confirms the findings linking the application of electric fields and subsequent changes in astrocyte proliferation and cell division.

The orientation of cell division was also examined when studying astrocyte proliferation. When looking at the measured angle representing the cleavage furrow, the calculated r-value from cells exposed to a field strength of 400 $^{mV}/_{mm}$ was 0.23, while the r-value from cells at a control field (0 $^{mV}/_{mm}$) was 0.17. Based on these numbers alone, there didn't appear to be a difference due to an electric field; however, these r-values may not be entirely accurate due to the diametric nature of the data. In order to test the directionality of the electric induced-orientation of cell division, a Rayleigh's test for directionality was carried out. When using the critical values and desired level of significance ($\alpha = 0.05$), the null hypothesis that measured angles from a field strength of 400 $^{mV}/_{mm}$ were uniformly distributed was rejected, indicating orientation of the axis of division in response to an electric field. The null hypothesis was not rejected for the measured angles from a field strength of 0 $^{mV}/_{mm}$, establishing that the orientation of division was completely random in control cells. A v-test for directionality further compared the circular mean from cells exposed to an electric field (93.1^{O}) to a more standard angle matching the x-axis or y-axis (90^{O}). The null hypothesis that the measured angles were randomly scattered was rejected; therefore, the alternative hypothesis that the cell axis of orientation towards 90^{O}, or parallel to the applied electric field vector, was accepted as valid. Therefore, an electric field of physiological field strength induced orientation of the mitotic spindle apparatus in a particular direction, thus controlling the axis of cell division.

Electric Field-Induced Astrocyte Morphology Changes

As cells change their maturation state, their external morphologies and intracellular make-ups shift to reflect their current state. These shifts in morphology can occur during cellular differentiation, often seen during development, or cellular dedifferentiation upon injury. In astrocytes, these internal changes were tracked using fluorescent dyes for the nucleus and intermediate filaments GFAP & vimentin.

Over the 12 hour period of the electric field application (400 $^{mV}/_{mm}$), astrocytes shifted from a flattened polygonal shape, typically seen in mature astrocytes, to a rounded bipolar shape associated with immature astrocytes. These changes in surface morphology, both in response to an electric field and in absence of one (0 $^{mV}/_{mm}$), can be seen in Figure 3.8. Control cells showed a predominantly polygonal population of cells – only 8.9% of the cells tracked in ImageJ displayed a bipolar morphology within the first hour of time-lapse recording. Over the next eleven hours, the number of bipolar cells decreased to 1.7%, indicating a shift to a polygonal morphology. However, within the first hour of applying an electric field of 400 $^{mV}/_{mm}$, astrocytes immediately shifted their external appearance, with 69.7% of tracked cells showing a bipolar morphology. At hour 12, 68.5% of the cells still had a bipolar shape, showing that the change in morphology was maintained over the course of the electric field application; this slight variation was due to the nature of electric field induced-cell migration, indicating that the exact same group of cells was not present in a region of interest for the full 12 hours. Contrary to what is seen with the application of an electric field, control cells shift towards the polygonal morphology over time, most likely due to the lack of migration & lack of increased proliferation. The shifts in surface morphology over time are visualized in Figure 3.9.

Figure 3.8: Quantifying Astrocyte Surface Morphology Changes
(a) Immediately following application of an electric field with a field strength of 400 $^{mV}/_{mm}$, astrocytes began to shift from a flattened, polygonal morphology to a more rounded bipolar shape with pronounced processes extending in opposite directions. This shift in morphology mostly occurs within the first hour, before mass directional movement of cells. **(b)** The ImageJ plug-in CellCounter was used to tag polygonal & bipolar cells as two separate categories; polgonal cells were marked as pink and bipolar cells were marked as blue. The numbers of both cell types were counted at hour 0, 1, 6, 12 of the time-lapse recordings.

(a)

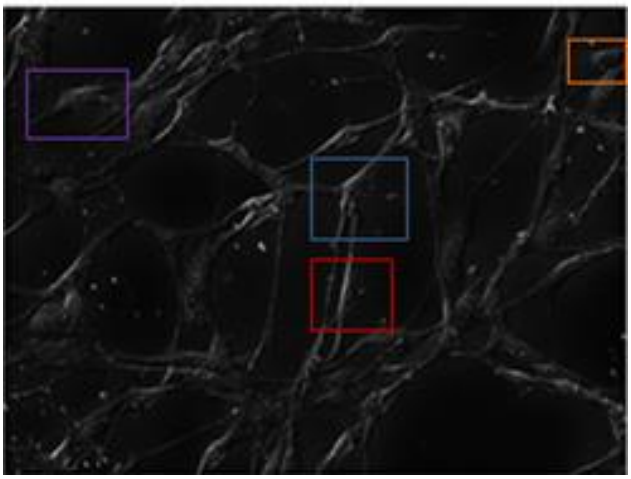

t = 0 hrs

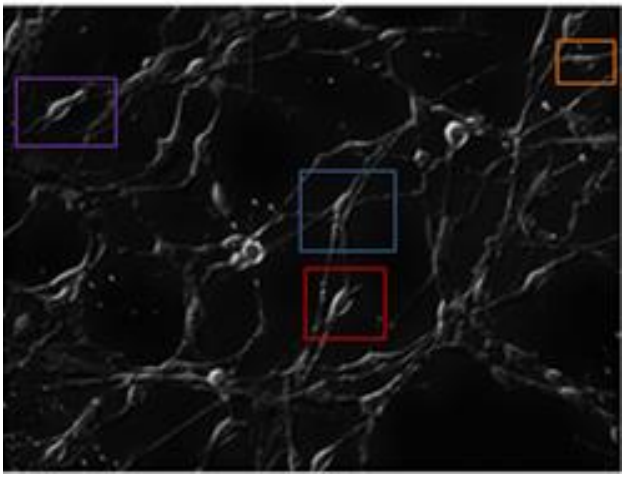

t = 0.5 hrs

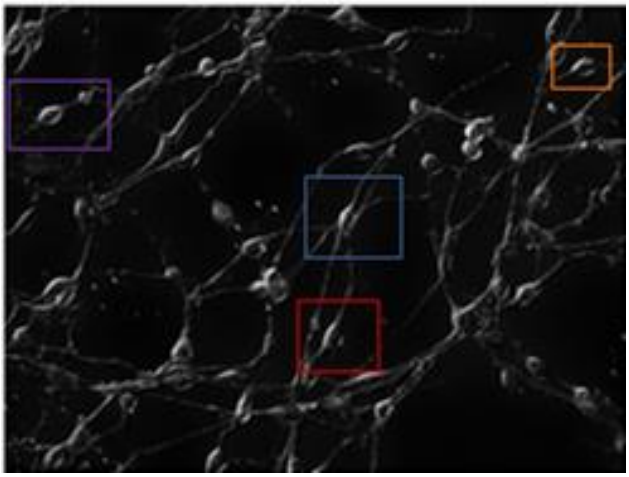

t = 1 hrs

(b)

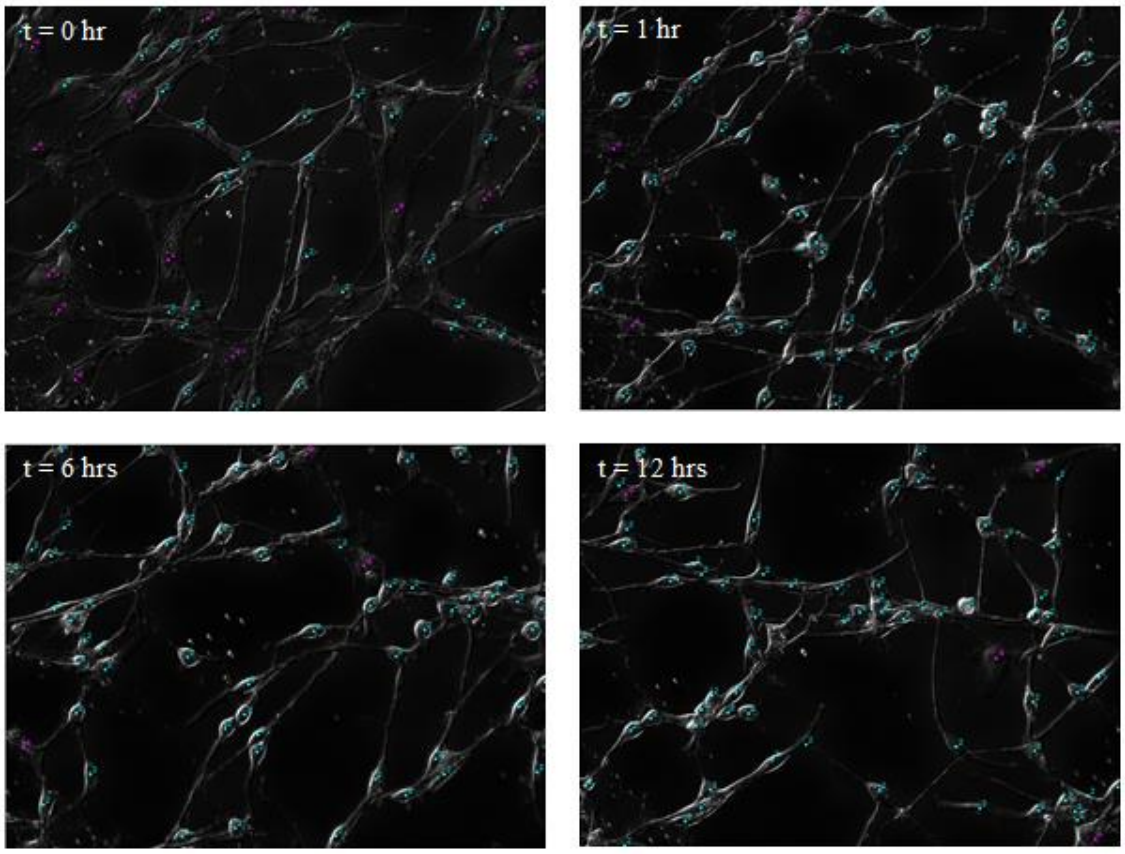

Figure 3.9: Changes in Astrocyte Surface Morphology
Within the first hour of time-lapse recording, cells lacking an electric field (0 $^{mV}/_{mm}$) showed predominantly polygonal cells, shown in orange. Only 8.9% of the cells displayed a bipolar state, shown in purple, and over the course of 12 hours, the number of bipolar cells dwindled down to 1.7%. Without an electrical cue in the form of the electric field, astrocytes assumed a polygonal state, additionally showing limited migration & proliferation, and showed no tendency to shift into the bipolar state. However, over a 12 hour exposure to an electric field of strength 400 $^{mV}/_{mm}$, the astrocytes displayed a rapid shift towards the bipolar morphology. Within the first hour, 69.7% of the cells had a bipolar morphology and 68.5% of the astrocytes still displayed a bipolar morphology at the end of recording. This change in external morphology was maintained throughout the cell exposure of electric fields; the slight variations in numbers were due to the constant migration of astrocytes, resulting in a different group of cells in the region of interest every few hours. Since bipolar morphologies are typically associated with immature astrocytes, this rise in bipolar cells may indicate that an electric field may lead to the reversion of astrocytes to an earlier maturation state, while control cells shifted into a population of mature astrocytes.

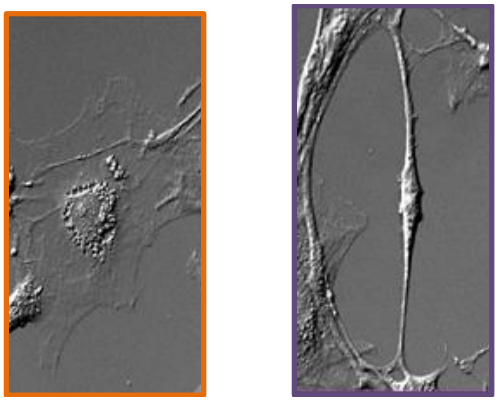

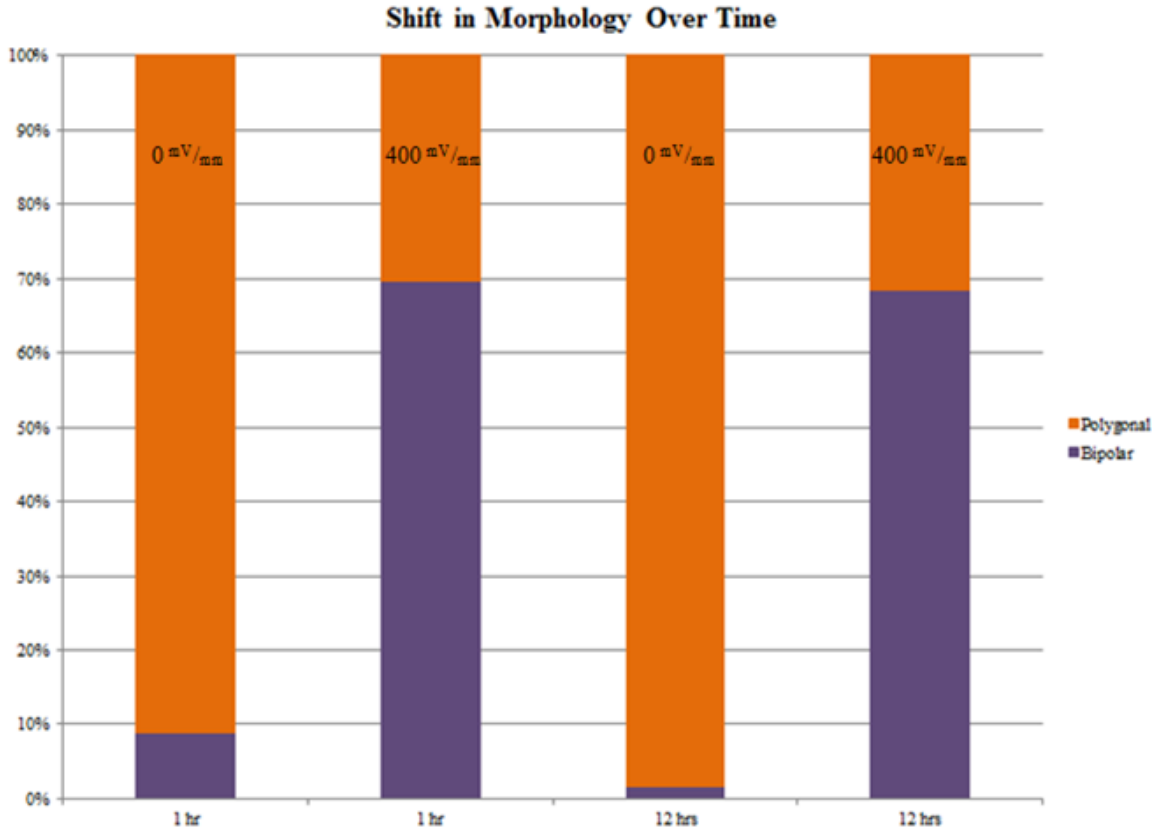
Shift in Morphology Over Time
100%
90%
80%
70%
60%
50%
40%
30%
20%
10%
0%
0 mV/mm
400 mV/mm
0 mV/mm
400 mV/mm
1 hr
1 hr
12 hrs
12 hrs
Polygonal
Bipolar

Staining for nuclear elements and cytoskeleton proteins, as presented in Figure 3.10, highlighted the internal changes in morphology that occur following exposure to an electric field. Astrocytes showed an increase in the amount of intermediate filament vimentin that is expressed, with cells exposed to a field strength of 100 $^{mV}/_{mm}$ displaying large amounts of the protein throughout the cell. This protein, generally associated with immature astrocytes, is seen minimally in control cells (0 $^{mV}/_{mm}$). The change in vimentin expression indicates that astrocytes undergo dedifferentiation into an earlier maturation state, resembling a neural precursor-like cell, in response to an electric field.

The nuclei, which are identified by the DAPI-stained DNA, were clearly larger in cells exposed to an electric field; additionally, the nuclear stain also appeared lighter, indicating that the nuclear elements had spread out and become more diffuse. These nuclear changes indicate that the DNA had transitioned from the tightly-packed hetereochromatin to the loosely-packed euchromatin structure seen during active transcription. The electric field appears to influence the regulatory controls over DNA transcription, leading to the expression of a variety of mRNA and proteins.

While this staining was carried out at an electric field strength of 100 $^{mV}/_{mm}$, the similarities observed in induced astrocyte behaviors between field strengths 400 $^{mV}/_{mm}$ and 100 $^{mV}/_{mm}$ indicate that cells exposed to a field strength of 400 $^{mV}/_{mm}$ would display the same changes in cytoskeletal protein composition. The proportional relationship between the applied electric field strength and the intensity of both astrocyte migration & astrocyte proliferation suggests that at 400 $^{mV}/_{mm}$, astrocytes would show even higher levels of vimentin expression and nuclear conformational changes.

Figure 3.10: Changes in Astrocyte Intracellular Morphology
The red fluorescent stain outlined the astrocyte-specific intermediate filament vimentin while the blue DAPI stain labeled nuclear elements. After exposure to an electric field of 100 $^{mV}/_{mm}$, the levels of vimentin appear to have been up-regulated, with a larger, brighter red stain appearing throughout the cell. The nuclear stain also appears larger and more diffuse; this change in nuclear packing indicates a shift in DNA elements into a more open, active euchromatin conformation. Euchromatin is associated with higher levels of gene expression and protein production, accounting for the observed rise in vimentin. The increase in vimentin, a marker of immature astrocytes, and shift in DNA conformation to favor transcription indicate that in response to an electric field, astrocytes may revert to an earlier maturation state resembling a neural precursor-like cell. Similar changes in morphology can be expected when cells are exposed to an electric field of 400 $^{mV}/_{mm}$.

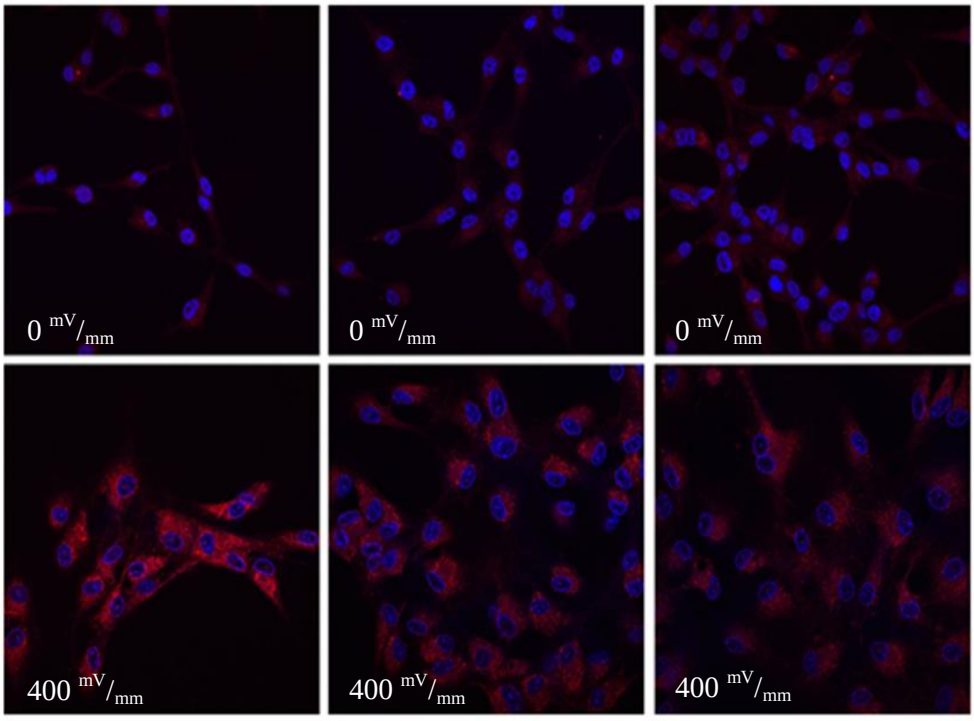
0 mV/mm
0 mV/mm
0 mV/mm
400 mV/mm
400 mV/mm
400 mV/mm

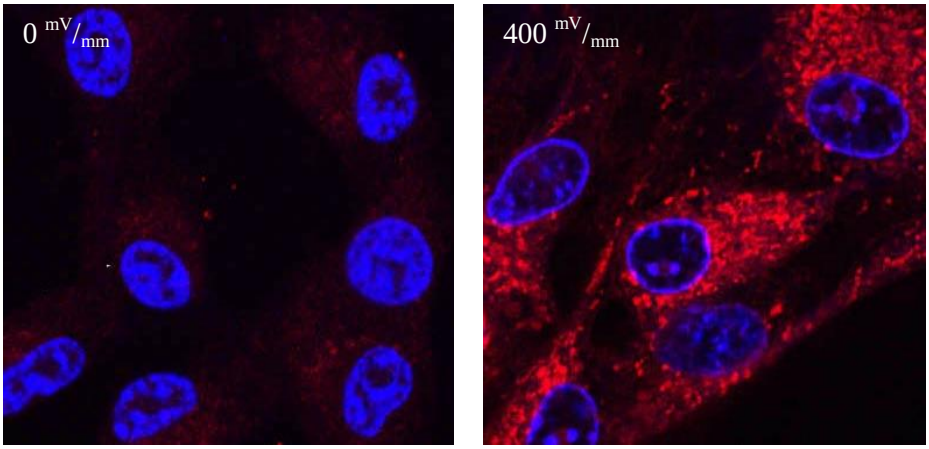
0 mV/mm
400 mV/mm

CHAPTER 4 Discussion

When examining electric fields *in vivo*, adult mammalian tissue exhibit electric fields between 1 & 5 $^{mV}/_{mm}$ (Cao et al., 2013), while developing mammalian tissue exhibit electric fields ranging between 20 & 50 $^{mV}/_{mm}$ (Hotary & Robinson, 1994), showing an elevation in electric current flow. Similar changes in outward current flow are seen in injured mammalian tissue (Khan et al., 1994), where injury potentials with field strengths between 40 & 200 $^{mV}/_{mm}$ are generated (Barker et al., 1982). Injured non-mammalian tissue from vertebrates capable of regeneration, however, show a much more elevated outward current than similarly injured tissue in mammals, generating injury potentials with higher electric field strengths (200+ $^{mV}/_{mm}$) (Borgens et al, 1977). This difference in post-injury electric field strengths appears to be crucial for the varying levels of enhanced wound healing and subsequent regeneration seen in vertebrate tissue.

Following a traumatic neural or spinal injury, some of the initial events that occur *in vivo* include changes in astrocyte directional migration, astrocyte proliferation rate, and changes in astrocyte surface & cytoskeletal morphology. These responses to injury mimic the cellular events seen during embryonic development. An applied external electric field with a field strength of 400 $^{mV}/_{mm}$ was used to emulate the *in vivo* conditions seen in post-injury regenerating tissue; using electric fields, it may be possible to coax astrocytes to exhibit these behaviors *in vitro*. The results from these electric field studies have demonstrated that electric fields have a graded effect on astrocyte behaviors over a 12 hour exposure period. While the overall changes in cell movement, proliferation, and morphology have been observed during both development and post-injury healing, electric field-

induced enhancement of changes in astrocyte behavior and maturity may be the central link between electric field strengths and tissue regeneration.

Astrocytes Influenced by Electric Fields

Astrocytes were shown to exhibit directional movement towards the positive anode in response to an electric field strength of 400 $^{mV}/_{mm}$, with an average velocity of 26.62 $^{\mu m}/_{hr}$ and an average overall displacement of 186.81 μm over a 12 hour period. At this field strength, the maximum velocity observed during a one hour time period was 132.5 $^{\mu m}/_{hr}$; while this number may be an outlier and not represent the average astrocyte, it demonstrates how far an astrocyte is capable of moving in an hour. Astrocytes receiving no electric field (0 $^{mV}/_{mm}$) had an average velocity of 12.40 $^{\mu m}/_{hr}$ with an average displacement of 67.5 μm; however, the bulk of this movement was completely random, with cells often moving in a circular fashion. This corroborates previous *in vitro* scratch studies that have shown that astrocytes move with velocities between 10-30 μm/hr, with an average velocity of 12 $^{\mu m}/_{hr}$ (Kornyei et al., 2000). The application of electric fields clearly enhances astrocyte migration by not only increasing the speed at which the cells move but by also providing a direction for movement.

During the application of an electric field of 400 $^{mV}/_{mm}$ over a 12 hour period, astrocytes showed symmetric division resulting in two identical progeny cells, with the axis of division parallel to the electric field vector. Comparing the cumulative number of divisions seen with an electric field of 400 $^{mV}/_{mm}$ (172) and lacking an electric field (38) showed a 4.5-fold increase in cell division. Similarly, the average rate of cell division was elevated 1.5- to 2-fold during the first 24 hours post-injury in areas adjacent to a wound (Kornyei et al., 2000). Therefore, the application of an electric field mimicking those seen in regenerating animals caused increased proliferation of astrocytes.

Additionally, electric fields have a graded effect on astrocyte behaviors. At the four field strengths tested, the average directional migration velocities at 400 $^{mV}/_{mm}$ (26.62 $^{\mu m}/_{hr}$), 100 $^{mV}/_{mm}$ (22.75 $^{\mu m}/_{hr}$), 10 $^{mV}/_{mm}$ (19.04 $^{\mu m}/_{hr}$), and 0 $^{mV}/_{mm}$ (12.40 $^{\mu m}/_{hr}$) show a linear trend. A linear regression analysis showed that the regression correlation coefficient, represented by r, calculated from a trend line fit to the data was 0.99. Since a r-value of 1 indicates complete linearity, this indicates that the induced cell velocity is proportional to the applied electric field strength. Additionally, the astrocytes exposed to 400 $^{mV}/_{mm}$ or 100 $^{mV}/_{mm}$ showed strong directional movement towards the anode, while astrocytes exposed to 10 $^{mV}/_{mm}$ or 0 $^{mV}/_{mm}$ showed no clear directional movement, often circling around the original starting point.

Similar to migration, a correlation between astrocyte proliferation rates and electric field strength was also noted. At each field strength, the average cumulative cell divisions observed per region of interest over a 12 hour period at 400 $^{mV}/_{mm}$ (8.6), 100 $^{mV}/_{mm}$ (7.0), 10 $^{mV}/_{mm}$ (2.0), and 0 $^{mV}/_{mm}$ (1.9) show a linear trend, though less pronounced. The r-value from the fitted trend line was 0.86, meaning that there is correlation between electric field strength and proliferation rate. However, the absence of complete linearity may be due to the fact that there is a large gap between the number of divisions at higher field strengths (400 $^{mV}/_{mm}$ & 100 $^{mV}/_{mm}$) and those at lower field strengths (10 $^{mV}/_{mm}$ & 0 $^{mV}/_{mm}$).

The morphology of astrocytes also undergo a shift in response to an electric field of 400 $^{mV}/_{mm}$. Within the first hour of electric field exposure, astrocytes immediately shift from a polygonal, flattened morphology into a bipolar shape, with a more rounded nucleus and two processes extending in opposite directions. After the full 12 hours, 96.9% of the cells in any particular region of interest had a bipolar shape; this contrasts greatly with control cells, where 0.05% of cells retain a bipolar morphology. When using staining to examine cytoskeletal protein expression, astrocytes showed a clear increase in the expression of the intermediate filament vimentin, which is classically

observed in immature astrocytes. Additionally, the nucleus appeared larger and slightly more diffuse, indicating that the nuclear elements have opened into a euchromatin form that is associated with active transcription.

Applied Electric Fields Mimic Injury Potentials

When tested with a range of electric field strengths, the resultant astrocyte behaviors were found to be proportional to the field strength. Whereas moderate directional cell migration and increased cell proliferation were seen at 100 $^{mV}/_{mm}$, mimicking injury potentials seen in non-regenerating mammals, much more robust migration and proliferation were seen at a field strength of 400 $^{mV}/_{mm}$, which corresponds to injury potentials in regenerating non-mammals. At 10 $^{mV}/_{mm}$, which is approximately equivalent to endogenous electric fields present in adult mammalian tissue, and the control 0 $^{mV}/_{mm}$, average cell velocities were much lower, with no clear directional movement, and lower levels of cell division was observed.

The strength of the applied electric field appears to be crucial for the intensity of induced cell behaviors. This may explain why amphibians, producing high strength injury potentials in damaged tissue, undergo regeneration while mammals do not. Although mammals do initiate similar astrocytic responses following an injury, the level of this activity is not rapid and comprehensive enough to match the short time frame available for successful structural and functional recovery, instead leading to the creation of an inhibitory post-injury environment. The application of an electric field equivalent to an injury potential generated by a vertebrate capable of regeneration, however, would allow mammalian astrocytes to enhance their post-injury efforts, promoting central nervous system regeneration.

Astrocyte Dedifferentiation in Regeneration

Astrocytes are capable of undergoing cellular dedifferentiation, reverting to a neural precursor-like cell that displays intracellular markers and characteristics of immature radial glial cells, under specific extracellular and tissue conditions (Laywell et al., 2000). One of these conditions includes post-injury damaged tissue, with astrocytes undergoing dedifferentiation in response to hypothermia (Yu et al., 2006), neurotoxic compounds (Wachter et al., 2010) and mechanical injury (Yang et al., 2009) in mammals. Increased levels of the intermediate filament vimentin, a cytoskeletal protein found in immature astrocytes, are observed; while increased levels of GFAP are also observed *in vivo*, this increase is transient and therefore unreliable to truly establish astrocyte dedifferentiation. The external morphology of these cells also shifts to a more bipolar shape, resembling radial glial cells seen during neurodevelopment. Now resembling neural precursor-like cells, the cells, often found at the edge of the wound, undergo high levels of cell division – these daughter cells can differentiate into neurons or glial cells as required for central nervous system regeneration (Walder et al., 2003).

Similar changes in astrocyte behaviors are seen after the application of an electric field of physiological strength (400 $^{mV}/_{mm}$), indicating electric field-induced astrocyte dedifferentiation into a maturation state resembling a neural precursor-like cell. The shift in external morphology to a bipolar shape and the shift in internal cytoskeletal proteins, mainly the increase in vimentin, mimic what is seen *in vivo* post-injury. Additionally, the observed shift in the packing of DNA elements from hetereochromatin to the more open euchromatin conformation is connected with earlier maturation states. This 'unwrapping' of DNA indicates increased transcription and translation of a variety of proteins – in addition to changing the cytoskeletal makeup of astrocytes, transcription & translation factors, molecules for chemotaxis, cell cycle mediators and channels & transporters that are integrated into the cellular plasma membrane can all be generated and/or released for other uses.

The signaling protein sonic hedgehog (Shh), crucial for normal patterning of the central nervous system in development and maintenance of neural stem cells (Palma et al. 2005), is believed to be one of the modulators of astrocyte dedifferentiation. The expression of Shh is increased post-injury, and blocking Shh signaling using a neutralizing antibody prevents cell dedifferentiation. Shh regulates numerous genes and proteins involved with cell proliferation and potential regeneration, including the transcription factor Gli2 and the protein cyclin D1, leading to altered gene expression and cell cycles (Yang et al., 2012). While other proteins may be involved in regulating astrocyte dedifferentiation and associated gene expression, this control over DNA transcription seen following electric field application could play a crucial role in coordinating multiple astrocytic behaviors, an important role in post-injury tissue regeneration.

In response to an electric field, astrocytes revert to a bipolar shape similar to that associated with radial glia, cells which are capable of migration during neurodevelopment, and migrate towards the positively-charged anode. This is similar to cells moving *in vivo* towards the injury site, which is experiencing a shift in positively-charged sodium ions in response to disruptions to the epithelium. The sudden displacement of sodium ions that generates the injury potential is possibly the initial cue for astrocyte migration to the injury site. The Na-H exchanger (NHE-1) in particular is a membrane protein that can amplify these migratory cues (Denker & Barber, 2002); in response to the changing sodium levels, the NHE-1 can coordinate adhesion molecules with the cytoskeleton for directional migration to occur.

Additional changes in membrane potentials from various voltage-gated channels and intracellular signaling cascades can redistribute components of the plasma membrane as well as recruiting extracellular proteins can also promote astrocyte movement. In particular, voltage-gated calcium (Ca^{++}) channels, which are known to regulate intracellular calcium concentrations & cell signaling pathways, seem a likely candidate for the observed dedifferentiation and resulting migration, since

they are expressed much more highly in immature astrocytes and not detected in mature astrocytes (Achour et al., 2010). Inwardly rectifying potassium (K^+) channels, which play a role in astrocyte potassium buffering and are up-regulated post-injury (Bordley et al., 2000), and other voltage-gated potassium channels can recruit integrins, or proteins that modulate cell attachments, and aid cell migration (Brown & Dransfield, 2008). This directional cell movement results in a larger number of cells possessing neural precursor-like characteristics at the injury site, possibly leading to broader, more active regeneration with a higher chance of functional recovery.

After the injury potential is established *in vivo* and astrocytes have migrated to the injury site, astrocytes then release cytokines and other chemical guidance cues for further cell migration to the damaged tissue. These additional molecules and cells then form both the structural and biochemical aspects of the glial scar, blocking off the damaged area. However, tissue from animals capable of regenerating do not release extracellular substances used in the glial scar. Mammalian astrocyte dedifferentiation produces a cell similar to the astrocytes seen in regenerating non-mammalian damaged tissue. Since preventing the glial scar from forming appears to be one of the main mechanisms that regenerating tissue uses, applied electric fields could be used to induce this cell maturation state, preventing the release of molecules associated with the glial scar and promoting regeneration.

At the site of injury, the damaged areas show high levels of cell division so that the resultant daughter cells can begin to repair and fill the damaged tissue. This change in proliferation rate, both *in vivo* & *in vitro*, indicates a change in cell cycle regulation through changes in concentration of cyclins, cyclin dependent kinases, and other related proteins. Electric field studies have shown that the axis of division is oriented parallel to the applied electric field vector; therefore, the mitotic spindle aligns perpendicular with the electric field vector. The orientation of the cell division axis is critical for normal growth and development, as it determines the fate of future daughter cells

making it an important aspect of healing and regeneration (Thery et al, 2007). The appropriate cell-cell contacts and adherens junctions are required for the proper orientation of mitotic spindles and symmetrical division (Gotz & Huttner, 2005). The daughter cells can then integrate into the developing central nervous system tissue as mature neurons or glial cells (Ge et al., 2012).

These changes in astrocyte proliferation are believed to be controlled by signals that both trigger and sustain increased cell division over a lengthy period of time. Fibroblast growth factor (FGF) is an important signaling molecule during neural development that is up-regulated post-injury and sustains the proliferation of neural progenitor cells, improving both neural survival and functional recovery of the central nervous system (Teng et al., 1998). Following tail amputation, the application of FGF reduced neuron death and improved spinal cord regeneration in newts (Zhang et al., 2000). However, a similar application of FGF to a rat brain triggered reactive astrogliosis, which can often be inhibitory to neurite outgrowth and regeneration (Eclancher, 1996). This difference between regenerating and non-regenerating animals indicates that mammalian astrocytes have lost the ability to dedifferentiate and associated regenerative abilities (Ferretti et al., 2003). An applied electric field could be the activating factor to trigger mammalian cell dedifferentiation, unlocking the potential to regenerate the central nervous system that is readily seen in amphibians.

Applied Electric Fields & Human Regeneration

As the research done with electric field studies continues to grow, thereby expanding our knowledge of electrophysiology, externally applied electric fields are beginning to be implemented in a wide variety of therapies. Endogenous electric fields with high field strengths have been observed extensively in amphibians, existing around sites of injury and promoting regeneration of entire limbs or organs. Mammalian cells show similar changes in behavior and physiology in response to an applied electric field *in vitro*, with the effects of electric fields on various cell types now being

studied more extensively (as presented in Table 1.1). Focusing on the influence electric fields have on astrocytes, in conjunction with their roles post-injury, can help create an effective therapy for human central nervous system regeneration.

A common mammalian model used to study the application of electric fields is the wounded cornea, due to the potential difference created post-injury from disruption of continuous ion transport. Human corneal epithelial cells show directional migration and altered frequency and orientation of cell division in response to an electric field; these induced behaviors are believed to be caused by various growth factors and the redistribution of their associated receptors within the plasma membrane (McCaig, 2011). Rabbit cornea also show nerves sprouting from the ophthalmic nerve, moving towards the damaged area in parallel nerve bundles, with the direction and extent of growth being controlled by the electric field. Similarly, human keratinocytes also move and reorient themselves in response to an electric field, using growth factors, such as EGF, and ions channel/receptors (Pullar, 2011). Applied electric fields are believed to override any other cues present in the environment, altering transcription and signaling pathways to enhance wound healing and wound closure rates in humans (Zhao et al., 2010). Current wound treatments also target the endogenous electric field, using pharmacological therapies to enhance the electric field strength, often by altering the sodium current. The Dermacorder, a newly developed instrument that non-invasively measures the electric fields generating by wounds in human skin, can be used to further monitor and enhance wound healing (Nuccitelli, 2011).

Applied electric fields also have effects on vasculature, musculature, and bone. Angiogenesis can be enhanced using an electric field by activating pro-angiogenic pathways (involving growth factors such as VEGF) as well as influencing the migration, elongation, alignment, and division of endothelial cells, even regulating the direction of new blood vessel formation (Wang et al, 2011). Electric fields can also change multiple aspects of the musculoskeletal system, altering the cellular

behaviors of bovine chondrocytes, rabbit fibroblasts, and human osteoblasts & osteoclasts (Gunja et al, 2011). Following a fracture, an applied electric field can stimulate bone growth and increase bone rejoining by changing the gene expression of growth factors and signaling molecules (Ciombor & Aaron, 2005). Some therapies have even utilized an implant that provides a constant electric field to the fractured area in humans (Goldstein et al., 2010).

When examining the central nervous system, post-injury potentials similar to those seen at the epithelium are observed in mammals such as rodents, cats, dogs, and guinea pigs. Neural regeneration does not readily occur in mammals due to the post-injury inhibitory environment; however, applied electric fields can be used to direct outgrowing neurites through this inhibition, controlling the direction and rate of growth of rodent future axons & dendrites. When using *in vivo* animal models, rats with central nervous system injuries (spinal cord compression) that were exposed to an electric field showed marked behavioral recovery, especially when compared to sham animals not receiving electric fields (Wallace et al., 1987). Guinea pigs with transected spinal cords also showed both reduced axonal degeneration and axonal regrowth in response to electric fields (Zuberi et al., 2008). Interestingly, this regrowth was seen in the glial scar, with the growth cone often projecting through the glial scar to the opposite side of the spinal cord (Borgens & Bohnert, 1997). This implies that the electric field overrides the inhibitory cues and molecules present post-injury that inhibit this level of regeneration. The regeneration of certain ascending fibers and pathways led to functional motor improvement (Borgens et al., 1986). Additional *in vivo* electric field studies using dogs with severe spinal cord injuries showed similar results, with improved motor functions when compared to sham dogs (Borgens et al., 1999).

The results seen in mammals have led to initial human clinical trials using applied electric fields to treat humans paralyzed due to spinal cord injuries, leading to total sensory & motor loss. An implant that provided an electric field internally to the spine led to recovery of limited motion and light

sensations in the upper and lower extremities in 14 patients over the course of a year (Shapiro et al., 2005). This *in vivo* method has shown that electric fields are capable of reestablishing damaged ascending (sensory) and descending (motor) axonal pathways. However, electric fields alone only lead to slight, partial regeneration.

The work done on applied electric fields of physiological strengths in conjunction with astrocytes and growing neurites (Alexander et al., 2006) indicates that more pronounced and overall regeneration is possible in the human central nervous system. Further electric field studies done with astrocytes show that their electric field-induced behaviors, including directing outgrowing neurites and astrocyte dedifferentiation to a neural precursor-like cell, strengthen this idea. Additionally, human neural stem cells, which can be recruited to damaged areas of the brain and spine, migrate *in vitro* in response to an applied electric field (Feng et al., 2012), showing that other components of the human central nervous system respond similarly to electric fields. The electric field studies done both *in vitro* and *in vivo* have shown that electric fields have the potential to control and amplify regeneration of various human tissues and systems, including the central nervous system. Electrical fields, when used with the normally inhibitory astrocytes, can lead to major strides in human central nervous system regeneration.

Electric Fields & Other Glial Cells

The damaged central nervous system, while capable of regeneration, often fails to do so due to the inhibitory environment encountered post-injury. Astrocytes, the predominant glial cells found in the mammalian central nervous system, have a major role in creating this inhibition. Applied electrical fields are capable of overriding currently existing chemical cues *in vivo*; in the case of astrocytes, induced cell behaviors may then enhance central nervous system regeneration. The effects of electric fields on other glial cells have not been extensively studied; since other glial cells are linked

with development and maintenance of the post-injury environment, they may play similar roles in post-injury regeneration (Qiu et al., 2000). Due to the multiple factors and cell types involved in potential central nervous system regeneration, a combination of therapies would most likely produce the most successful results, with the highest potential to regain structure and functionality post-injury.

Oligodendrocytes, which arise from many of the same progenitor cells as astrocytes, produce a combination of proteins & lipids to form a myelin sheath around axons in the central nervous system (Bradl & Lassmann, 2010). In opossum newborns, the onset of myelination coincides with the loss of regenerative capacity (Ghooray & Martin, 1993) – this indicates that myelin proteins, such as the common myelin-associated glycoprotein MAG, inhibit mammalian central nervous system regeneration. Following an injury, damaged neurons typically lose their myelin sheath; adult oligodendrocytes are incapable of re-myelinating axons post-injury (Vick et al., 1992). This unattached myelin, as well as the forming glial scar at the injury site, exposes neurites to myelin-associated inhibitors, further preventing regeneration. Using specific antibodies against these inhibitory substances to block their effects, however, would permit regeneration at the site of injury (Chen et al., 2000). An injured opossum spinal cord, when treated with an antibody against the Nogo protein, displayed neurite outgrowth patterns consistent with those seen in younger animals that are capable of spinal cord regeneration (Varga et al., 1995). Similar outcomes in other mammals such as rats (Dyer et al., 1998) highlight the role that oligodendrocytes and myelin play in repressing central nervous system regeneration.

While oligodendrocytes produce myelin sheaths in the central nervous system, Schwann cells conduct a similar role in the peripheral nervous system. The presence of Schwann cells may be one of the key differences contributing to peripheral nervous system regeneration, possibly by creating an environment more permissive to neurite outgrowth (Bradl & Lassman, 2010). Schwann cells are

capable of regenerating and re-innervating neurons (Huebner & Strittmatter, 2009) as well as re-myelinating post-injury surviving axons (Blight & Young, 1989) in rats & cats. A graft of peripheral nervous tissue, when inserted into the spinal cord, enhances growth of central nervous system axons (Richardson et al., 1980), with Schwann cells directing neurite growth in a manner similar to astrocytes (Thompson & Buettner, 2006). Applying an electric field *in vitro* enhanced this Schwann cell-directed neurite outgrowth in rats (Koppes et al., 2010), and Schwann cells displayed anodal migration in response to an electric field *in vitro* (McKasson et al., 2008). The similarities between induced cell behaviors in astrocytes and Schwann cells, including their influence on growing neurites and directional migration, indicates that Schwann cells could also be used to promote regeneration.

Due to the multiple factors and cell types involved in potential central nervous system regeneration, a combination of therapies would most likely produce the most successful results, with high structural and functional recovery post-injury. Pharmacological approaches have already begun to use multiple approaches simultaneously – using chondroitinase ABC to break down the inhibitory glial scar component CSPG alongwith anti-Nogo-A antibody to neutralize myelin-associated inhibitors has led to greater numbers of axons regenerating than using each treatment singularly (Zhao et al., 2013). Glial cells can also be used to enhance the minimal spontaneous regeneration that is seen *in vivo*, while electric fields used with glia cells can override any other chemical guidance cues and induce neurite outgrowth in a specific direction. Both oligodendrocytes (Ankerhold & Stuermer, 1999) and Schwann cells (Nagoshi et al., 2011) undergo cellular dedifferentiation post-injury, similar to that seen in astrocytes. If oligodendrocytes showed dedifferentiation in response to an applied electric field, this could lead to remyelination of newly formed central nervous system axons, a critical step for functional recovery which is typically carried out by limited oligodendrocytes precursor cells *in vivo* (Keirstead & Blakemore, 1999). Post-injury astrocytes have been shown to inhibit the differentiation of these oligodendrocytes

precursor cells, highlighting not only the importance of each cell type but also their roles in tandem (Wang et al., 2011). Using a combination of electric fields to switch glia into neural precursor-like cells, pharmacological agents to negate the effects of growth inhibitors, and even the possible use of implanted bridges pre-coated with growth factors to direct neurite outgrowth (McCaig et al., 2000) may be the best method to treat central nervous system injuries and recover full functionality.

Cell Culture Limitations

Currently, the work done with electric fields involving their influence on astrocytes and potential in central nervous system regeneration has been *in vitro*. The nature of cell cultures, with flasks reaching confluency and needing to be split into new ones, indicates that astrocytes in cultures do not mature to the degree that occurs *in vivo* (Banker & Goslin, 1992). When replicating these findings *in vivo* in an animal model, the different environment may lead to slightly varied responses to an applied electric field. The cell culture media contains astrocyte-specific growth factors used to optimize cell growth, while the plates are coated in extracellular matrix proteins (poly-L-lysine, fibronectin) – these conditions are not seen *in vivo*. An animal model or *in vivo* system also experiences shifts in temperature, pH, and CO_2 concentrations that aren't seen in artificial conditions. On a broader level, autocrine and paracrine signaling between astrocytes and other component of the nervous system (neurons, macroglia, vasculature) may alter the extent to which astrocytes, as well as other cells, respond to electric fields. The applied electric field may also be diminished or distorted *in vivo* due to differences in tissue conductivity and the presence of a glial scar and its related molecules post-injury.

The levels of the electric field-induced cell behaviors may also differ when shifting from *in vitro* to *in vivo*. Astrocyte migration occurs much more quickly when cells are not attached to each other than when they are connected to each other or form a sheet. *In vitro*, migrating cells tend to move

into open spaces, where they are often loosened from neighboring cells and released from contact inhibition. The lack of 'open' spaces and the retention of these intercellular connections between astrocytes indicate that electric field-induced migration may be more difficult in an *in vivo* system. Additionally, as cells reach confluency, the rate of cell proliferation decreases (Kornyei et al., 2000), which is not a concern when regenerating damaged tissue – the rate of *in vivo* astrocyte proliferation, therefore, may be even higher than believed.

The dedifferentiated astrocyte, which now resembles radial glia, also demonstrate symmetrical division. During development, however, radial glia (which later turn into astrocytes) show symmetric, proliferative divisions and asymmetric, neurogenic divisions that lead to differing daughter cells, some of which are capable of becoming neurons. This is due to the attachment of radial glial cells to nervous tissue and the orientation of their axis of division. The electric field causes orientation of the mitotic spindle and cleavage furrow; however, since the glia weren't attached to anything *in vitro*, no asymmetric divisions were observed. An *in vivo* system, however, may allow further asymmetric divisions that lead to a larger population of neural precursor-like cells; further signaling with components of the central nervous system can then allow these cells to differentiate into neurons, replacing the lost cells while integrating themselves into damaged tissue.

The astrocytes used in these electric field studies were derived from post-natal rat cerebellum. There are three types of mammalian cerebellar astrocytes – the conventional 'bushy' protoplasmic astrocytes, the rare 'smooth' protoplasmic astrocytes, and Bergmann glial cells (Yamada & Watanabe, 2002). Bergmann glia, which are associated with formation & maintenance of the cerebellum during development and make up about 15% of the adult cerebellum, retain features found in cortical radial glial cells. These cells have low levels of GFAP and high levels of vimentin & nestin, resembling immature astrocytes (Gotz, 2013). Radial glial cells, which function as adult neural stem cells, are commonly found in the spinal cord of lower vertebrates (Reichenbach &

Wolburg, 2013), which indicates a greater level of regenerative plasticity in these animals. Mammalian cerebellar astrocytes were therefore chosen for these electric field studies due to the presence of Bergmann glial cells in order to mimic the cell types encountered in the mammalian spinal cord. Since the cerebellum is considered a more primitive neural structure, there may be less evolutionary dissimilarities between regenerating and non-regenerating animals, giving mammalian astrocytes exposed to an electric field a higher chance of duplicating cell behaviors seen in amphibian astrocytes.

However, the presence of Bergmann glia and other astrocytes with more immature phenotypes may skew the staining and misrepresent the level to which cytoskeletal changes are occurring during dedifferentiation. These astrocytes, while staining positively for GFAP, always express far more vimentin regardless of an electric field. It is possible that this lack of GFAP may be due to the fact that astrocyte cultures never reach complete maturity due to culturing conditions. To measure the true extent of dedifferentiation and changes in protein production seen in response to an electric field of 400 $^{mV}/_{mm}$, astrocytes from a different subpopulation of the rat brain (ex. cortical, hippocampal) can be tested and subsequently stained.

Future Electric Field Studies

Nearly all previous studies conducted on electric fields and their effects on cell types have focused on a limited number of field strengths. Since showing that the intensity of astrocyte responses depends on the applied electric field strength, previous studies can be revisited to see whether other cell types display graded behaviors or even entirely different cell behaviors in response to an electric field. After finishing the current studies on electric fields and astrocytes, future work with central nervous system regeneration would also include *in vitro* electric field studies on other glial cells, possibly from varying regions of the nervous system as well as different mammals, before

moving to an *in vivo*, animal model or human study. In order to enhance structural and functional post-injury recovery, electric fields could also be combined with pharmacological treatments and coated bridges placed at the injury site.

However, there are aspects of an *in vivo* system that may affect the overall response to applied electric fields, such as the impact of intracellular and intercellular signaling between multiple aspects of the central nervous system, and the wide variability of development in different regions of the brain, both within the same animal and when compared to humans. As the size of an animal increases, so does the size of its brain (and its individual components), becoming increasingly complex – humans and primates possess additional layers of astrocytes with characteristic domains and processes (Oberheim et al., 2006). These unpredicted factors and interactions suggest that electric field studies should first be carried out *in vitro* on slice cultures before moving to animal models.

Conclusions

Electric fields are present throughout development and following injury, playing critical roles in controlling mammalian regeneration. This study demonstrated that in response to an applied electric field strength of physiological field strength, astrocytes exhibit directional cell migration, increased cell proliferation, and cytoskeletal changes indicative of cell dedifferentiation. This effect of electric fields on interdependent astrocyte behaviors is crucial for central nervous system regeneration and can be used to develop therapies to promote the regrowth of damaged neural and spinal pathways following a traumatic injury, ultimately leading to full functional recovery.

Literature Cited

Abbott NJ, Ronnback L, Hansson E. Astrocyte-endothelial interactions at the blood brain barrier. *Nature Reviews Neuroscience*. 2006; 7(1):41-53.

Achour BS, Pont-Lezica L, Bechade C, Pascual O. Is astrocyte calcium signaling relevant for synaptic plasticity? *Neuron Glia Biology*. 2010; 6(3):147-155.

Alexander J, Fuss B, Colello R. Electric field-induced astrocyte alignment directs neurite outgrowth. *Neuron glia biology*. 2006; 2(2):93-103.

Altizer AM, Moriarty LJ, Bell SM, Schreiner CM, Scott WJ, Borgens RB. Endogenous electric current is associated with normal development of the vertebrate limb. *Developmental Dynamics*. 2001; 221(4):391-401.

Altizer AM, Stewart SG, Albertson BK, Borgens RB. Skin flaps inhibit both the current of injury at the amputation surface and regeneration of that limb in newts. *Journal of Experimental Zoology*. 2002; 293:467-477.

Ankerhold R, Stuermer CA. Fate of oligodendrocytes during retinal axon degeneration and regeneration in the goldfish visual pathway. *Journal of Neurobiology*. 1999;41(4):572-584.

Babona-Pilipos R, Popovic MR, Morshead CM. A galvanotaxis assay for analysis of neural precursor cell migration kinetics in an externally applied direct current electric field. *Journal of Visualized Experiments*. 2012; 68.

Banker G, Goslin K. Astroglia in culture. In: Banker G, Goslin K, eds. *Culturing nerve cells.* 2nd ed. Cambridge, MA: Massachusetts Institute of Technology; 1992:309-336.

Barker AT, Jaffe LF, Vanable JWJ. The glabrous epidermis of cavies contains a powerful battery. *American Journal of Physiology*. 1982; 242(3):R358-R366.

Batter DK, Corpina RA, Roy C, Spray DC, Hertzberg EL, Kessler JA. Hetereogeneity in gap junction expression in astrocytes culutured from different brain regions. *Glia*. 1992; 6(3):213-221.

Berman JM, Awayda MS. Redox artifacts in electrophysical recordings. *American Journal of Physiology*. 2013; 304(7):C604-C613.

Blight AR, Young W. Central axons in injured cat spinal cord recover electrophysical function following remyelination by schwann cells. *Journal of Neurological Science*. 1989; 91(1-2):15-34.

Bonfanti L, Peretto P. Adult neurogenesis in mammals - a theme with many variations. *European Journal of Neuroscience*. 2011; 34(6):930-950.

Bordey A, Hablitz JJ, Sontheimer H. Reactive astrocytes show enhanced inwardly rectifying K+ currents in situ. *NeuroReport*. 2000; 11(14):3151-3155.

Borgens RB, Blight AR, Murphy DJ, Stewart L. Transected dorsal column axons within the guinea pig spinal cord regenerate in the presence of an applied electric field. *Journal of Comparative Neurology*. 1986; 258:168-180.

Borgens RB, Bohnert DM. The responses of mammalian spinal axons to an applied DC voltage gradient. *Experimental Neurology*. 1997; 145:376-389.

Borgens RB, Toombs JP, Breur G, et al. An imposed oscillating electric field improves the recovery of function in neurologically complete paraplegic dogs. *Journal of Neurotrauma*. 1999; 16(7):639-657.

Borgens RB, Vanable JW, Jaffe LJ. Bioelectricity and regeneration: Large currents leave the stumps of regenerating newt limbs. *Proceedings of the National Academy of Sciences of the United States of America*. 1977; 74(10):4528-4532.

Borgens RB, Shi R, Mohr TJ, Jaeger CB. Mammalian cortical astrocytes align themselves in a physiological voltage gradient. *Exp Neurol*. 1994; 128(1):41-49.

Bradl M, Lassmann H. Oligodendrocytes: Biology and pathology. *Acta Neuropathologica*. 2010; 119(1):37-53.

Brighton CT, Okereke E, Pollack SR, Clark CC. *In vitro* bone-cell response to a capacitively coupled electric field. the role of field strength, pulse pattern, and duty cycle. *Clinical Orthopaedics and Related Research*. 1992; 285(255):262.

Brockes JP. Amphibian limb regeneration: Rebuilding a complex structure. *Science*. 1997; 276:81-87.

Brown SB, Dransfield I. Electric fields and inflammation: May the force be with you. *Scientific World Journal*. 2008; 8(1280):1294.

Buffo A, Rite I, Tripathi P, et al. Origin and progeny of reactive gliosis: A source of multipotent cells in the injured brain. *Proceedings of the National Academy of Sciences of the United States of America*. 2008;105(9):3581-3586.

Cao L, Wei D, Reid B, et al. Endogenous electric currents might guide rostral migration of neuroblasts. *EMBO Reports*. 2013; 14(2):184-190.

Chao PH, Roy R, Mauck RL, Liu W, Valhmu WB, Hung CT. Chondrocyte translocation response to direct current electric fields. *Journal of Biochemical Engineering*. 2000; 122(3):261-267.

Chen MS, Huber AB, van der Haar ME, et al. Nogo-A is a myelin-associated neurite outgrowth inhibitor and an antigen for monoclonal antibody IN-1. *Nature*. 2000; 403(6768):434-439.

Ciombor DM, Aaron RK. The role of electrical stimulation in bone repair. *Foot and ankle clinics*. 2005; 10(4):579-593.

Colello RJ, Alexander JK. Electrical fields: Their nature and influence on biological systems. In: Morkoc H, ed. *Advanced semiconducter and organic nano-techniques.* San Diego, California: Elsevier; 2003:319-346.

Cork RJ, McGinnis ME, Tsai J, Robinson KR. The growth of PC12 neurites is biased towards the anode of an applied electric field. *Journal of Neurobiology*. 1994; 25(12):1509-1516.

Davies MP, An RH, Doevendans P, Kubalak S, Chien KR, Kass RS. Development changes in ionic channel activity in the embryonic murine heart. *Circulation Research*. 1996; 78(1): 15-25.

Dawley EM, O Samson S, Woodard KT, Matthias KA. Spinal cord regeneration in a tail autotomizing urodele. *Journal of Morphology*. 2012; 273(2):211-225.

Denker SP, Barber DL. Cell migration requires both ion translocation and cytoskeletal anchoring by the Na-H exchanger NHE1. *Journal of Cell Biology*. 2002; 159(6):1087-1096.

Doetsch F. The glial identity of neural stem cells. *Nature Neuroscience*. 2003;6(11):1127-1134.

Doetsch F, Caille*f* I, Lim DA, Garci*f*a-Verdugo JM, Alvarez-Buylla A. Subventricular zone astrocytes are neural stem cells in the adult mammalian brain. *Cell*. 1999; 97(6):703-716.

Dyer JK, Bourque JA, Steeves JD. Regeneration of brainstem-spinal axons after lesion and immunological disruption of myelin in adult rat. *Experimental Neurology*. 1998; 154(1):12-22.

Eclancher F, Kehrli P, Labourdette G, Sensenbrenner M. Basic fibroblast growth factor (bFGF) injection activates the glial reaction in the injured adult rat brain. *Brain Research.* 1996; 737(1-2):201-214.

Ekmark-Lewén S, Lewén A, Israelsson C, et al. Vimentin and GFAP responses in astrocytes after contusion trauma to the murine brain. *Restorative Neurology & Neuroscience*. 2010; 28(3):311-321.

Erickson CA, Nuccitelli R. Embryonic fibroblast motility and orientation can be influenced by physiological electric fields. *Journal of Cell Biology*. 1984; 98(1):296-307.

Fawcett J. Astrocytes and axon regeneration in the central nervous system. *Journal of Neurology*. 1994; 241:S25-S28.

Feng JF, Liu J, Zhang XZ, et al. Guided migration of neural stem cells derived from human embryonic stem cells by an electric field; stem cells. *Stem Cells*. 2012; 30(2):349-355.

Ferretti P, Zhang F, O'Neill P. Changes in spinal cord regenerative ability through phylogenesis and development: Lessons to be learnt. *Developmental Dynamics*. 2003; 226(2):245-256.

Ferrier J, Ross SM, Kanehisa J, Aubin JE. Osteoclasts and osteoblasts migrate in opposite directions in response to a constant electrc field. *Journal of Cellular Physiology*. 1986; 129(3):283-288.

Filous AR, Miller JH, Coulson-Thomas YM, Horn KP, Alilain WJ, Silver J. Immature astrocytes promote CNS axonal regneration when combined with chondroitinase ABC. *Developmental Neurobiology*. 2010; 70(12):826-841.

Floyd TL. Ohm's law, energy, and power. In: *Electric circuit fundamentals.* 7th ed. Upper Saddle River, New Jersey: Pearson Prentice Hall; 2007:74-100.

Freeman MR. Specification and morphogenesis of astrocytes. *Science*. 2010; 330(6005):774-748.

Ge WP, Miyawaki A, Gage FH, Jan YN, Jan LY. Local generation of glia is a major astrocyte source in postnatal cortex. *Nature*. 2012; 484(7394):376-380.

Gentzkow GD. Electrical stimulation to heal dermal wounds. *Journal of Dermatological Surgery and Oncology*. 1993; 19(8):753-758.

Ghooray GT, Martin GF. The development of myelin in the spinal cord of the north american opossum and its possible role in loss of rubrospinal plasticity. *Brain Research. Developmental Brain Research*. 1993; 72(1):67-74.

Ghooray GT, Martin GF. Development of radial glia and astrocytes in the spinal cord of the north american opossum (didelphis virginiana). *Glia*. 1993; 9(1):1-9.

Giaume C, Venance L. Intracellular calcium signaling and gap junctional communication in astrocytes. *Glia*. 1998; 24(1):50-64.

Goldstein S, Sprague S, Petrisor BA. Electrical stimulation for fracture healing: Current evidence. *Journal of Orthopaedic Trauma*. 2010; 24:S62-S65.

Gotz M. Radial glial cells. In: Kettenmann H, Ransom BR, eds. *Neuroglia.* 3rd ed. New York, NY: Oxford University Press; 2013:50-61.

Gotz M, Huttner WB. The cell biology of neurogenesis. *Nature Reviews Molecular Cell Biology*. 2005; 6(10):777-788.

Gruler H, Nuccitelli R. Neural crest cell galvanotaxis: New data and a novel approach to the analysis of both galvanotaxis and chemotaxis. *Cell Motility and the Cytoskeleton*. 1991; 19(2):121-133.

Gunja NJ, Hung CT, Bulinski JC. Effects of DC electric fields on migration of cells of the musculoskeletal system. In: Pullar CE, ed. *The physiology of bioelectricity in development, tissue regeneration, and cancer.* 1st ed. Boca Raton, FL: CRC Press; 2011:186-200.

Haugland RP. Antibodies, avidins, and lectins. In: *Handbook of fluorescent probes and research chemicals.* 5th ed. Eugene, OR: Molecular Probes, Inc.; 1992.

Hinkle L, McCaig CD, Robinson KR. The direction of growth in differentiationg neurones and myoblasts from frog embryos in an applied electric field. *Journal of Physiology*. 1981; 314:121-135.

Hotary KB, Robinson KR. Endogenous electrical currents and voltage gradients in xenopus embryos and the consequences of their disruption. *Developmental Biology*. 1994; 166(2):789-800.

Hotary KB, Robinson KR. Evidence of a role for endogenous electric fields in chick embryo development. *Development*. 1992; 114(4):985-996.

Huang R, Peng L, Hertz L. Effects of a low-voltage static electric field on energy metabolism in astrocytes. *Bioelectromagnetics*. 1997; 18:77-80.

Huebner EA, Strittmatter SM. *Results & Problems in Cell Differentiation*. 2009; 43:339-351.

Illingworth CM, Barker CT. Measurement of electrical currents emerging during the regeneration of amputated fingertips in children. *Clinical Physics & Physiological Measurement*. 1980; 1:87-89.

Iten LE, Bryant SV. Stages of tail regeneration in the adult newt, notophtalmus viridescens. *Journal of Experimental Zoology*. 1976; 196(3):283-292.

Jaffe LF, Poo MM. Neurites grow faster towards the cathode than the anode in a steady field. *Journal of Experimental Zoology*. 1979; 209(1):115-128.

Jenkens LS, Duerstock BS, Borgens RB. Reduction of the current of injury leaving the amputation inhibits limb regeneration in the red spotted newt. *Developmental Biology*. 1996; 178:251-262.

Khan T, Myklebust J, Swiontek T, Sayers S, Dauzvardis M. Electrical field distribution within the injured cat spinal cord: Injury potentials and field distribution. *Journal of Neurotrauma*. 1994; 11(6):699-710.

Koppes AN, Seggio AM, Thompson DM. Neurite outgrowth is significantly increased by the simultaneous presentation of schwann cells and moderate exogenous electric fields. *Journal of Neural Engineering*. 2011; 8(4).

Kornyei Z, Czirok A, Vicsek T, Madarasz T. Proliferative and migratory responses of astrocytes to *in vitro* injury. *Journal of Neuroscience Research*. 2000; 61(4):421-429.

Laywell ED, Rakic P, Kukekov VG, Holland EC, Steindler DA. Identification of a multipotent astrocytic stem cell in the immature and adult mouse brain. *Proceedings of the National Academy of Sciences of the United States of America*. 2000; 97(25):13883-13888.

Li GN, Hoffman-Kim D. Evaluation of neurite outgrowth anisotropy using a novel application of circular analysis. *Journal of Neuroscience Methods*. 2008; 174:202-214.

Li L, El-Hayek YH, Liu B, Chen Y, Gomez E, Wu X. Direct-current electrical field guides neuronal stem/progenitor cell migration. *Stem Cells*. 2008; 26(8):2193-2200.

Lin F, Baldessari F, Gyenge CC, Sato T, Chambers RD, Santiago JG, Butcher EC. Lymphocyte electrotaxis in vitro and in vivo. *Journal of Immunology*. 2008; 181(4): 2465-2471.

Liu Y, Rao MS. Glial progenitors in the CNS and possible lineage relationships among them. *Biology of the Cell*. 2004; 96(4): 279-290.

Lodish H, Berk A, Kaiser C, et al. Transmembrane transport of ions and small molecules. In: *Molecular cell biology*. 6th ed. New York: W. H. Freeman and Company; 2008:470-472.

Mao XG, Xue XY, Zhang X. The potential of the brain: Plasticity implications for de-differentiation of mature astrocytes. *Cellular and Molecular Neurobiology*. 2009; 29(8):1105-1108.

Marr PG. Directional (circular) statistics. http://webspace.ship.edu/pgmarr/Geo441/Lectures/Lec%2016%20-%20Directional%20Statistics.pdf. Updated 2011. Accessed 03/13, 2013.

Masaki H, Ide H. Regeneration potency of mouse limbs. *Development, Growth & Differentiation*. 2007; 49:89-98.

McCaig CD. Electrical signals control corneal epithelial cell physiology and wound repair. In: Pullar CE, ed. *The physiology of bioelectricity in development, tissue regeneration, and cancer.* 1st ed. Roca Baton, FL: CRC Press; 2011:121-135.

McCaig CD, Sangster L, Stewart R. Neurotrophins enhance electric field-directed growth cone guidance and directed nerve branching. *Developmental Dynamics*. 2000; 217(3):299-308.

McCaig C, Rajnicek A, Song B, Zhao M. Controlling cell behavior electrically: Current views and future potential. *Physiol Rev*. 2005; 85(3):943-978.

McKasson MJ, Huang L, Robinson KR. Chick embryonic schwann cells migrate anodally in small electric fields. *Experimental neurology*. 2008; 211(2):585-587.

Merkle FT; Tramontin AD, Garcia-Verdugo JM, Alvarez-Buylla A. Radial glia give rise to adult neural stem cells in the subventricular zone. *Proceedings of the National Academy of Sciences of the United States of America*. 2004; 101(50):17528-17532.

Messerli MA, Graham DM. Extracellular electric fields direct wound healing and regeneration. *The Biological Bulletin*. 2011; 221:79-92.

Meyer A, Zardoya R. Recent advantages in the molecular phylogeny of vertebrates. *Annual Review of Ecology, Evolution, and Systematics*. 2003; 34:311-318.

Miller MW, Nowakowski RS. Use of bromodeoxyuridine-immunocytochemistry to examine the proliferation, migration, and time of origin of cells in the central nervous system. *Brain Research*. 1988; 457(1):44-52.

Montgomery DL. Astrocytes: Form, functions, and roles in disease. *Vetinary Pathology*. 1994; 31:145-167.

Morest DK, Silver J. Precursors of neurons, neuroglia, and ependymal cells in the CNS: What are they? where are they from? how do they get where they are going? *Glia*. 2003; 43(1):6-18.

Nag S. Morphology and properties of astrocytes. *Methods in Molecular Biology*. 2011; 686:69-100.

Nagoshi N, Shibata S, Hamanoue M, et al. Schwann cell plasticity after spinal cord injury shown by neural crest lineage tracing. *Glia*. 2011; 59(5):771-784.

Neugebauer KM, Tomaselli KJ, Lilien J, Reichardt LF. N-cadherin, NCAM, and integrins promote retinal neurite outgrowth onastrocytes *in vitro*. *Journal of Cell Biology*. 1988; 107(3):1177-1187.

Nuccitelli R. Measuring endogenous electric fields. In: Pullar CE, ed. *The physiology of bioelectricity in development, tissue regeneration, and cancer.* 1st ed. Boca Raton, FL: CRC Press; 2011:1-15.

Nuccitelli R. Endogenous ionic currents and DC electric fields in multicellular animal tissues. *Bioelectromagnetics*. 1992; 1:147-157.

Oberheim NA, Wang X, Goldman S, Nedergaard M. Astrocytic complexity distinguishes the human brain. *Trends in neurosciences*. 2006; 29(10):547-553.

Okada TS. A brief history of regeneration research. *Journal of Bioscience*. 1996; 21(3):261-271.

Orlov ML. Linear Regression. http://chemistry.oregonstate.edu/courses/ch361-464/ch464/RegrssnFnl.pdf. Updated 1996. Accessed 03/03, 2013.

Palma V, Lim DA, Dahmane N, et al. Sonic hedgehod controls stem cell behavior in the postnatal and adult brain. *Development*. 2005; 132(2):335-344.

Patel N, Poo MM. Orientation of neurite growth by extracellular electric fields. *The Journal of neuroscience*. 1982; 2(4):483-496.

Poss KD, Wilson LG, Keating MT. Heart regeneration in zebrafish. *Science*. 2002; 298:2188-2190.

Prochiantz A. Neuronal growth and shape. *Developmental Neuroscience*. 1985; 7:189-198.

Pullar CE. Physiological electric fields can direct keratinocyte migration and promote healing in chronic wounds. In: Pullar CE, ed. *The physiology of bioelectricity in development, tissue regeneration, and cancer.* 1st ed. Boca Raton, FL: CRC Press; 2011:138-153.

Purves D, Lichtman J. Mechanisms of directed axon outgrowth. In: *Principles of neural development.* 1st ed. Massachusetts: Sinauer Associates Inc.; 1985:119-130.

Qiu J, Cai D, Filbin MT. Glial inhibition of nerve regeneration in the mature mammalian CNS. *Glia*. 2000; 29(2):166-174.

Raff MC, Abney ER, Cohen J, Lindsay R, Noble M. Two types of astrocytes in cultures of developing rat white matter: Difference in morphology, surface gangliosides, and growth characteristics. *Journal of Neuroscience*. 1983; 3(6):1289-1300.

Rajnicek AM, Gow NA, McCaig CD. Electric field-induced orientation of rat hippocampal neurones *in vitro*. *Experimental Physiology*. 1992; 77(1):229-232.

Reichenbach A, Wolburg H. Astrocytes and ependymal glia. In: Kettenmann H, Ransom BR, eds. *Neuroglia*. 3rd ed. New York, NY: Oxford University Press; 2013:35-49.

Reid B, Song B, McCaig CD, Zhao M. Wound healing in rat cornea: The role of electric currents. *Federation of American Societies for Experimental Biology*. 2005; 19(3):379-386.

Reid B, Song B, Zhao M. Electric currents in xenopus tadpole tail regeneration. *Developmental Biology*. 2009; 335(1):198-207.

Richardson PM, McGuinness UM, Aguayo AJ. Axons from CNS neurons regenerate into PNS grafts. *Nature*. 1980; 284(5753):264-265.

Ridet JL, Malhotra SK, Privat A, Gage FH. Reactive astrocytes: Cellular and molecular cues to biological function. *Trends in neurosciences*. 1997; 20(12):570-577.

Rodnight RB, Gottfried C. Morphological plasticity of rodent astroglia. *Journal of Neurochemistry*. 2013; 124(3):263-275.

Sauer H, Rahimi G, Hescheler J, Wartenberg M. Effects of electric fields on cardiomyocyte differentiation of embryonic stem cells. *Journal of Cellular Biochemistry*. 1999; 75(4):710-723.

Seifert AW, Kiama SG, Seifert MG, Goheen JR, Palmer TM, Maden M. Skin shedding and tissue regeneration in african spiny mice (acomys). *Nature*. 2012; 489(7417):561-565.

Shapiro S, Borgens RB, Pascuzzi R, et al. Oscillating field stimulation for complete spinal cord injury in humans: A phase 1 trial. *Journal of Neurosurgery Spine*. 2005; 2(1):3-10.

Sharif A, Legendre P, Pre*f*vot V, et al. Transforming growth factor alpha promotes sequential conversion of mature astrocytes into neural progenitors and stem cells. *Oncogene*. 2007; 26(19):2695-2706.

Sher F, Boddeke E, Copray S. Ezh2 expression in astrocytes induces their dedifferentation toward neural stem cells. *Cellular Reprogamming*. 2011; 13(1):1-6.

Sheridan DM, Isseroff RR, Nuccitelli R. Imposition of a physiological DC electric field alters the migratory response of human keratinocytes on extracellular matrix molecules. *Journal of Investigative Dermatology*. 1996; 106(4):642-646.

Singh BN, Koyano-Nakagawa N, Garry JP, Weaver CV. Heart of newt: A recipe for regeneration. *Journal of Cardiovascular Translational Research*. 2010; 3:397-409.

Sofroniew MV, Vinters HV. Astrocytes: Biology and pathology. *Acta Neuropathologica*. 2010; 119(1):7-35.

Sofroniew MV. Molecular dissection of reactive astrogliosis and glial scar formation. *Trends in neurosciences*. 2009; 32(12):638-647.

Somjen GG. Nervenkitt: Notes on the history of the concept of neuroglia; GLIA. *Glia*. 1988; 1:2-9.

Song B, Pu J, Reid B, Zhao Z, Zhao M. Application of direct current electric fields to cells and tissues *in vitro* and modulating wound electric field *in vivo*. *Nature Protocols*. 2007; 2(6):1479-1489.

Song B, Zhao M, Forrester JV, McCaig CD. Nerve regeneration and wound healing are stimulated and directed by an endogenous electric field *in vivo*. *Journal of Cell Science*. 2004; 117(20):4681-4690.

Song B, Zhao M, Forrester JV, McCaig CD. Electrical cues regulate the orientation and frequency of cell division and the rate of wound healing *in vivo*. *Proceedings of the National Academy of Sciences of the United States of America*. 2002; 99(21):13577-13582.

Stern JE, Filosa JA. Bidirectional neuro-glial signaling modalities in the hypothalamus: Role in neurohumoral regulation. *Auton Neurosci*. 2013; 175(1-2):51-60.

Stewart S, Rojas-Munoz A, Izpisua Belmonte JC. Bioelectricity and epimorphic regeneration. *Bioessays*. 2007; 29(11):1133-1137.

Teng YD, Mocchetti I, Wrathall JR. Basic and acidic fibroblast growth factors protect spinal motor neurones *in vivo* after experimental spinal cord injury. *European Journal of Neuroscience*. 1998; 10(2):798-802.

Terman JR, Wang XM, Martin GF. Repair of the transected spinal cord at different stages of development in the north american opossum, didelphis virginiana. *Brain Research Bulletin*. 2000; 53(6):845-855.

Thery M, Jimenez-Dalmaroni A, Racine V, Bornens M, Julicher F. Experimental and theoretical study of mitotic spindle orientation. *Nature*. 2007; 447(7143):493-496.

Thomspon DM, Buettner HM. Neurite outgrowth is directed by schwann cell alignment in the absence of other guidance cues. *Annals of Biomedical Engineering*. 2006; 34(1):161-168.

Varga ZM, Schwab ME, Nicholls JG. Myelin-ascoaited neurite growth-inhibitory proteins and supression of regeneration of immature mammalian spinal cord in culture. *Proceedings of the National Academy of Sciences of the United States of America*. 1995; 92(24):10959-10963.

Vick RS, Neuberger TJ, DeVries GH. Role of adult oligodendrocytes in remyelination after neural injury. *Journal of Neurotrauma*. 1992; 9:S93-S103.

Wachter B, Schürger S, Rolinger J, et al. Effect of 6-hydroxydopamine (6-OHDA) on proliferation of glial cells in the rat cortex and striatum: Evidence for de-differentiation of residentastrocytes. *Cell and Tissue Research*. 2010; 342(2):147-160.

Walder S, Zhang F, Ferretti P. Up-regulation of neural stem cell markers suggests the occurence of dedifferentiation in regenerating spinal cord. *Development Genes and Evolution*. 2003; 213(12):625-630.

Wallace MC, Tator CH, Piper I. Recovery of spinal cord function induced by direct current stimulation of the injured rat spinal cord. *Neurosurgery*. 1987; 20(6):878-884.

Wang E, Yin Y, Bai H, Reid B, Zhao Z, Zhao M. Electrical control of angiogenesis. In: Pullar CE, ed. *The physiology of bioelectricity in development, tissue regeneration, and cancer*. 1st ed. Boca Raton, FL: CRC Press; 2011:156-175.

Wang ET, Zhao M. Regulation of tissue repair and regeneration by electric fields. *Chinese Journal of Traumatology*. 2010; 13(1):55-61.

Wang Y, Cheng X, He Q, et al. Astrocytes from the contused spinal cord inhibit oligodendrocyte differentiation of adult oligodendrocyte precursor cells by increasing the expression of bone morphogenetic proteins. *Journal of Neuroscience*. 2011; 31(16):6053-6058.

Wanner I. An *in vitro* trauma model to study rodent and human astrocyte reactivity. *Methods in Molecular Biology*. 2012; 814:189-219.

Xu H, Yang Y, Tang X, et al. Bergmann glia function in granule cell migration during cerebellum development. *Molecular Neurobiology*. 2013; 47(2):833-844.

Yamada K, Watanabe M. Cytodifferentiation of bergmann glia and its relationship with purkinje cells. *Anatomical Science International*. 2002; 77(2):94-108.

Yang H, Cheng XP, Li JW, Yao Q, Ju G. De-differentiation response of cultured astrocytes to injury induced by scratch or conditioned culture medium of scratch-insulted astrocytes. *Cellular and Molecular Neurobiology*. 2009; 29(4):455-473.

Yang H, Feng GD, Olivera C, et al. Sonic hedgehog released from scratch-injured astrocytes is a key signal necessary but not sufficient for the astrocyte de-differentiation. *Stem Cell Research*. 2012; 9(2):156-166.

Yao L, Pandit A, Yao S, McCaig CD. Electric field-guided neuron migration: A novel approach in neurogenesis. *Tissue Engineering: Part B*. 2011; 13(3):143-153.

Yu T, Cao G, Feng L. Low temperature induced de-differentiation of astrocytes. *Journal of Cellular Biochemistry*. 2006; 99(4):1096-1107.

Zar JH. *Biostatistical analysis*. 4th ed. Upper Saddle River, NJ: Prentice Hall; 1999.

Zhang F, Clarke JD, Ferretti P. FGF-2 Up-regulation and proliferation of neural progenitors in the regenerating amphibian spinal cord *in vivo*. *Developmental Biology*. 2000; 225(2):381-391.

Zhao M, Agius-Fernandez A, Forrester JV, McCaig CD. Orientation and directed migration of cultured corneal epithelial cells in small electric fields are serum dependent. *Journal of Cell Science*. 1996; 109:1405-1414.

Zhao M, Forrester JV, McCaig CD. A small, physiological electric field orients cell division. *Proceedings of the National Academy of Sciences of the United States of America*. 1999; 96(9):4942-4946.

Zhao M, McCaig CD, Agius-Fernandez A, Forrester JV, Araki-Sasaki K. Human corneal epithelial cells reorient and migrate cathodally in a small applied electric field. *Current Eye Research*. 1997; 16(10):973-984.

Zhao M, Penninger J, Isseroff RR. Electrical activation of wound-healing pathways. *Advances in Skin & Wound Care*. 2010; 1:567-573.

Zhao RR, Andrews MR, Wang D, et al. Combination treatment with anti-nogo-A and chondroitinase ABC is more effective than single treatments at enhancing functional recovery after spinal cord injury. *European Journal of Neuroscience*. 2013.

Zuberi M, Liu-Snyder P, Ul Haque A., Porterfield DM, Borgens RB. Large naturally-produced electric currents and voltage traverse damaged mammalian spinal cord; journal of biological engineering. *Journal of Biological Engineering*. 2008; 2(17).

VITA

Doel Dhar was born in Culpeper, Virginia, on January 17, 1990. She graduated from Thomas Jefferson High School for Science & Technology, Alexandria, Virginia in June 2007. She received her Bachelor of Science degree, majoring in Neuroscience and minoring in Biochemistry, from the College of William & Mary, Williamsburg, Virginia in December 2010.